

INFORMATION TO USERS

The most advanced technology has been used to photograph and reproduce this manuscript from the microfilm master. UMI films the text directly from the original or copy submitted. Thus, some thesis and dissertation copies are in typewriter face, while others may be from any type of computer printer.

The quality of this reproduction is dependent upon the quality of the copy submitted. Broken or indistinct print, colored or poor quality illustrations and photographs, print bleedthrough, substandard margins, and improper alignment can adversely affect reproduction.

In the unlikely event that the author did not send UMI a complete manuscript and there are missing pages, these will be noted. Also, if unauthorized copyright material had to be removed, a note will indicate the deletion.

Oversize materials (e.g., maps, drawings, charts) are reproduced by sectioning the original, beginning at the upper left-hand corner and continuing from left to right in equal sections with small overlaps. Each original is also photographed in one exposure and is included in reduced form at the back of the book.

Photographs included in the original manuscript have been reproduced xerographically in this copy. Higher quality 6" x 9" black and white photographic prints are available for any photographs or illustrations appearing in this copy for an additional charge. Contact UMI directly to order.

U·M·I

University Microfilms International
A Bell & Howell Information Company
300 North Zeeb Road, Ann Arbor, MI 48106-1346 USA
313/761-4700 800/521-0600

Order Number 9108807

**Surgery simulation: A computer graphics system to analyze and
design musculoskeletal reconstructions of the lower limb**

Delp, Scott Lee, Ph.D.

Stanford University, 1990

Copyright ©1990 by Delp, Scott Lee. All rights reserved.

U·M·I

300 N. Zeeb Rd.
Ann Arbor, MI 48106

NOTE TO USERS

**THE ORIGINAL DOCUMENT RECEIVED BY U.M.I. CONTAINED PAGES WITH
PHOTOGRAPHS WHICH MAY NOT REPRODUCE PROPERLY.**

THIS REPRODUCTION IS THE BEST AVAILABLE COPY.

**SURGERY SIMULATION:
A COMPUTER GRAPHICS SYSTEM TO ANALYZE AND DESIGN
MUSCULOSKELETAL RECONSTRUCTIONS OF THE LOWER LIMB**

A DISSERTATION
SUBMITTED TO THE DEPARTMENT OF MECHANICAL ENGINEERING
AND THE COMMITTEE OF GRADUATE STUDIES
OF STANFORD UNIVERSITY
IN PARTIAL FULFILLMENT OF THE REQUIREMENTS
FOR THE DEGREE OF
DOCTOR OF PHILOSOPHY

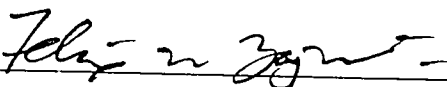
By

Scott Lee Delp

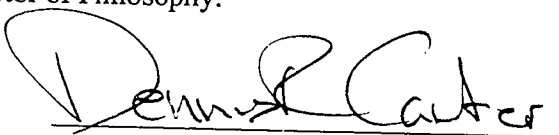
August 1990

© Copyright by Scott Lee Delp 1990
All Rights Reserved

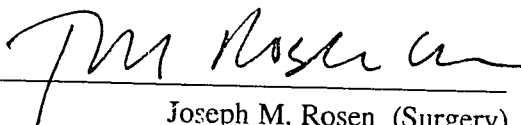
I certify that I have read this thesis and that in my opinion it is fully adequate, in scope and quality, as a dissertation for the degree of Doctor of Philosophy.


Felix E. Zajac, III (Principal Advisor)

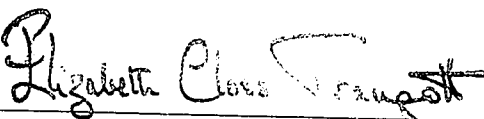
I certify that I have read this thesis and that in my opinion it is fully adequate, in scope and quality, as a dissertation for the degree of Doctor of Philosophy.


Dennis R. Carter (Mechanical Engineering)

I certify that I have read this thesis and that in my opinion it is fully adequate, in scope and quality, as a dissertation for the degree of Doctor of Philosophy.


Joseph M. Rosen (Surgery)

Approved for the University Committee on Graduate Studies:


Dean of Graduate Studies

Abstract

Function can sometimes be restored to patients with movement disabilities via surgical reconstruction of musculoskeletal structures. Surgical reconstructions, however, often compromise the capacity of muscles to generate force and moments about the joints. Patients that cannot generate sufficient joint moments are left with weak or dysfunctional limbs. The goal of this dissertation is to understand the connection between the parameters of various surgical procedures and the moment-generating capacity of the lower-limb muscles.

A graphics-based model of the human lower limb was developed to study the effects of musculoskeletal reconstructions on muscle function. The lines of action of forty-three muscle-tendon complexes were defined based on their relationships to three-dimensional bone surface models. A model for each muscle-tendon complex was formulated to compute its force-length relation. The kinematics of the lower limb were defined by modeling the hip, knee, ankle, subtalar, and metatarsophalangeal joints. Thus, the maximum isometric force and joint moments that each muscle-tendon complex develops can be computed at any body position. Since the model is implemented on a computer graphics workstation, the model parameters can be graphically manipulated according to various surgical techniques. For example, the origin-to-insertion path of a muscle-tendon complex can be altered to simulate a tendon transfer. The results of the simulated surgeries are displayed in terms of presurgery and postsurgery muscle forces, joint moments, and other biomechanical variables.

The model of the lower limb has been used to analyze tendon surgeries and pelvic osteotomies. The analysis of tendon lengthenings indicated that the forces generated by the ankle plantarflexors are extremely sensitive to surgical lengthening of tendon, while other muscles are much less sensitive. Quantifying the sensitivity of the muscle forces and joint moments to changes in tendon length provides important new data needed to design effective tendon surgeries. Simulations of the Chiari pelvic osteotomy suggest that osteotomies performed with high angulation shorten the hip abductors and may lead to the commonly observed weakness of the hip abductors. Simulated surgeries showed that horizontal osteotomies preserve the moment-generating capacity of the hip abductors and may therefore decrease the number of patients who limp after surgery.

Just as computer graphics systems have enhanced other areas of design and analysis, an interactive, graphics-based model of the human lower limb can facilitate the design and analysis of surgical procedures.

Acknowledgements

I am deeply thankful to have had the opportunity to work with Professor Felix E. Zajac. As my principal advisor, Felix has been a constant source of insight and encouragement. His enthusiasm, attention to detail, and friendship will continue to influence my work in the years to come.

I thank Professors Joseph Rosen and Dennis Carter, the other members of my reading committee, for the many discussions we have had related to biomechanics and surgery simulation. My regular meetings at Dr. Rosen's home have been especially constructive.

I gratefully acknowledge the contributions of Peter Loan and my brother, Idd Delp. Pete, Idd and I began this project in 1986 when we digitized and displayed a human pelvis. Since then, Pete and I have worked together to develop much of the musculoskeletal modeling software that was used in this dissertation. Pete has written most of the software that is presented in Chapter 3. Idd has helped me to create illustrations, posters, and videos that describe the surgery simulation project. Without Pete and Idd this project would not have been possible.

Melissa Hoy and Eric Topp have been of tremendous assistance in developing the model of the lower limb that is presented in Chapter 4. Eric Topp is responsible for developing the "partial velocity" method for computing moment arms which is presented in Chapter 3.

Many physicians have helped give clinical direction to this work. Special thanks go to Dr. Eugene Bleck and Dr. Gerard Bollini for their help with the analysis of the Chiari osteotomy (Chapter 6). I also thank Dr. Bleck and Dr. George Rab for sharing their insights into tendon lengthenings and tendon transfers. I am grateful to George Rab for his careful review of Chapter 5.

I have benefitted from daily interactions with colleagues at Stanford University and the VA Rehabilitation Research and Development Center. Gary Beaupre', Dave Brown, Carol Cady, Gayle Curtis, B. J. Fregly, Michael Gordon, Gon Khang, Artimus Kuo, Tracy Orr, Marcus Pandey, Lisa Schutte, Pamela Stevenson, Marjolein van der Meulen, and Gary Yamaguchi have been helpful. Scott Tashman has been especially helpful in providing insight into gait analysis in cerebral palsy. Thanks to Jim Bishop and Pat McCarty for helping me get things done at the VA and for keeping the refrigerator stocked.

I thank Don Stredney for providing data describing the shank and foot bones, Michael Roberts for help with the anatomical study of the Chiari osteotomy, and Scott Fisher and Steve Pieper for transferring our lower-limb model into NASA's virtual environment.

Finally, and most importantly, I thank my family for their love and support. Comprehensive thanks are not possible, so I have chosen some examples. Brother Gary, in a foolish act of pure love, read and commented on the entire first draft of this dissertation. Brother Bryan called the night before qualification exams with the one thing I did remember during the exam — “drive for the hoop and score.” Brother Idd, worked with me until 4:00 AM to finish the illustration and layout of this document, and then cooked me breakfast. Mom responded to my request to borrow food money with “How about if I fly out and cook your dinners for a month.” Dad, you taught me how to revitalize myself by canoeing in the Canadian wilderness. It's time for a little wilderness.

This work was supported by the Rehabilitation Research and Development Service, Department of Veterans Affairs; the Aerospace Human Factors Research Group at NASA Ames Research Center; and a National Science Foundation Predoctoral Fellowship.

Scott L. Delp
Palo Alto, California
August, 1990

Contents

1 INTRODUCTION

- 1.1 *Focus of the Dissertation* 2
- 1.2 *Significance of this Research* 4
- 1.3 *Static Properties of Muscle and Tendon* 4
- 1.4 *Other Terminology* 7
- 1.5 *Thesis Overview* 9

2 BACKGROUND AND RELATED WORK

- 2.1 *Musculoskeletal Models* 10
- 2.2 *Three-dimensional Reconstructions from Medical Imaging Equipment* 11
- 2.3 *Computer Simulation of Tendon Transfers* 12
- 2.4 *Computer Modeling of Hip Reconstructions and Osteotomies* 13
- 2.5 *Our Model in Relation to These Others* 13
- 2.6 *Major Assumptions* 13
 - We assume full muscular activation* 13
 - Comparing the model results to experimental data is problematic* 14
 - We do not account for muscle-tendon adaptation over time* 15
 - We use model of a nominal lower extremity* 15

3 MUSCULOSKELETAL MODELING SOFTWARE

- 3.1 *Introduction* 16
- 3.2 *Defining a Musculoskeletal Model* 17
 - Defining the Body Segments* 18
 - Defining the System Kinematics* 18
 - Modeling the Muscles* 20
 - Computing Moment Arm, Muscle-tendon Length and Force* 22
- 3.3 *Interacting with a Model* 24
- 3.4 *Software Design Goals* 27

4 LOWER-EXTREMITY MODEL

4.1	<i>Musculoskeletal Geometry</i>	29
4.2	<i>Joint Models</i>	31
4.3	<i>Muscle-tendon Parameters</i>	34
4.4	<i>Model Output</i>	36
4.5	<i>Computed Joint Moments Compared to Experimental Data</i>	37
	<i>Ankle Moments</i>	38
	<i>Knee Moments</i>	40
	<i>Hip Moments</i>	43
4.6	<i>Sensitivity Study</i>	47
4.7	<i>Example Surgery Simulation</i>	49
4.8	<i>Assumptions and Limitations</i>	50
4.9	<i>Advantages of Graphics</i>	51

5 ANALYSIS OF TENDON LENGTHENINGS

5.1	<i>Abstract</i>	53
5.2	<i>Introduction</i>	53
5.3	<i>Methods</i>	54
5.4	<i>Results</i>	55
	<i>Effect of Optimal Fiber Length</i>	57
	<i>Effect of Tendon Length</i>	57
	<i>Effect of Pennation</i>	58
	<i>Relative Importance of Fiber Length, Tendon Length, and Pennation Angle</i>	59
	<i>Effect of Moment Arm</i>	59
	<i>Sensitivity of Joint Moments</i>	60
5.5	<i>Discussion</i>	63
	<i>Confidence in Muscle-Tendon Parameters</i>	63
	<i>Assumptions and Limitations</i>	64
	<i>Clinical Implications</i>	66

6 ANALYSIS OF THE CHIARI PELVIC OSTEOTOMY

6.1	<i>Abstract</i>	68
6.2	<i>Introduction</i>	68
6.3	<i>Methods</i>	69
	<i>Surgical Model</i>	70
	<i>Musculoskeletal Model</i>	71
	<i>Simulations of Surgery</i>	72
6.4	<i>Results</i>	72
6.5	<i>Discussion</i>	77
6.6	<i>Conclusion</i>	79

7 CONCLUSION

7.1	<i>Contributions</i>	80	
7.2	<i>Applications and Extensions of Musculoskeletal Modeling Software</i>		80
7.3	<i>Applications and Extensions of Lower-Extremity Model</i>	82	
7.4	<i>Clinical Applications</i>	82	
	<i>Summary of Clinical Findings</i>	82	
	<i>Application to Muscle-Tendon Surgery</i>	82	
	<i>Application to Osteotomies</i>	84	
	<i>Application to Joint Replacements</i>	84	
	<i>Applications to Complex Reconstructions</i>	85	
7.5	<i>Future Work</i>	85	

APPENDIX A	<i>Muscle input file</i>	89
-------------------	--------------------------	----

APPENDIX B	<i>Joint input file</i>	100
-------------------	-------------------------	-----

APPENDIX C	<i>Format of bone files</i>	106
-------------------	-----------------------------	-----

REFERENCES	107
-------------------	-----

Illustrations

Figure

1.1	<i>Surgery simulation system</i>	2
1.2	<i>Normalized force-length property of muscle</i>	5
1.3	<i>Orientation of muscle fibers and tendon in a pennated muscle</i>	6
1.4	<i>Normalized force-length relationship for tendon</i>	6
3.1	<i>Structure of musculoskeletal modeling software</i>	17
3.2	<i>Muscle-tendon actuator model</i>	20
3.3	<i>Definition of terms used in moment arm calculations</i>	22
3.4	<i>Display highlighting the model viewer</i>	25
3.5	<i>Display highlighting the joint editor</i>	26
3.6	<i>Display highlighting the plotmaker utility</i>	27
4.1	<i>Three-dimensional representation of musculotendinoskeletal geometry</i>	30
4.2	<i>Location of the body-segmental reference frames</i>	31
4.3	<i>Geometry for determining knee moments and kinematics</i>	32
4.4	<i>Knee extensor moment arm vs. knee angle</i>	33
4.5	<i>The ankle, subtalar, and metatarsophalangeal joint axes</i>	33
4.6	<i>Passive hip moment vs. hip flexion angle</i>	36
4.7	<i>Comparison of computed and experimental plantarflexion moments</i>	36
4.8	<i>Plantarflexion moment vs. ankle angle with knee extended</i>	38
4.9	<i>Plantarflexion moment vs. ankle angle with knee flexed</i>	38
4.10	<i>Dorsiflexion moment vs. ankle angle</i>	39
4.11	<i>Knee extension moment vs. knee angle with the hip extended</i>	41
4.12	<i>Knee extension moment vs. knee angle with the hip flexed</i>	41
4.13	<i>Knee flexion moment vs. knee angle with hip extended</i>	42
4.14	<i>Knee flexion moment vs. knee angle with hip flexed</i>	42
4.15	<i>Hip extension moment vs. hip angle with knee flexed</i>	43
4.16	<i>Hip extension moment vs. hip angle with knee extended</i>	43

4.17	<i>Hip flexion moment vs. hip angle with knee flexed</i>	44
4.18	<i>Hip abduction moment vs. hip abduction angle</i>	45
4.19	<i>Hip adduction moment vs. hip abduction angle</i>	46
4.20	<i>Hip rotation moment vs. hip rotation angle</i>	46
4.21	<i>Change in joint angle at which four actuators develop peak force</i>	47
4.22	<i>Decrease in muscle force at the joint angle of peak force</i>	48
4.23	<i>Display from a simulated surgery</i>	49
5.1	<i>Body position for which forces and moments are presented</i>	55
5.2	<i>Change in tendon length resulting in a 50% decrease in muscle force</i>	56
5.3	<i>Soleus force vs. ankle angle with elastic and inelastic tendon</i>	58
5.4	<i>The effect of pennation on the soleus force vs. ankle angle curve</i>	58
5.5	<i>Force vs. joint angle for muscles with different moment arms</i>	60
5.6	<i>Ankle moments before and after simulated tendon lengthening</i>	61
5.7	<i>Knee moments before and after simulated tendon lengthening</i>	62
5.8	<i>Hip moments before and after simulated tendon lengthening</i>	62
6.1	<i>Surgical parameters</i>	70
6.2	<i>Musculoskeletal coordinates for the gluteus medius</i>	71
6.3	<i>Comparison of computed and experimental hip abductor moments</i>	73
6.4	<i>Results of two surgery simulations</i>	74
6.5	<i>The effect of surgical parameters on gluteus medius abductor moment</i>	76
A1	<i>Reading the muscle input file</i>	89
B1	<i>Reading the joint input file</i>	100

Tables

4.1	<i>Muscle-tendon parameters for 43 muscle-tendon complexes</i>	35
5.1	<i>Parameters for commonly lengthened muscle-tendon complexes</i>	56
6.1	<i>Gluteus medius parameters at anatomical position</i>	75

1 Introduction

Muscles and tendons actuate movement by developing force and generating moment about the joints. When human movement is impaired by disease or trauma, function can sometimes be restored with surgical reconstruction of musculoskeletal structures. For example, patients with muscular spasticity often undergo tendon transfer and tendon lengthening operations aimed at correcting gait abnormalities. In osteoarthritic patients, bones are reconstructed to alter the joint geometry or to accommodate an endoprosthesis. Surgical reconstructions and joint pathologies often compromise the capacity of muscles to generate force and moment about joints. For instance, when a tendon is lengthened or reattached in a new location, the muscle fibers may be too long or too short to generate active force. When a joint becomes deformed from disease, the moment arms of the muscles that cross the joint may be reduced, thus decreasing the moment that can be generated at that joint. Patients that cannot generate sufficient muscle force or joint moment are left with weak or dysfunctional limbs.

At present, there are few quantitative tools to evaluate the effects of surgical procedures on muscle function. Surgeons rely on their experience and qualitative information from clinical exams to make surgical decisions. However, the combined effects of muscle-tendon properties and skeletal geometry in determining moment-generating characteristics of each muscle are complex and have not been quantified. The absence of a quantitative understanding has limited the success of many musculoskeletal reconstructions and hampers the development of new procedures.

Computer models can assist in understanding the biomechanical consequences of musculoskeletal reconstructions. Since musculoskeletal mechanics are complex, computer models are needed to understand the effects of surgery on the interactions of bone, muscle, and tendon. Alternatively, developing effective surgical procedures without computer models takes years of experience with many patients *for each surgeon*. Computer models can be especially useful to less experienced surgeons for investigating the effects of surgical decisions on a model rather than on a patient. Computer models can also be useful to biomechanical engineers and experienced surgeons for analyzing problematic surgeries and designing new procedures.

Computer graphics are an essential part of computer models for simulating surgery. Computer graphics are helpful to visualize the three-dimensional geometry of the musculoskeletal

system and to facilitate communication among engineers and surgeons. During the past two decades, computer graphics systems for engineering and scientific applications have been under vigorous development. Since graphics effectively link the planning and conceptualizing ability of the human user with high-speed computational machines, graphics tools have become an essential part of engineering design and scientific analysis. However, the use of computer graphics in the design and analysis of surgical procedures is in its infancy. The primary reason is that few systems have been developed that give insight into the biomechanics of surgical procedures.

1.1 Focus of the Dissertation

The goal of this dissertation is to study the biomechanical consequences of surgical reconstructions of the lower extremity. To this end, a computer graphics-based model of the lower extremity was developed to simulate the effects of musculoskeletal reconstructions on muscle function. The model calculates the maximum isometric force and joint moment that each muscle can develop for any body position. Since the model is implemented on a computer-graphics system, one can manipulate the model parameters according to various surgical techniques. The results of the simulated surgeries are then displayed in terms of pre- and post-surgery muscle forces and joint moments (Figure 1.1). The thesis of this dissertation is that the use of such

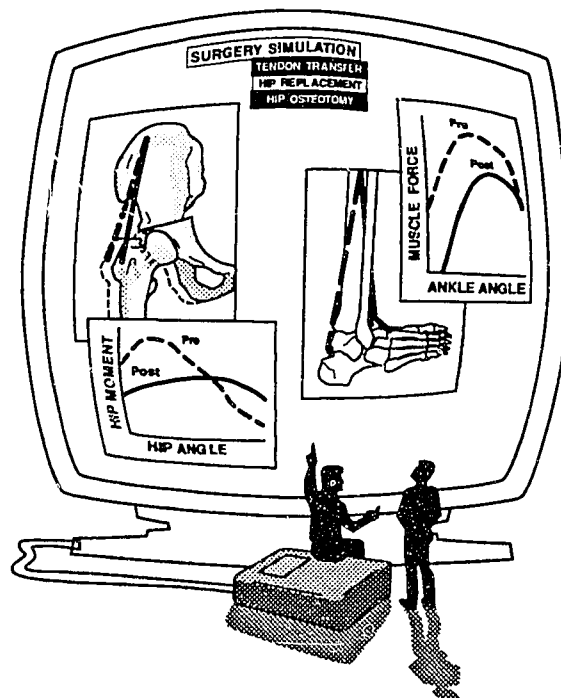


Figure 1.1. Surgery simulation system. Computer simulation of surgical procedures can help to understand how surgically changing the musculoskeletal system affects the force- and moment-generating capacity of the muscles. The two windows on the left show the biomechanical consequences of a simulated hip osteotomy. The two windows on the right show the muscle force curves before and after a simulated tendon transfer.

models will facilitate the design of surgical procedures by providing information about the variables that affect surgical outcomes. We expect that better understanding of the biomechanical consequences of surgical interventions will improve the design of surgical procedures and thus the functional results.

Our model-based studies of musculoskeletal surgeries focus on such questions as:

- How much can a tendon be lengthened before muscle weakness occurs?
- Precisely where should the tendon of a transferred muscle be attached so that the muscle can generate force over a desired range of joint motion?
- Why does muscle weakness occur after some pelvic osteotomies, but not others?

The three main contributions of this dissertation are:

- (1) **Musculoskeletal modeling software** was developed that enables users to develop, alter, and analyze models of a wide variety of musculoskeletal structures. The particular structure to be analyzed (e.g., the lower extremity) is specified by defining the surfaces of the bones, the kinematics of the joints, and the geometry and force-generating properties of the muscles. From the bone, joint, and muscle data, the software calculates the maximum isometric force and joint moment that each muscle can develop for any body position. The software has been implemented on a computer graphics workstation so that users can easily view and interact with the musculoskeletal models. Also, since the software can be used to analyze many different musculoskeletal structures, it can be used to study diverse problems in biomechanics.
- (2) A three-dimensional **model of the lower extremity** was developed using the musculoskeletal modeling software. That is, the bone geometry and the joint kinematics were specified for the entire lower extremity. This model also defines the origin-to-insertion paths and specifies the muscle-tendon parameters (i.e., peak force, fiber length, fiber angle, and tendon length) for every muscle such that the isometric joint moments computed with the model correspond closely to joint moments measured during maximum voluntary contraction experiments. This lower-extremity model can be used to study surgical procedures, as done here, or to calculate muscle-tendon lengths, moment arms, *etc.* during movements such as bicycling and walking.
- (3) The lower-extremity model was used to **analyze several clinical problems**. Surgical lengthening of tendon was analyzed to determine the sensitivity of muscle force to changes in tendon length. The Chiari osteotomy [23] was analyzed to study how the procedure might be performed to reduce the number of patients who limp after surgery. Sensitivity tests were performed that indicate which parameters have the greatest potential to affect the outcome of these surgical procedures.

1.2 Significance of this Research

In an article on surgery simulation, Mann states: "Musculoskeletal disorders are reported as a major, if not dominant, source of morbidity nationally. NIH surveys ranking chronic diseases place arthritis and orthopaedic problems ahead of even heart disease. The Veterans Administration reports that, among its patient population, musculoskeletal diseases rank second in frequency of complaints, fourth in hospital admissions, and fifth in surgical procedures. Among children, much rehabilitation and surgical attention is devoted to postural and gait abnormalities. Conservative estimates put the national cost of direct care for musculoskeletal disease at \$20 billion a year [83]."

Many people who suffer from neuromuscular or musculoskeletal diseases (e.g., stroke, cerebral palsy, arthritis, and spinal cord injury) may benefit from the insights gained from surgery simulations, since musculoskeletal reconstructions are commonly performed on these individuals. Improved surgical outcomes will benefit these individuals not only in the short-term, but also in the long-term, since their future rehabilitation needs may be reduced. Unsatisfactory surgical outcomes often require revision or "second try" surgeries. For example, in several series of patients who have undergone surgical lengthening of tendon to correct gait abnormalities, the revision rate was over 40% [98, 118]. Potentially, simulation studies that quantify the sensitivity of muscle force to changes in tendon length will reduce the need for revision surgeries in patients treated with tendon lengthening.

Another potential benefit of surgery simulation is improved communication between engineers, clinicians, and patients. I have found that surgeons quickly grasp the concepts needed to understand the simulation results in a short tutorial session with the computer-graphics system. These sessions have fostered a great deal of interaction among engineers, physicians, and other health scientists. Also, with a computer graphics display, a surgeon could demonstrate to a patient and his or her family what is causing a problem, what surgery is planned, and what benefits are expected from the surgery. Using the model to improve physician-patient communication is a long-term benefit that has not yet been realized.

1.3 Static Properties of Muscle and Tendon

This dissertation is concerned with the isometric (static) properties of muscle and tendon, so it will be helpful to review some of the basic properties of these tissues. An excellent introduction to muscle properties is presented by Lieber [74]. Zajac gives a more comprehensive review of both muscle and tendon properties [150]. I will briefly summarize the isometric properties of muscle and tendon. Those familiar with these ideas can skip this section without loss of continuity. My intention is to introduce some basic properties of muscle and tendon and define some key terms, not to discuss the details of muscle-tendon modeling.

The sarcomere is the fundamental unit of force generation in muscle. Each sarcomere is about $2\text{-}3\mu\text{m}$ in length and about $1\mu\text{m}$ in diameter. A muscle fiber is composed of a large number of sarcomeres in series. Thus, the length of a muscle fiber depends on the number of sarcomeres in series and the length of each sarcomere. In general, the muscle fibers within a given muscle are of similar length; however, fiber lengths vary significantly between muscles. A bundle of muscle fibers form a muscle fascicle. A whole muscle can be considered to be a set of muscle fascicles that are arranged in parallel. The physiologic cross-sectional area (PCSA) of a muscle can be estimated by measuring the volume of the muscle and dividing by the average fiber length. The peak isometric force that can be generated by a muscle is proportional to its PCSA (see Section 4.3 for details).

The force developed by a muscle also depends on its length. The force-length relationship can be obtained by stimulating a muscle maximally and measuring the force developed at different muscle lengths. Given a nominal muscle force-length curve (Figure 1.2), the force-length property of an individual muscle can be estimated by specifying its **peak isometric muscle force** (F_o^M) and **optimal muscle-fiber length** (ℓ_o^M) (i.e., the fiber length at which active force peaks). †

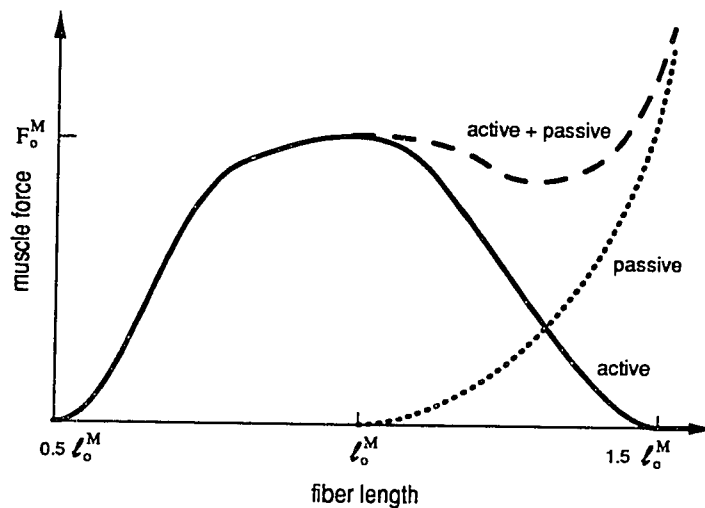


Figure 1.2. Normalized force-length property of muscle. When fully activated, muscle develops peak active force (F_o^M) at optimal fiber length (ℓ_o^M). Passive (i.e., not activated) muscle develops force when stretched beyond (ℓ_o^M). The active + passive force is equal to the sum of active and passive components.

† A few words about notation will be helpful. F denotes force and ℓ denotes length. Superscripts indicate the tissue under consideration. Thus, F^M refers to the force in muscle, ℓ^M to the length of muscle, and ℓ^T to the length of tendon. Subscripts denote the conditions under which force and length are considered. That is, F_o^M denotes the peak, or optimum, muscle force. ℓ_o^M refers to optimal muscle-fiber length. ℓ_s^T denotes tendon slack length, or length at which tendon begins to develop force when stretched.

Muscle force is transmitted to the skeleton via tendon. Thus, the properties of muscle and tendon must be integrated into a model of the muscle-tendon complex (i.e., “muscle-tendon actuator”). In such a model, muscle can be considered as a set of equally-long fibers that are in series with tendon. These fibers may be oriented such that they are in line with the tendon, as in a parallel-fibered muscle, or at an angle (the **pennation angle**, α) to the tendon (Figure 1.3). The model for a pennate muscle is equivalent to a parallel-fibered muscle when the pennation angle is 0° .

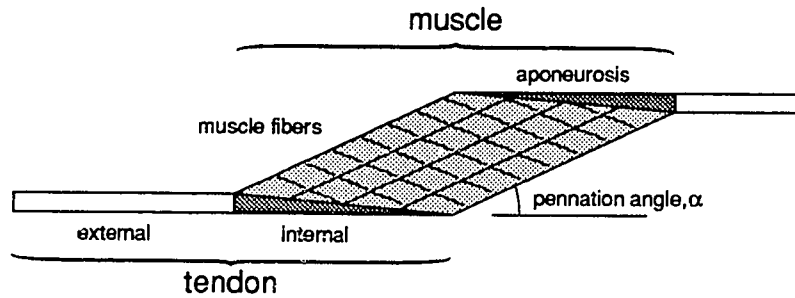


Figure 1.3. Orientation of muscle fibers and tendon in a pennated muscle. Muscle fibers are assumed to lie in parallel and be of equal length. Fibers may be oriented at an angle (pennation angle) with respect to the tendon. Tendon consists of a component internal (i.e., the aponeurosis) and external to the muscle belly. Adapted from Zajac [150].

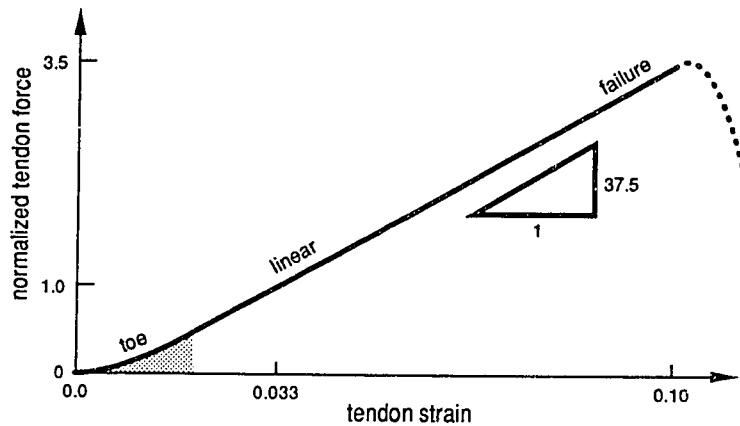


Figure 1.4. Normalized force-length relationship for tendon. Tendon is more compliant in the toe region than in the linear region and fails at about 10% strain. Tendon force is normalized by peak isometric muscle force (F_o^M in Figure 1.2). Tendon strain is defined by tendon stretch divided by tendon slack length (ℓ_s^T), where ℓ_s^T is length at which tendon begins to develop force on elongation. Adapted from Zajac [150].

The static properties of tendon must be included in a muscle-tendon model. Given a normalized force-length curve for tendon (Figure 1.4), the force-length property of an individual tendon can be determined by specifying F_o^M and its tendon slack length (l_s^T) [150]. Data suggest that the properties of internal and external tendon are identical [110], so “tendon” is considered to consist of both internal and external portions. Thus, tendon length includes the length of internal and external tendon. The length of tendon at which force begins to develop when stretched is called the **tendon slack length** (l_s^T).

To summarize, both muscle and tendon have force-length properties. These properties can be scaled to represent an individual muscle-tendon complex by specifying four parameters [150]. Peak isometric force (F_o^M) and optimal fiber length (l_o^M) scale the muscle force-length property. F_o^M and tendon slack length (l_s^T) scale the tendon force-length property. Pennation angle (α) specifies the angle between the muscle fibers and the tendon.

Muscle-tendon force rotates the joints by generating moments about the joints. The moment of force about a joint (**joint moment**) is the product of tendon force and **moment arm**. A muscle has a moment arm for each degree of freedom of the joint(s) it spans. For example, the semitendinosus muscle, which spans the hip and the knee, has a moment arm for each degree of freedom in the hip and knee joints. We have developed a complex method to calculate moment arms for all types of joints (see Section 3.4). However, it is often helpful to think of the moment arm as the lever arm of a muscle. So, in the most simple terms, joint moment equals tendon force times its lever arm. The **maximum isometric joint moment** is equal to the moment generated by a muscle, or set of muscles, when the muscles are maximally activated and held at constant length.

Clinically, muscular strength is quantified in terms of a patient’s ability to generate moment about the joints. Physical therapists and other health professionals who use strength testing equipment, such as a Cybex II dynamometer, to measure joint moment often refer to joint moments as torque. Those who cannot generate “normal” moments about a joint are considered to be weak at that joint. If a patient cannot generate the moments needed to actuate a certain movement, they may require assistive devices to perform the task, compensate for their weakness by moving abnormally, or avoid the movement altogether. For example, a patient that cannot generate sufficient moments to extend the knee and hip may need assistance to get up from a couch or a toilet.

1.4 Other Terminology

This section defines some terms that are frequently used in this dissertation.

tendon transfer - a surgery in which a tendon is detached from one location and then reattached in a new location. Thus, a muscle that normally generates extension moment can be transferred so that it generates flexion moment after surgery.

tendon lengthening - a surgery in which tendon is lengthened. Tendon lengthenings are often performed to correct postural and gait abnormalities. For example, the Achilles tendon is often lengthened in patients that walk on their toes (an equinus deformity) because of hyperactive or tight calf muscles.

osteotomy - a surgery in which a bone is cut into two pieces, and then the pieces are realigned. This procedure is usually performed to reconstruct a diseased joint.

musculoskeletal geometry - the geometric relationships among muscles and bones. These relationships determine the length and moment arms of each muscle-tendon complex.

muscle-tendon parameters - peak isometric force (F_o^M), optimal fiber length (l_o^M), fiber pennation angle (α), and tendon slack length (l_s^T).

maximum isometric joint moment of a muscle - the moment generated by a muscle when it is maximally activated and held at constant length.

maximum isometric joint moment of a muscle group - the moment generated by a group of muscles (e.g., knee flexors) when they are maximally activated and held at constant length.

muscle strength - the peak isometric joint moment that can be generated by a muscle, or group of muscles, over a specified range of joint motion. This is often determined from the maximum isometric joint moment vs. joint angle curve (e.g., Figures 4.8 - 4.20).

total joint moment - the sum of the moments generated by all the muscles that contribute to a joint moment. For example, total hip flexion moment is the sum of the moments generated by all muscles that have hip flexion moment arms.

moment curve - the maximum isometric joint moment vs. joint angle curve (e.g., Figures 4.8 - 4.20).

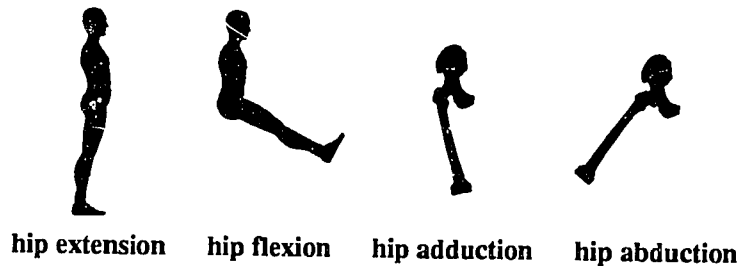
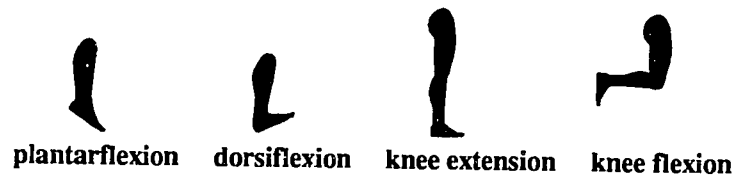
muscle force curve - the maximum isometric muscle force vs. joint angle curve (e.g., Figure 5.3).

passive joint moment - the moment of passive muscle force about a joint. Muscle that is not activated develops force when stretched beyond a certain length (Figure 1.2). For example, even when the muscles are not excited, force develops in the hamstrings when the hip is flexed (see Figure 4.6). The moment generated by muscles from stretching the fibers beyond a certain length is termed passive joint moment.

active + passive joint moment - the moment of active + passive muscle force about a joint. This is the moment that is measured when the muscles are activated and stretched beyond a certain length (i.e., when both active and passive force are developed).

active joint moment - the moment of active muscle force about a joint. The moment of active force (Figure 1.2) about the joints is plotted in the "active only" curves of Figures 4.8 - 4.20.

aponeurosis - the part of tendon that is internal to the muscle belly (Figure 1.3).

joint motions -**1.5 Thesis Overview**

The next chapter describes related work and outlines some of the major assumptions of this dissertation. Chapter 3 describes the musculoskeletal modeling software and details how to define musculoskeletal models using this software system. Chapter 4 presents the model of the lower extremity, discusses its limitations, and presents an example surgery simulation. This chapter presents some of the details that were excluded from our recent journal article [30]. The files that define the lower-extremity model within the musculoskeletal modeling software (e.g., by specifying the muscle-tendon paths) are contained in the Appendices A and B. Chapters 5 and 6 apply the lower-extremity model to study specific clinical problems. Chapter 5 discusses how tendon lengthening surgeries affect the moment-generating capacity of the muscles. Chapter 6, an analysis of the Chiari pelvic osteotomy [23], is the result of my first surgery simulations [29]. This analysis was performed before the lower-extremity model was implemented on the computer graphics system. Chapter 7, the conclusion, summarizes the key contributions of this dissertation and discusses possible future directions of the surgery simulation project.

Since much of the work I have done for this dissertation was performed in collaboration with others, I use the pronoun “we” throughout this document. In Chapters 2 and 4, “we” refers to myself, Peter Loan, Melissa Hoy, Eric Topp, and Felix Zajac. In Chapter 3, “we” refers to myself and Peter Loan. In Chapter 5, “we” refers to myself and Felix Zajac. In Chapter 6, “we” refers to myself, Eugene Bleck, Felix Zajac, and Gerard Bollini.

2 Background and Related Work

To put our surgery simulation project into a larger context, this chapter reviews the research of other investigators in the area of musculoskeletal modeling and surgery simulation. Section 2.1 presents other biomechanical models of the musculoskeletal system and shows how these models can be enhanced with computer graphics. Section 2.2 discusses surgery simulators that make use of data from medical imaging equipment. Sections 2.3 and 2.4 outline biomechanical analyses of specific surgical procedures that relate closely to our simulations. Based on this introduction, the remainder of the chapter contrasts our simulations with these previous investigations and describes some of the basic assumptions of this dissertation.

2.1 Musculoskeletal Models

Other investigators have developed models of the lower extremity to evaluate muscular forces and moments during walking [56], kicking [57], and other activities (see [150, 151] for review). In general, these studies have emphasized the calculation of muscle forces using optimization theory, but did not focus on musculoskeletal geometry. Recently, White *et al.* [140] reported a model describing the variability of musculoskeletal geometry (origin and insertion coordinates) for gait analysis. A similar model [13] has been adapted by Rab to calculate muscle-tendon lengths during normal and pathological walking [111]. Other models demonstrating the effects of musculoskeletal geometry on muscle function exist [62, 81, 86, 108, 123], but these have not been applied to analyze surgical procedures. Models of the lower extremity have been applied to study surgeries such as total hip reconstructions [69], osteotomies [15], and tendon transfers [32]. However, since these models were not implemented on computer-graphics workstations, they provided no means to visualize the geometric changes caused by the surgery, nor did they enable the user to graphically alter the model parameters.

The advantages of using interactive graphics to model the musculoskeletal system were first described in 1977 [143]. Since that time, advances in computer and display technology have significantly expanded the potential to visualize and interact with models of musculoskeletal structures. For example, Wood *et al.* [145] have displayed upper-limb musculature as part of their efforts to design prosthetic arm controllers. To help design more effective tendon transfers, others have developed a graphics-based system to simulate hand biomechanics [16, 128]. Garg and Walker used a computer-graphics model to study the effects of prosthesis design on knee

motion [46]. All of these studies were significantly enhanced by computer graphics. However, no graphics-based model has been reported to study how surgical changes in musculoskeletal geometry affect the moment-generating characteristics of the lower-extremity muscles.

The geometry of the musculoskeletal system is complex. Computer display is therefore helpful to visualize the three-dimensional geometric relationships among the muscles and bones, and to understand how these relationships are changed during surgery. Musculoskeletal geometry is important to the function of muscles because it determines the moment arm of each muscle and thus the moment about a joint of a given muscle force. Geometry also determines muscle-tendon length (i.e., origin to insertion length) for a specific body position. Since muscle-tendon force depends on muscle-tendon length [150], accurate specification of musculoskeletal geometry is necessary to calculate both muscle-tendon force and moment arm, the two multiplicative factors that determine the moment of muscle force about a joint.

2.2 Three-dimensional Reconstructions from Medical Imaging Equipment

Predicting the outcome of surgical procedures has been of interest for many years. In the past, surgeons and engineers have used clay, wood, or plastic models to visualize the geometric changes that occur during surgery. Recent advances in medical imaging technology, such as computed tomography (CT) and magnetic resonance (MR), have made it possible to display and manipulate realistic computer-generated images of anatomical structures (see [4, 39, 47] for review). Because of the immediate practical applications, medical imaging groups commonly present examples related to surgery simulation. Vannier and colleagues pioneered many of the early applications related to planning and evaluation of craniofacial surgery [135]. Three-dimensional reconstructions from CT data are now being used to plan total hip reconstructions, osteotomies, and allograft procedures [93]. Groups at the University of Pennsylvania [59], University of North Carolina [109] and the Mayo Clinic [114] have also developed interactive systems to analyze medical images.

Sometimes CT reconstructions are used to create plastic models via computer-aided manufacturing technology [40]. The solid models have been used to plan routine craniofacial reconstructions or to experiment with unique surgeries prior to actual operations [88]. The solid models are also used to design custom prostheses [53, 113]. Where available, three-dimensional image reconstruction systems are used routinely in patient management. The cost is high, however, and only a limited number of stand-alone systems are available [71]. Further, while this method is well-suited to visualize a patient's anatomy, it does not provide a means to understand how a planned surgery will affect muscle strength.

The key advantage of surgery simulators based on medical image technology is that they allow the user to visualize a patient's anatomy in three dimensions. Some systems allow users to manipulate the images by cutting bones to plan osteotomies [93, 132]. Others allow one to measure linear and curvilinear distances from three-dimensional surface displays [129]. However,

none of these image-based systems have incorporated the mechanical properties of muscle and tendon or the kinematic properties of the joints. This is the fundamental difference between image-based surgery simulators and our model-based approach. Although both approaches take advantage of computer display of anatomical structures, our objective is to understand how surgical changes in musculoskeletal geometry, joint kinematics, and other parameters affect muscle strength. This is not possible without a biomechanical model.

A computer-aided surgery system that includes both biomechanical analysis and three-dimensional reconstructions from CT scans is under development at the Massachusetts Institute of Technology [54, 83]. The system combines motion analysis, optimization models, CT data, and computer graphics display. Although Mann *et al.* have made significant progress with motion analysis [84], CT processing [126], and computer graphics [20, 78], no analyses of clinical problems using computer-aided surgery have yet been reported.

2.3 Computer Simulation of Tendon Transfers

Dul *et al.* developed a biomechanical model to simulate tendon transfers at the ankle [32]. An optimization scheme was used to predict muscle forces before and after an anterior transfer of the posterior tibial tendon. Estimates of muscle force were based on muscle cross-sectional area, but did not take tendon length into account. However, Hoy *et al.* suggest that tendon length is an important factor influencing the ability of muscles to generate active force, especially for muscles crossing the ankle [62]. Although the tendon transfer simulations agree with clinical findings (i.e., the mechanical conditions for normal standing and walking are met by the surgery), they provide no insight into how surgical variables affect the clinical result. Dul *et al.* conclude that biomechanical models can assist engineers and surgeons in analyzing the mechanical effects of tendon-transfers, but make no clinical recommendations based on their results [32]. Our goal is to understand how the surgical variables affect the functional result and thus to provide insight into how the design of tendon transfer surgeries can be improved.

A system for interactive simulation of tendon-transfer surgeries in the hand is being developed for clinical use at Louisiana State University in conjunction with the Hansen's Disease Center [16]. Initially this system was based on the kinematics of the thumb joints only. Now, it includes motion of the fingers and three long flexors of the thumb and fingers [128]. The user can simulate the kinematics of a patient's impaired hand, try out a proposed tendon transfer on the computer model, and display the results on a graphics workstation. The hand model can be customized to an individual patient by specifying muscle weaknesses and ranges of joint motion found from clinical exams. Once the patient parameters are specified, a tendon-transfer surgery can be simulated by choosing from a set of commonly performed operations. The outcome of simulated surgeries are evaluated in terms of moment arms and muscle-tendon excursions (i.e., changes in origin-to-insertion length). A model of muscle and tendon has not been included in this system, so muscle-tendon forces and joint moments cannot be calculated.

2.4 Computer Modeling of Hip Reconstructions and Osteotomies

A computer model has been developed at University of Iowa to investigate the mechanism by which proximal femoral osteotomies relieve pain [15]. In this model, muscle moments were calculated from kinematic and force plate data using optimization algorithms to distribute the total joint moment among the muscles of the lower extremity. Once muscle forces were calculated, joint force was computed. Osteotomies were simulated by adjusting the muscle attachment coordinates and recomputing the muscle and joint forces. The primary conclusion of this study was that proximal femoral osteotomies do not significantly reduce the joint force, and thus a different explanation for the success of femoral osteotomies should be explored.

The University of Iowa group used a similar approach to optimize the geometry in total hip replacements [69]. They determined that the hip joint force could be minimized by positioning the femoral head as far medially, anteriorly, and inferiorly as possible. This early study clearly demonstrated the utility of using computer models of the musculoskeletal system to analyze the biomechanical consequences of surgical reconstructions.

2.5 Our Model in Relation to These Others

The fundamental goal of the dissertation is to understand the connection between the parameters of various surgical procedures and the forces and joint moments that can be developed by the muscles (i.e., muscle strength). To achieve this objective, we have developed a computer model of the human lower extremity. The model is based on the three-dimensional geometry of the muscles and bones, the kinematic properties of the joints, the force-generating properties of muscle, and the elastic properties of tendon. With this model we can compute each muscle's maximum (i.e., fully activated) isometric force and its moment about the joints for any body position. We can then change the musculoskeletal model according to various surgical techniques to determine how the simulated surgery affects the force- and moment-generating capacity of the muscles.

To develop this model we have had to make many simplifying assumptions. While the previous section noted some of the limitations of previous investigations, the following section describes some of the assumptions and limitations of our model.

2.6 Major Assumptions

This section discusses the major assumptions of our musculoskeletal model.

We assume full muscular activation. To test the validity of our model, we compare calculated joint moments with experimental joint moments reported by others (e.g., Figures 4.8 - 4.20). Since we assume that the muscles are fully activated and held isometric, we compare calculated moments to isometric moments measured during maximum voluntary contractions (MVC). Support for the assumption of full muscular activation during MVC is abundant [6, 7]. However,

recent evidence suggests that a MVC may yield less than the maximum force that a muscle can develop because not all the motor units are fully excited during sustained voluntary contractions [35, 36]. In any case, the forces or moments measured during MVC represent a standard measure of muscular performance [36]. Muscular strength is defined in this dissertation as the peak isometric joint moment that can be generated by a muscle, or group of muscles, over a specified range of joint motion. For an individual muscle, it is determined by the muscular activation, musculoskeletal geometry, and parameters of the specific muscle-tendon complex. By assuming full activation, we can isolate the effects of surgically changing musculoskeletal geometry and muscle-tendon parameters on muscle strength.

Comparing the model results to experimental data is problematic. There are other problems associated with comparing computed joint moments with experimental joint moments. A complete, consistent set of experimental data indicating how the maximum isometric joint moments vary with joint angles does not exist. Researchers typically report moments for a single joint only (e.g., plantarflexion moment vs. ankle angle). Thus, we had to compare our simulated joint moments with experimental joint moments measured by a number of different research groups on a number of different populations. For some joints (e.g., the ankle), different research groups report very similar joint moment curves [63, 116]. We have confidence in these experimental data. Joint moment curves for the hip, however, vary significantly between research groups [72]. When reported experimental data are inconsistent, we had to select the data that we considered to be the most accurate based on the authors' descriptions of the experimental methods.

The redundancy of muscles is also a problem in comparing the calculated and measured joint moments. Many muscles may contribute to the moment about a joint, but only the total joint moment can be measured. So, total calculated moment may match the experimental moment, but how do we know if the individual muscle moments are reasonable?

Several conditions help us gain confidence in the moments generated by individual muscles. First, when comparing calculated and experimental joint moment curves, we are not just matching a single value. The moment curve's shape, magnitude, and joint angle at which moment peaks must all be considered. Also, many muscles generate moment about more than one axis of a joint, or span more than one joint. Yet, a single set of muscle-tendon parameters must yield reasonable moments for all joint axes. For example, the parameters chosen for hip muscles must yield both reasonable hip flexion-extension moments and hip abduction-adduction moments. Adjacent joint angles can also be varied to study moments generated by biarticular muscles. For instance, simulated and experimental plantarflexion moment curves can be compared for different knee angles (see Figures 4.8 and 4.9). Herzog *et al.* described a similar method to determine the force-length relationship of selected biarticular muscles by varying adjacent joint angles [60].

A second set of constraints helped us to gain confidence in individual muscle moments. We used experimentally measured muscle-fiber lengths, pennation angles, and physiologic cross

sectional areas. Thus, only one parameter, tendon slack length, was varied to match simulated and experimental joint moments. For many muscles there is a very small range of tendon lengths that yields reasonable results (i.e., active force in a reasonable range of motion and not too much passive force). Thus, we are fairly confident in the muscle-tendon parameters that determine the moments of individual muscles. Chapter 4 compares computed and experimental moments and further discusses our confidence in the muscle moment curves.

We do not account for muscle-tendon adaptation over time. It is well known that muscle and tendon adapt to the loads imposed upon them. Adaptation is one basic mechanism of strength development. Muscles are exercised against progressively larger resistances, and over time, the muscle cross section increases in response. Muscle and tendon also adapt to imposed stretch, or to being held in a shortened position over a period of time [142]. Numerous experimental studies have investigated the effects of immobilization and exercise on the properties of muscle (e.g., [125]) and tendon (e.g., [144]). However, no comprehensive mathematical model that relates the combined effects of imposed forces and lengths, activations, and musculoskeletal geometry on the time-changing properties of the muscle-tendon complex has been validated. Consequently, we do not include such relationships in our model. If a mathematical model of muscle-tendon adaptation over time did exist, it could be easily incorporated into the model presented here. Presently, muscle-tendon adaptation can only be studied by changing the muscle-tendon parameters (e.g., muscle fibers can be shortened 10% to study the effects of immobilizing a joint in a flexed position).

We use model of a nominal lower extremity. We use a nominal model of the lower extremity to study how surgical changes affect muscle function. Our nominal model represents a subject that is about 1.8 meters tall and has the strength of a young, adult male. We have modeled an “average” lower extremity because we want to understand the basic interactions among muscle, tendon, and bone that affect muscle function before we study how these fundamental relationships vary among individuals. Understanding which parameters have the greatest potential to affect muscle function will help to define future, patient-specific models. Also, through sensitivity tests, the nominal model can be used to identify which parameters of a surgical procedure have the greatest potential to affect the surgical outcome (see Chapters 5 and 6).

There are several other assumptions associated with the using a nominal model to simulate surgeries. These are discussed in Sections 4.8, 5.4, and 6.5. The next chapter describes the musculoskeletal modeling software.

3 *Musculoskeletal Modeling Software*

As part of the surgery simulation project, we have created a computer graphics system that enables users to quickly develop, alter, and evaluate models of a wide variety of musculoskeletal structures. A model is specified by defining the surfaces of the bones, the geometry and force-generating properties of the muscles, and the kinematics of the joints. Once a model is defined, the isometric force and resulting joint moments that each muscle develops can be computed. The software has been implemented on a computer graphics workstation so that the user can efficiently view and interact with a model. This not only makes the development of a model very efficient, but enables the user to alter a model and instantly analyze the effects. Also, since the software can be used to develop and analyze models of many different musculoskeletal structures, it can enhance the productivity of biomechanics researchers working in diverse areas. This chapter describes the musculoskeletal modeling software and gives detailed examples of how to define models using this system.

3.1 Introduction

In designing the software we established four goals. Specifically, the software should:

- (1) be *general* enough so that many different musculoskeletal structures can be modeled,
- (2) provide *realistic* models of muscle and tendon, and allow accurate specification of joint kinematics,
- (3) provide an *interactive*, graphics-based environment so the model can be visualized, altered, and analyzed efficiently,
- (4) be *extensible* so that new features, such as a more complex muscle model or a bone cutting tool, can easily be added to the software system.

The software was developed using the C language on a Silicon Graphics IRIS 2400T, and has recently been ported to a Personal IRIS 4D/25. A window manager provides a multi-window environment. The program allows the user to load one or more musculoskeletal models by reading sets of input files. Once loaded, a model can be acted upon by a number of tools (Figure 3.1). Each tool is contained within its own window and has a distinct function, such as controlling the viewing of the models, altering the muscles, or making plots for analysis.

A musculoskeletal structure is specified with three types of input files. The “bone” files contain lists of the polygons that represent the bone surfaces. The “joint” file specifies the kine-

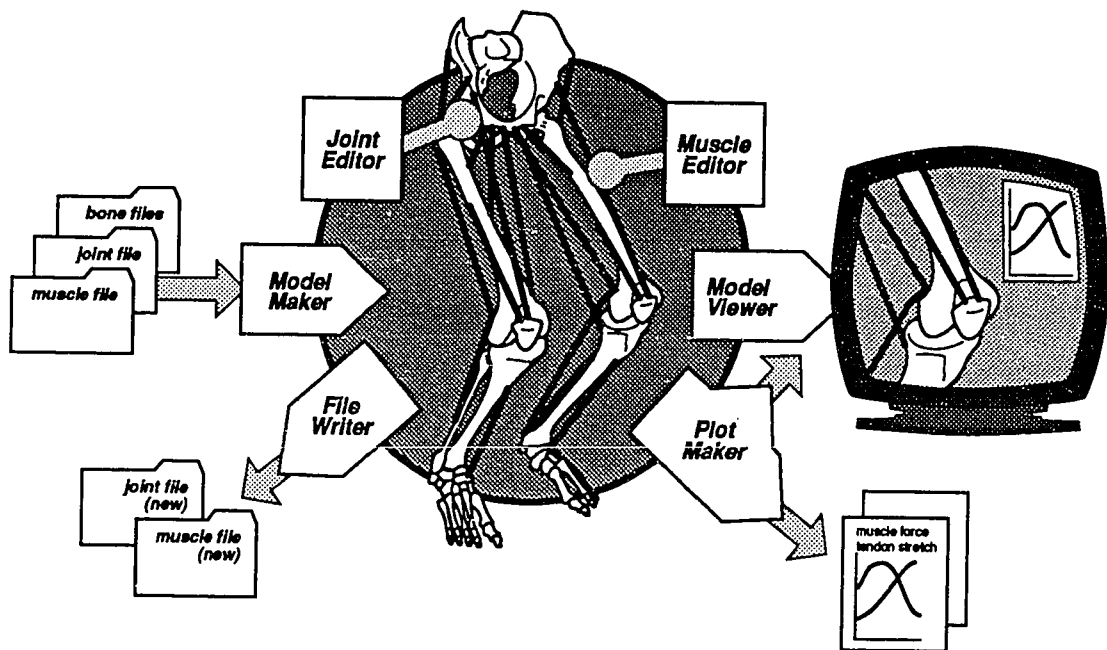


Figure 3.1. Structure of musculoskeletal modeling software. Input files describing the bone surfaces (bone files), joint kinematics (joint file), and muscle properties (muscle file) are read in to make a musculoskeletal model. A model can be altered using the joint editor, muscle editor, and model viewer. Information is extracted from the model by making plots or by exporting edited joint and muscle files.

matics of each joint. Finally, the “muscle” file contains a list of coordinates that describe the line of action of each muscle, and the parameters (described below) needed to compute isometric muscle force. The model maker (Figure 3.1) scans these input files and creates a data structure that represents the musculoskeletal model. The joint and muscle files are passed through a pre-processor so that C-style comments (demarcated with `/* */`) can be used within the files.

3.2 Defining a Musculoskeletal Model

A musculoskeletal model consists of a set of rigid body segments that are connected by joints. Muscles span the joints and thus develop moment about the joints. To define a model of a musculoskeletal structure, one must create the input files that define the body segments, joints, and muscles. I will use examples from our lower-extremity model to demonstrate how one defines a musculoskeletal model. Comprehensive examples of the muscle, joint, and bone files that describe the lower-extremity model are given in the appendices.

3.2.1 Defining the Body Segments

A body segment consists of one or more bones. In the joint file, the bones that make up each body segment are specified as shown in the following example.

```
/* EXAMPLE BODY SEGMENT */
beginsegment TIBIA
name: right_shank
files: 2
filenames: r_tibia.dat
           r_fibula.dat
endsegment
```

The files listed in the definitions of the body segments (e.g., `r_tibia.dat`) define polyhedra that describe the bone surfaces (see Appendix C for format of bone files). These bone surface data can be derived from CT or MR images, or digitizing bone surfaces. The vertices in each polyhedron are expressed in a Cartesian coordinate system that serves as the reference frame for the body segment (Figure 4.2 shows the reference frames for the lower-limb model). These reference frames are used to specify the position and orientation of one body segment with respect to another by defining joints, as described below.

3.2.2 Defining the System Kinematics

The body segments can be connected in any arrangement by defining joints. A joint specifies the transformations that relate the position and orientation of one body segment to another. The transformations consist of three orthogonal translations and three rotations around user-defined axes, and are performed in a user-defined order. Each translation and rotation is either a constant (i.e., independent of body position) or a function of a generalized coordinate. A generalized coordinate defines a degree-of-freedom in the musculoskeletal model (e.g., a joint angle). The functions that relate the translations and rotations to the generalized coordinates are called kinematic functions.

The joint file defines the joints, generalized coordinates, and the kinematic functions used in the joint definitions. Selected examples from the lower-extremity model illustrate the format for defining a joint, generalized coordinate, and kinematic function. For example, the femoral-tibial joint definition shown below specifies the transformations from the FEMUR segment to the TIBIA segment. The order of the transformations indicates that to move from the FEMUR reference frame to the TIBIA reference frame, a translation is performed first, followed by rotations around `axis1`, `axis2`, and `axis3`, respectively. The rotation axes are defined relative to the FEMUR reference frame, and can be changed by adjusting the axis definitions. The translation is broken into three orthogonal components (`tx`, `ty`, `tz`), where the `x`, `y`, and `z` directions are defined by the axes of the FEMUR reference frame. In this example, all the translations and rotations are either constants or functions of a single generalized coordinate (`knee_angle`); thus, there is

one degree-of-freedom in this joint definition. This joint is not a simple revolute because two of the translations (t_x, t_y) are functions (f_1, f_2) of `knee_angle`.

```

/* FEMORAL-TIBIAL JOINT DEFINITION */
beginjoint (FEMUR,TIBIA)      /* joint from FEMUR frame to TIBIA frame */
name knee
order t r1 r2 r3             /* translate, then rotate about axis1,
                             axis2, and axis3 */

axis1 0.0 0.0 1.0
axis2 1.0 0.0 0.0           /* rotation axis definitions */
axis3 0.0 1.0 0.0

tx function f1(knee_angle)   /* the kinematic function (f1) specifies */
ty function f2(knee_angle)   /* the relation between the generalized */
tz constant 0.0              /* coordinate (knee_angle) and tx, the */
r1 function f3(knee_angle)   /* translation in the x direction.*/
r2 constant 0.0
r3 constant 0.0
endjoint

```

Kinematic functions define translations and rotations as functions of the generalized coordinates. These functions can be derived from biomechanical investigations of joint motion. For example, Yamaguchi and Zajac have determined the anterior-posterior translation (t_x) between the femur and the tibia as a function of knee angle [146]. This functional relationship is specified by the kinematic function, f_1 , shown below. The (`knee_angle`, t_x) pairs are interpolated by a natural cubic spline using an algorithm by Forsythe and Malcolm [42]. Thus, the value of t_x can be determined by evaluating the cubic spline at any `knee_angle` (see Figure 3.5, below).

```

/* EXAMPLE KINEMATIC FUNCTION */
beginfunction f1             /* defines x-translation from femur to tibia */
/* knee_angle (degrees), tx (meters) */
(-120.0,-0.003)
(-100.0, 0.001)
(-80.0, 0.004)
(-60.0, 0.004)
(-40.0, 0.002)
(-20.0,-0.001)
(-10.0,-0.003)
( 0.0,-0.005)
endfunction

```

Each generalized coordinate must be defined in the joint file. The generalized coordinate, `knee_angle`, from the femoral-tibial joint definition, is defined below. Two ranges of motion are defined (in degrees), each of which can serve as the independent variable when making plots. Also included are the two keys that can be used to change the value of the generalized coordinate and thereby animate the model on the workstation display.

```

/* EXAMPLE GENERALIZED COORDINATE */
begincoord knee_angle
range 0.0 -90.0 knee_flexion
range 0.0 20.0 knee_hyperextension
keys k LEFTMOUSE           /* press these keys to flex the knee */
endcoord

```

3.2.3 Modeling the Muscles

A muscle, or “muscle-tendon actuator,” is defined by specifying its geometry and force-generating properties. The geometry of a muscle-tendon actuator is defined by a series of points that are connected by line segments. Each point is fixed to one of the body segments, and is expressed in that segment’s reference frame. A minimum of two points, origin and insertion, is required to define the muscle path. In cases where a muscle wraps over bone or is constrained by retinacula, intermediate “via” points can be introduced to further constrain the muscle path. By specifying a restricted range of joint angle over which these via points constrain the path, the number of line segments in the muscle path can change with joint motion. For example, a via point near the surface of a bone can be used to constrain a muscle path only in the range of joint angle where the path would otherwise pass through the bone.

The isometric force-generating properties of a specific muscle-tendon actuator are derived by scaling a generic, Hill-based model. The generic model [150], accounts for the static properties of both muscle [48] and tendon [144] (Figure 3.2).

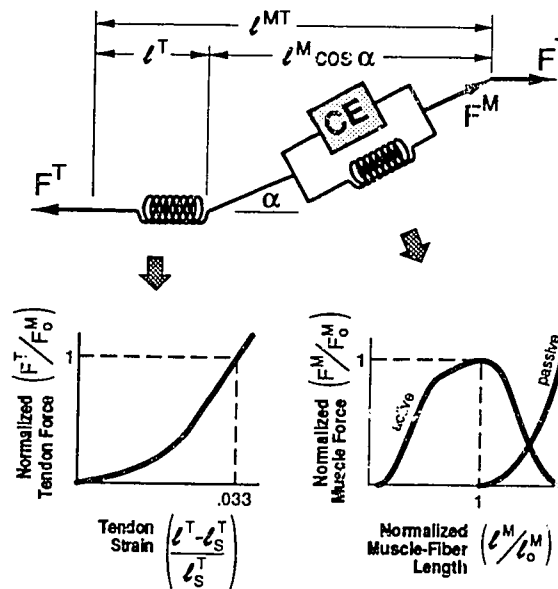


Figure 3.2. Muscle-tendon actuator model. The isometric properties of muscle are represented by an active contractile element (CE) in parallel with a passive elastic element. Isometric muscle force is assumed to be the sum of muscle force when it is inactive (passive) and when it is excited (active). The muscle is in series with tendon, which is represented by a non-linear elastic element. The forces in muscle (F^M) and tendon (F^T) are normalized by peak isometric muscle force (F_0^M). Tendon length (l^T) and muscle-fiber length (l^M) are normalized by optimal muscle-fiber length (l_0^M). Note that: $l^{MT} = l^T + l^M \cos \alpha$, and $F^T = F^M \cos \alpha$ where l^{MT} is the muscle-tendon length and α is the pennation angle. l_s^T is the tendon slack length. For a given muscle-tendon length and activation level the model determines muscle and tendon forces. From Delp et al. [30].

To scale the generic model to represent a specific actuator, the user must supply four parameters and three curves. The four parameters are: peak isometric muscle force (F_o^M), optimal muscle-fiber length (l_o^M), pennation angle (α), and tendon slack length (l_s^T) [150]. The process for determining these parameters is described in Section 4.3. The three curves are the normalized active and passive force-length relations of muscle, as well as the normalized force-length relation of tendon (Figure 3.2). These curves are defined by listing control points that are interpolated by natural cubic splines [42]. For example, the points defining the normalized tendon force-length relation are shown below. For a given tendon length (l^T), the tendon strain $((l^T - l_s^T) / l_s^T)$ is used to interpolate this function, yielding the normalized force value. This normalized force, multiplied by peak isometric muscle force (F_o^M), equals the force in the tendon.

```

beginendonforcelengthcurve
/* (tendon strain, normalized force) */
(0.0000,0.000)
(0.0013,0.011)
(0.0043,0.043)
(0.0088,0.123)
(0.0123,0.227)
(0.0333,1.000)
(0.0920,3.450)
endtendonforcelengthcurve

```

The muscle file (Appendix A) contains definitions of the muscles, as described above. A “default” muscle can be defined that describes the relationships that are usually identical for every muscle (e.g., the normalized force-length curves). If a particular muscle definition does not contain a certain parameter or curve, the parameter or curve is inherited from the default muscle. This greatly reduces the amount of information that must be specified in each muscle definition.

A sample lower-limb muscle, rectus femoris, is defined below. The path of this muscle is defined by three points, one in each of the PELVIS, FEMUR, and PATELLA reference frames. The point in the FEMUR frame is included in the muscle path only when the knee angle is between -120 and -80 degrees. This is done so that the muscle path wraps over the femur when the knee is flexed beyond -80 degrees. The muscle is a member of two groups (hip_flexion knee_extension), which means that the muscle name will appear in those two muscle-group menus on the workstation display. The muscle definition also lists the values for the four muscle-tendon parameters (F_o^M , l_o^M , l_s^T , α). Since the curves that specify the force-length relations of the muscle and tendon are not given in this sample muscle definition, they would be inherited from the default muscle.

```

/* EXAMPLE MUSCLE */
beginmuscleRectusFemoris
beginpoints
-0.029 -0.031 0.096 segment PELVIS
0.033 -0.403 0.001 segment FEMUR range knee_angle (-120,-80)
0.012 0.043 -0.001 segment PATELLA
endpoints

```

```

beginngroups hip_flexion knee_extension endgroups
/* The four muscle-tendon parameters are: */
force_max      780.0 /* Newtons */
optimal_fiber_length 0.0840 /* meters */
tendon_slack_length 0.3460 /* meters */
pennation_angle 5.0 /* degrees */
endmuscle

```

3.2.4 Computing Moment Arm, Muscle-tendon Length and Force

For every joint that a muscle spans, the muscle has a **moment arm** for each generalized coordinate used in the joint definitions. For example, since the RectusFemoris muscle, defined above, spans both the knee and hip, it has a moment arm for the knee angle and for each generalized coordinate (degree-of-freedom) at the hip. We calculate moment arms using the “partial velocity” method, which is defined by equations (1) - (4), below. These equations determine the moment arm of a muscle for a generalized coordinate, q_i , as follows (see Figure 3.3).

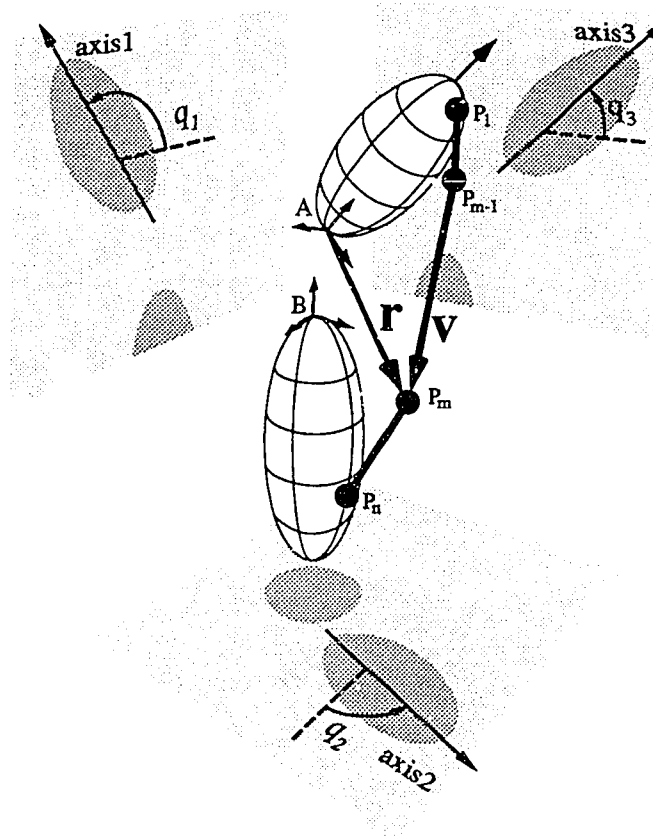


Figure 3.3. Definition of terms used in moment arm calculations. Points P_1 through P_n define the muscle path. P_1 through P_{m-1} are fixed in body A. P_m through P_n are fixed in body B. V is the vector from point P_{m-1} to P_m . F expresses point P_m in reference frame A. In general, six generalized coordinates (three rotation angles: q_1 , q_2 , q_3 , and three translation coordinates, not shown) are needed to characterize the orientation and position of body A relative to body B. The moment arm for each generalized coordinate is given by equation (4).

First, let \mathbf{u} , the translational component of the partial velocity, be defined as:

$$\mathbf{u} = \left(\frac{\partial t_x}{\partial q_i} \right) \mathbf{x} + \left(\frac{\partial t_y}{\partial q_i} \right) \mathbf{y} + \left(\frac{\partial t_z}{\partial q_i} \right) \mathbf{z} \quad (1)$$

where t_x , t_y , and t_z are the constants or kinematic functions that define the translation between the two reference frames. Next, let $\boldsymbol{\omega}$, the angular component of the partial velocity, be defined as:

$$\boldsymbol{\omega} = \left(\frac{\partial r_1}{\partial q_i} \right) \boldsymbol{\lambda}_1 + \left(\frac{\partial r_2}{\partial q_i} \right) \boldsymbol{\lambda}_2 + \left(\frac{\partial r_3}{\partial q_i} \right) \boldsymbol{\lambda}_3 \quad (2)$$

where r_1 , r_2 , and r_3 are the constants or kinematic functions that define the rotations about $\boldsymbol{\lambda}_1$ (axis1), $\boldsymbol{\lambda}_2$ (axis2), and $\boldsymbol{\lambda}_3$ (axis3), respectively. Then, ${}^A\mathbf{P}\mathbf{V}^{P_m}$, the partial velocity of the muscle point P_m in reference frame A, is:

$${}^A\mathbf{P}\mathbf{V}^{P_m} = \boldsymbol{\omega} \times \mathbf{r} + \mathbf{u} \quad (3)$$

where \mathbf{r} is P_m in reference frame A (Figure 3.3). Finally, the moment arm (ma) of the muscle for the generalized coordinate q_i is given by:

$$\text{ma} = {}^A\mathbf{P}\mathbf{V}^{P_m} \cdot \mathbf{V} \quad (4)$$

where \mathbf{V} is the vector along the muscle line of action (Figure 3.3). When the muscle line of action spans more than one joint (i.e., biarticular muscles) moment arms are computed by summing the partial velocity terms for each joint spanned. That is, equation (3) is used to determine the component of the partial velocity at each joint. These components are then summed to determine ${}^A\mathbf{P}\mathbf{V}^{P_m}$ which is used in equation (4).

This method is equivalent to computing moment arms with a vector cross product [62] for ball-and-socket and revolute joints. For planar joints that include kinematic constraints (e.g., the femoral-tibial joint defined above), this method gives the moment arm of a muscle about the instant center of rotation as determined from the joint kinematics. In the general case, the partial velocity method calculates a moment arm (ma) equal to the change in muscle-tendon length ($\partial \ell^{MT}$) with respect to a change in the generalized coordinate (∂q_i). That is, (4) is equivalent to

$$\text{ma} = \left(\frac{\partial \ell^{MT}}{\partial q_i} \right). \quad (5)$$

The advantage of the partial velocity method is that it provides a consistent technique to compute moment arms for all types of joints.

Muscle-tendon length is calculated as the sum of the lengths of the line segments that connect the points defining the muscle path. That is, if a muscle path is defined by points P_1 through

P_n , then muscle-tendon length (l^{MT}) is determined by first transforming the muscle points to a common reference frame and then computing

$$l^{MT} = \sum_{0 < i < n} |P_{i+1} - P_i| \quad (6)$$

To calculate the force in a muscle-tendon actuator, the following iterative algorithm was developed. Once the muscle-tendon length is computed, an initial guess of the muscle and tendon lengths is made. The force in the muscle is found by summing active force and passive force, each of which is calculated by using the length guess to interpolate the appropriate force-length curve. Similarly, the force in the tendon is found by using its length to interpolate the force-length curve of the tendon. In static equilibrium, the force in tendon (F^T) and muscle (F^M) are related by

$$F^T = F^M (\cos \alpha) \quad (7)$$

where α is the pennation angle (Figure 3.2) [150]. If the computed muscle and tendon forces indeed satisfy (7), then the muscle and tendon forces have been found. Otherwise, the muscle and tendon lengths are adjusted based on the slopes of their force-length curves at their respective lengths, and the process is repeated. This algorithm converges on a solution within about four iterations.

3.3 Interacting with a Model

An effective user interface is helpful both to develop and analyze musculoskeletal models. Four software tools: “model viewer, joint editor, muscle editor, and plot maker,” help the user to modify and study a model.

The **model viewer** allows the user to rotate, scale, and translate the model into any viewing perspective (Figure 3.4). The joints can also be manipulated by varying the values of the generalized coordinates by holding down the appropriate keys. The keys that control each generalized coordinate are specified in the generalized coordinate definitions. At any time, the model can be viewed as a shaded image or a wireframe object.

The **joint editor** enables the user to graphically manipulate the kinematics of any joint. Once a joint is selected, the three rotations and three translations that comprise the joint are displayed. If the rotations and translations are constants, they can be changed by typing in a new value. If they are functions of the generalized coordinates, they can be changed by moving, adding, or deleting control points of the splines that define the kinematic functions. For example, the user may choose to alter the kinematic functions that define the relative motion of the femur and tibia (Figure 3.5). The resulting motion can then be observed by flexing and extending the

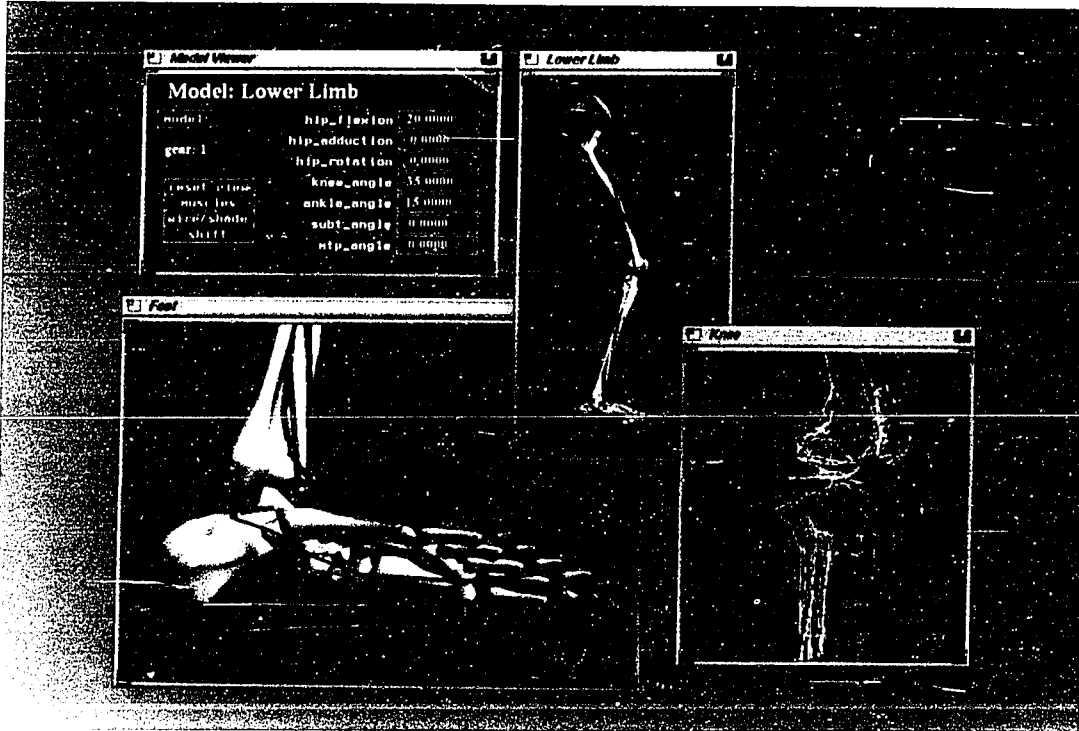


Figure 3.4. Display highlighting the model viewer. Each of the musculoskeletal models (Foot, Lower Limb, Knee) can be transformed into any viewing perspective. The joints in each model can be manipulated with the mouse or by typing in values of the generalized coordinates in the "model viewer" window (upper left).

knee. Graphical manipulation of joint kinematics is an efficient way to refine the model parameters to match experimental data and to alter the joint motion according to surgical procedures or various pathologies.

The **muscle editor** gives access to every parameter that describes a muscle. The muscle paths can be altered by first selecting a muscle from a screen menu and then choosing one or more of the points that define its path. The chosen muscle points can then be moved in the X, Y, and Z directions. An algorithm assists the user in attaching a muscle point to the bone by first finding the surface polygon closest to the muscle point and then moving the point toward that polygon.

At any time, a muscle point can be added or deleted, or the muscle can be restored to its original path. Graphical manipulation of the muscle-tendon paths provides an efficient way to define muscle paths when developing a model, and to alter muscle paths to simulate tendon transfer surgeries. In addition, each of the muscle-tendon parameters (F_o^M , ℓ_o^M , ℓ_s^T , α) and muscle activation can be changed by typing in a new value.

The **plot maker** utility allows the user to plot various computed properties of a muscle-tendon actuator. For example, the user may plot the effect of changing an actuator's tendon slack

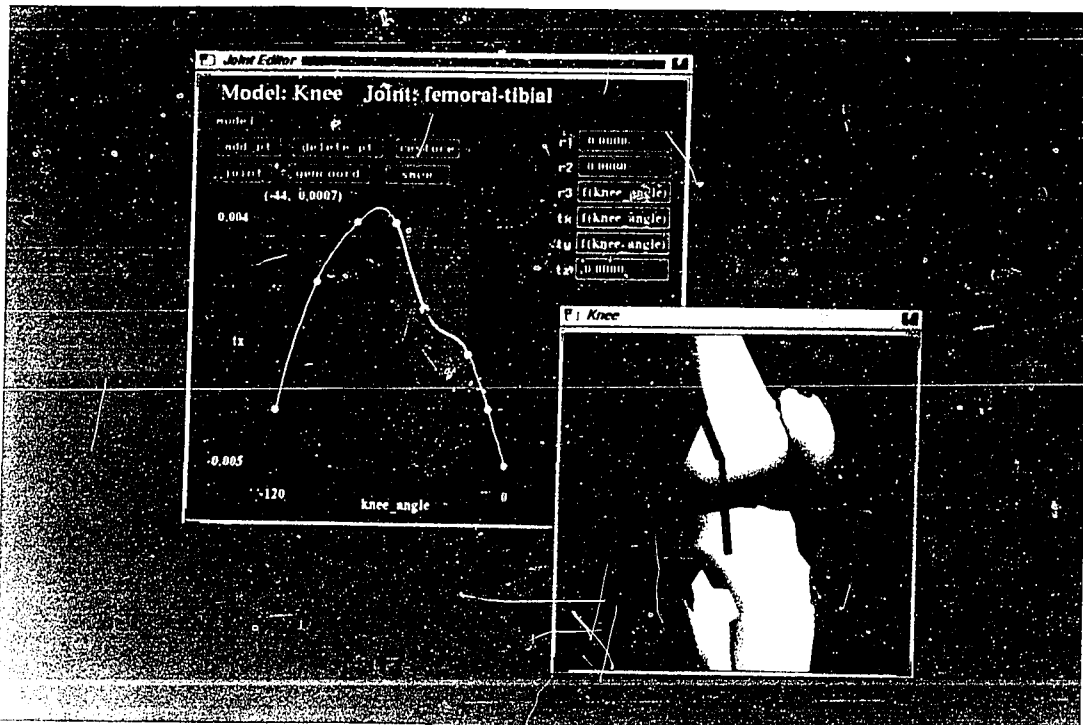


Figure 3.5. Display highlighting the joint editor. In the joint editor window (left) the user can alter the rotations ($r1$, $r2$, $r3$) and translations (tx , ty , tz) that comprise the joint. In this example, the tibial-femoral joint is being altered. The spline that defines the x -translation (tx) of the tibia as a function of the knee angle is being changed by moving the spline's control points with the mouse. Other translations and rotations that are functions of the knee angle ($r3$, ty) can be similarly altered. Constants ($r1$, $r2$, tz) can be changed by typing in new values. The effects of any change are immediately displayed in the view of the knee model (right window).

length (ℓ_s^T) or muscle-fiber length (ℓ_o^M) on isometric muscle force. To specify a plot, the user first chooses one of the six properties (muscle-tendon length, muscle-fiber length, tendon stretch, tendon force, moment arm, and joint moment) as the dependent variable, and then selects an independent variable (a generalized coordinate). Next, the user selects a muscle, or set of muscles, from menus that group them according to their functions. Figure 3.6 shows the menus used to specify the plots along with an example of the graphical output (soleus force versus ankle angle for two values of ℓ_s^T and ℓ_o^M).

In addition to these four tools, several file saving features have been implemented to enable the user to save musculoskeletal models and analyses of them. Joint and muscle files can be saved containing the same information as in the joint and muscle input files. Plots can be saved in Postscript files for printing or editing by other applications.

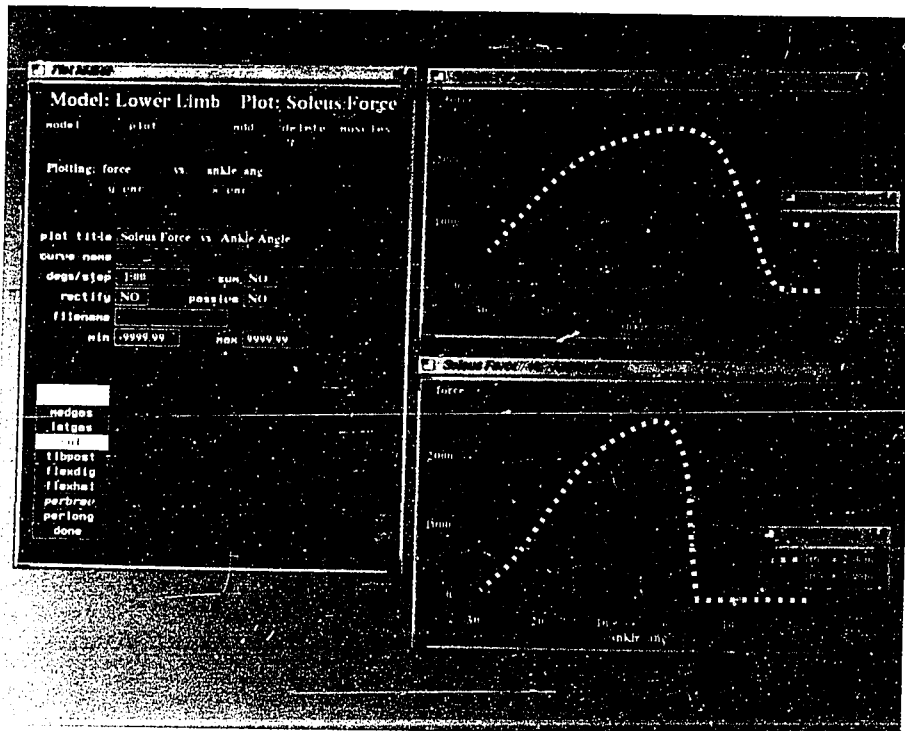


Figure 3.6. Display highlighting the plotmaker utility. The menus in the tool window (left) allow the user to specify the plotting parameters. The plots on the right show soleus active force versus ankle angle for two values of tendon slack length (l_s^T) (upper plot) and optimal muscle-fiber length (l_o^M) (lower plot). Negative ankle angles indicate plantarflexion; positive angles indicate dorsiflexion. Note that the angle of peak soleus force changes by 15° for a 1cm change in l_s^T (upper plot). Decreasing l_o^M not only changes the angle of peak force, but also decreases the range of ankle angles over which soleus develops active force (lower plot).

3.4 Software Design Goals

As stated in the introduction of this chapter, the software was designed to be *general*, *accurate*, *interactive*, and *extensible*. *Generality* was achieved by making the code completely independent of the particular system to be modeled. For example, all of the menus that contain muscle, joint, or body segment names are formed after the input files have been loaded, so they are not specific to any particular musculoskeletal structure. Also, the software can handle any number of muscles and body segments that are connected in arbitrary ways. Thus, the hindlimb of a cat or the upper limb of a human can be modeled in as straightforward a manner as a human leg.

It is important to discuss the limitations in the *accuracy* of models developed using our software. In the past, biomechanists have represented muscle-tendon paths as single lines from origin to insertion [13, 56, 57]. In our system, each muscle-tendon path can be described by a series of line segments. This is accurate for muscles with small areas of origin and insertion (e.g., tibialis posterior). However, muscles with large areas of attachment would be more realistically

modeled by defining them as volumes. As a compromise, muscles with large attachment areas (e.g., gluteus medius) can easily be split into several compartments (e.g., anterior, middle, and posterior). Our method of computing muscle-tendon force is based on a generic model of muscle and tendon [150] that can be scaled to represent a wide range of muscle architectures. However, our implementation of the model described by Zajac [150] characterizes only the isometric properties of muscle. To calculate muscle forces during movements, our muscle-tendon model must be enhanced to include force-velocity effects and other dynamic properties. The joint modeling technique allows any conceivable kinematic joint to be modeled. The only limitation is that the kinematic functions used to define joint motion cannot involve polynomials higher than third order (cubic splines). Joint models that move according to the forces in muscles, ligaments, and other surrounding tissues may provide a more realistic means to represent joint motion.

A set of window-oriented tools allows the user to *interact* with musculoskeletal models by changing any parameter of a model without leaving the program. Once created, a musculoskeletal model can be viewed, manipulated, and analyzed using screen menus, the mouse, and user-defined keys. The graphics display enhances the user's ability to extract information from the models.

We have developed a basic set of software tools for simulating the biomechanical consequences of surgical procedures. Additional capabilities could enhance the existing surgery simulations. For example, to simulate osteotomies, it might be desirable to implement a bone-cutting tool. This would allow the user to orient a cutting plane in order to cut and reposition sections of bone.

To achieve *extensibility* in the software we have implemented the editing and analysis tools as a set of distinct, modular components. Thus, little of the existing code would need to be changed to extend the capabilities of the program. Rather, to add a new tool to the program, three subroutines must be created to handle: (i) drawing the tool window, (ii) updating data structures, and (iii) processing keyboard and mouse input. These three subroutines must be registered with the event handler, which processes all input by calling the appropriate subroutines. A single window is associated with each tool, allowing for a clean segregation of input events. Also, each tool has its own private data structure and can change the public data structures of the models and plots, but not the structures of the other tools.

To maximize portability, the software will be converted to "X-windows" (an emerging graphics standard) using the "Motif" toolkit. This will reduce future conversion efforts and provide a more standard user interface. Other potential enhancements to the musculoskeletal modeling software are discussed in Chapter 7.

The next chapter describes the model of the human lower limb that we have developed using this software.

4 *Lower-Extremity Model*

Using the software described in Chapter 3, we have developed a model of the lower extremity. This model represents a subject that is about 1.8 meters tall and has the strength of a young, adult male. The model computes the maximum isometric force and joint moment that each muscle can develop at any body position. Using a computer-graphics workstation, the model can be altered according to various surgical procedures to study how surgical changes in musculoskeletal geometry (e.g., origin-to-insertion path) and muscle-tendon parameters (e.g., optimal muscle-fiber length and tendon slack length) affect the moment-generating capacity of the muscles.

This chapter first describes our lower-extremity model and compares the joint moments calculated with the model to experimentally measured joint moments. The sensitivity of muscle force to optimal muscle-fiber length and tendon slack length is analyzed and an example surgery simulation is presented. Finally, the limitations of the model are discussed.

4.1 Musculoskeletal Geometry

To acquire the bone surface data, we first marked the surfaces of bones with a mesh of polygons, and then determined the coordinates of the vertices with a three-dimensional digitizer (Polhemus Navigation Sciences, Colchester, Vermont). These coordinates were used to create files describing the surfaces of the pelvis and thigh bones. Data describing the shank and foot bones were provided by Stredney [124]. The format of these “bone files” is shown in Appendix C.

Based on the anatomical landmarks of these bone surface models, we defined the paths (i.e., the lines of action) of forty-three muscle-tendon actuators. Each muscle-tendon path is represented as a series of line segments. Origin and insertion are necessary landmarks and, in some cases, are sufficient for describing the muscle path (e.g., soleus is represented by a single line segment). In other cases, where the muscle wraps over bone or is constrained by retinacula, intermediate “via points” were introduced to represent the muscle path more accurately (e.g., peroneus longus is represented by a series of six line segments, see Figure 4.1). The number of muscle via points can depend on body position. For example, the quadriceps tendon wraps over the distal femur when the knee is flexed beyond some angle, but not when the knee is extended. Thus, additional via points, called “wrapping points,” are introduced for knee flexion angles greater than 80° so that the quadriceps tendon wraps over the bone, rather than passes through the bone, in that range of knee motion.

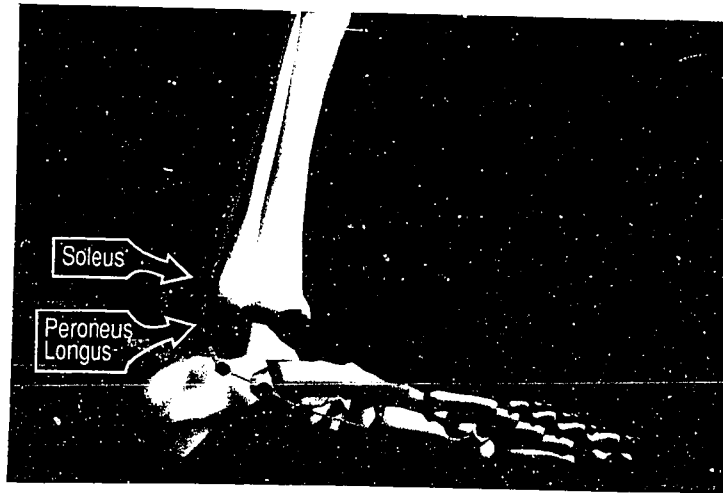


Figure 4.1. Three-dimensional representation of the musculo-tendinoskeletal geometry of the shank, foot, and toes. Some muscle-tendon actuators are represented as single line segments (e.g., soleus). Others are represented as a series of line segments (e.g., peroneus longus).

On the computer graphics system, we visually compared our muscle paths with paths defined by a commonly used set of muscle coordinates [13]. In the anatomical position, the paths are similar. However, interactively changing the skeletal configuration from the anatomical position revealed that several muscle paths (e.g., iliacus, psoas, sartorius, rectus femoris) reported by Brand *et al.* [13] passed through the bones or deeper muscles. This occurred because each muscle path reported by Brand *et al.* is defined by only two points that were measured on cadavers in the anatomical position. Displaying the muscle paths along with the bone surface models was helpful because it clearly showed where muscle via points and wrapping points were needed to properly constrain the muscle-tendon paths. We also compared moment arms calculated from our muscle paths with measurements we took from cadavers and from cross-sectional anatomy texts [38], as well as with moment arms reported in the literature (e.g., [32, 96, 146]). These comparisons showed that our muscle paths are anatomically accurate, and generate moment arms that are consistent with previous investigations over a wide range of joint motions. The coordinates that define all the muscle paths are listed in the “muscle file” contained in Appendix A.

Despite our effort to define accurate muscle paths, there are some muscles that pass through the bones or deeper muscles with extreme hip flexion and extension, and thus yield unrealistic moment arms. Specifically, GMAX3 (the most inferior component of gluteus maximus) passes through the ischial tuberosity beyond 60° of hip flexion. GMAX1 and GMAX2 (the superior and middle components of gluteus maximus) pass through deeper muscles beyond about 80° of flexion. Iliacus and psoas paths were also difficult to define. Both these muscles pass through the hip capsule beyond 5° of hip extension. It is difficult to introduce wrapping points to

constrain the paths of the hip muscles over specific ranges of motion because the intersections of the muscles with the bones, other muscles, and the joint capsule depend on all three hip angles (flexion, adduction, rotation). This problem could be solved by checking for intersections between the muscles and other tissues as the body position is changed. However, since checking for intersections is computationally intensive, this approach would decrease display speed considerably.

4.2 Joint Models

We modeled the lower extremity as seven rigid-body segments: (1) pelvis, (2) femur, (3) patella, (4) tibia/fibula, (5) talus, (6) foot (comprising the calcaneus, navicular, cuboid, cuneiforms, and metatarsals), and (7) toes (phalanges), with reference frames fixed in each segment (Figure 4.2). The relative motion of these segments is defined by models of the hip, knee, ankle, subtalar, and metatarsophalangeal joints. The "joint file" that specifies the kinematics of all the joints is contained in Appendix B.

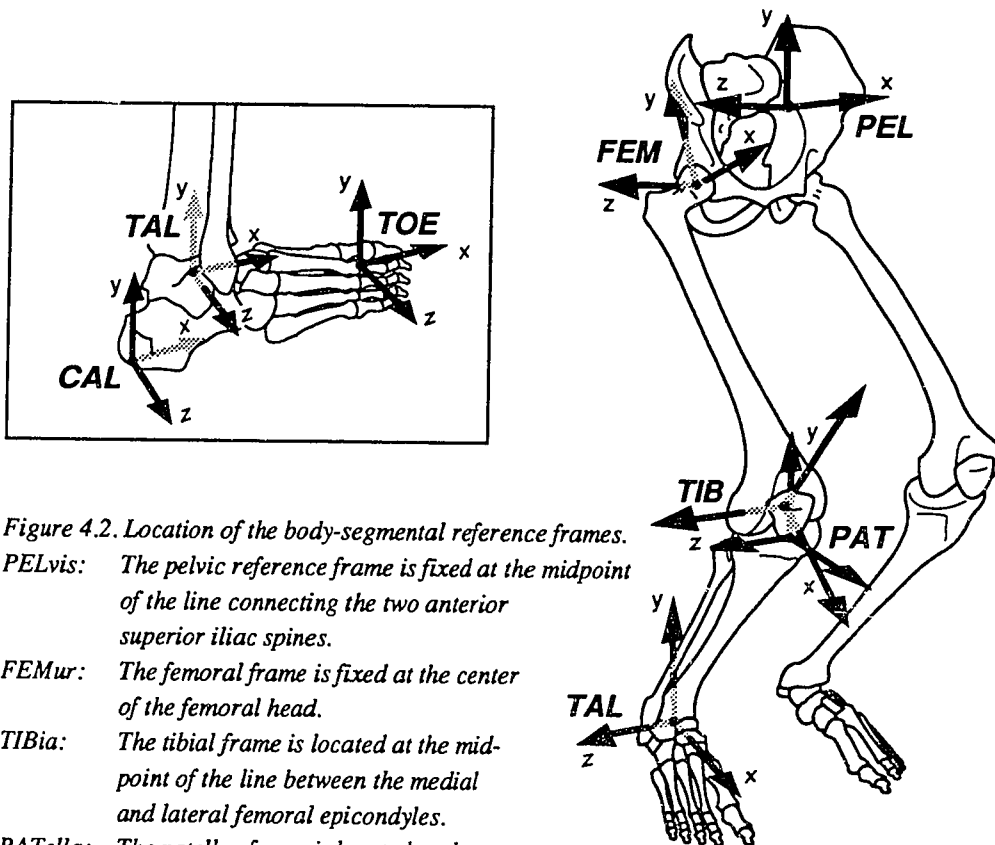


Figure 4.2. Location of the body-segmental reference frames.
PELvis: The pelvic reference frame is fixed at the midpoint of the line connecting the two anterior superior iliac spines.

FEMur: The femoral frame is fixed at the center of the femoral head.

TIBia: The tibial frame is located at the midpoint of the line between the medial and lateral femoral epicondyles.

PATella: The patellar frame is located at the most distal point of the patella.

TALus: The talar frame is located at the midpoint of the line between the apices of the medial and lateral maleoli.

CALcanus: The calcaneal frame is located at the most inferior, lateral point on the posterior surface of the calcaneus.

TOE: The toe frame is located at the base of the second metatarsal.

We characterized the hip as a ball-and-socket joint. The transformation between the pelvic and femoral reference frames is thus determined by successive rotations of the femoral frame about three orthogonal axes fixed in the femoral head.

We modified a planar model of the knee [146] to characterize the knee extensor mechanism. This single-degree-of-freedom model accounts for the kinematics of both the tibiofemoral joint and the patellofemoral joint in the sagittal plane as well as the patellar levering mechanism. We specified the transformations between the femoral, tibial, and patellar reference frames as functions of the knee angle. Tibiofemoral kinematics were determined as follows. The femoral condyles were represented as an ellipse; the tibial plateau was represented as a line segment (Figure 4.3). The transformation from the femoral reference frame to the tibial reference frame was then determined so that the femoral condyles remain in contact with the tibial plateau throughout the range of knee motion. The tibiofemoral contact point depends on the knee angle and was specified according to data reported by Nisell *et al.* [97]. Assuming that the length of the patellar ligament (ℓ_{pl} in Figure 4.3) is constant, the angle between the patellar ligament and the tibia (ϕ in Figure 4.3) determines the translation vector from the tibial reference frame to the patellar reference frame [133]. Rotation of the patella with respect to the tibia (β in Figure 4.3)

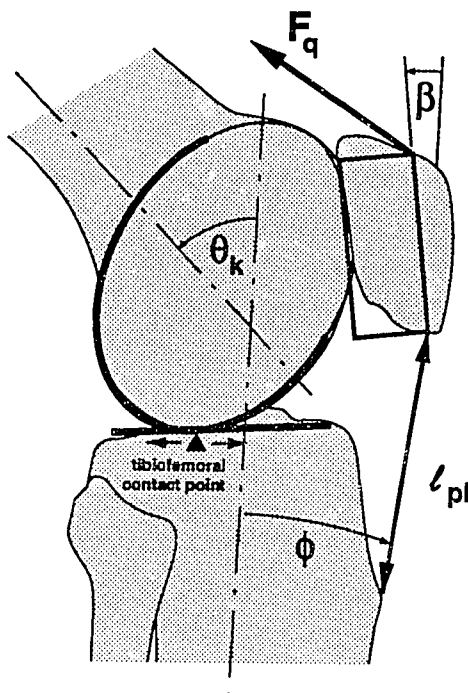
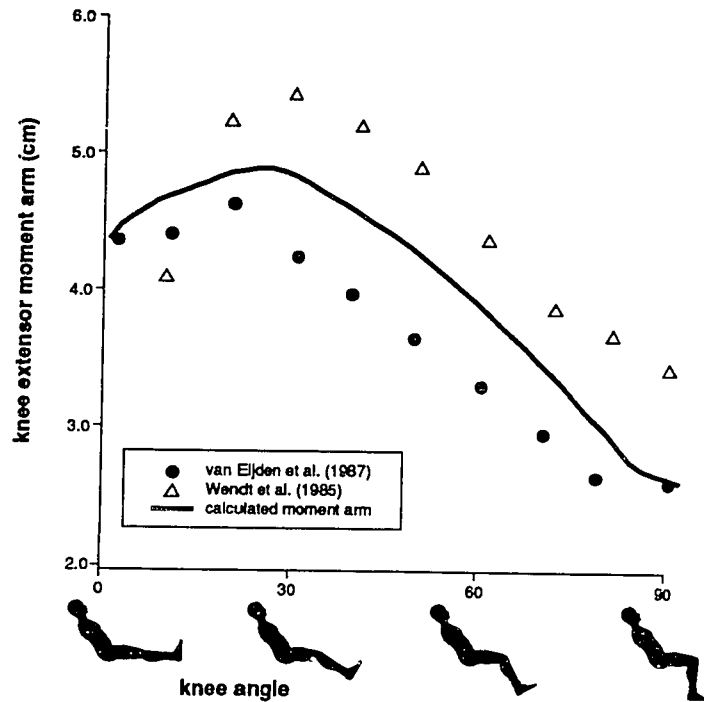


Figure 4.3. Geometry for determining knee moments and kinematics in the sagittal plane. θ_k is the knee angle; ϕ is the patellar ligament angle; β is the angle between the patella and the tibia; F_q is the quadriceps force; ℓ_{pl} is the length of the patellar ligament. From these kinematics, the moment of the quadriceps force about the instant center of knee rotation can be computed. Adapted from Delp *et al.* [30].

was specified according to experimental measurements of patellar rotation [133]. Moment arms calculated from these kinematics correspond closely to moment arms that have been measured experimentally (Figure 4.4).

Figure 4.4. Knee extensor moment arm vs. knee angle. The moment arm calculated for rectus femoris (solid line) corresponds closely with knee extensor moment arms measured by van Eijden et al. [134] and Wendt et al. [139]. Moment arms calculated for the vastus lateralis, vastus medialis, and vastus intermedius are slightly smaller (about 5mm) than the rectus femoris moment arm, but vary with knee angle in a similar way.



We modeled the ankle, subtalar, and metatarsophalangeal joints as frictionless revolute joints (Figure 4.5). Inman has described the location and orientation of axes for each of these joints [65]. When displayed, these axes produced realistic motion of the ankle and subtalar joints (i.e., the bone surface models did not collide or disarticulate), but unrealistic motion of the metatarsophalangeal joint (the phalanges separated from the metatarsals). We therefore rotated the metatarsophalangeal axis (-8° right-handed rotation about a vertical axis) to minimize disarticulation of that joint.

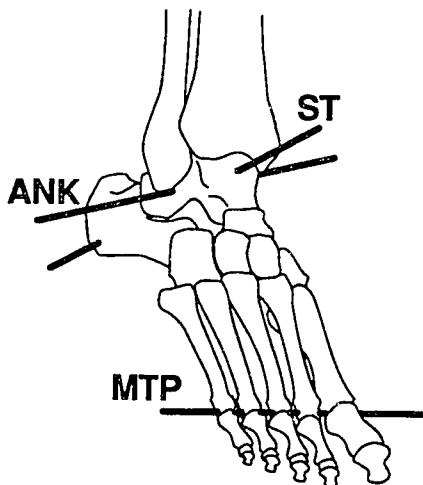


Figure 4.5. The ankle (ANK), subtalar (ST), and metatarsophalangeal (MTP) joints are modeled as revolute joints with axes oriented as shown. From Delp et al. [30].

4.3 Muscle-tendon Parameters

Section 3.2.3 describes a generic model of muscle and tendon that can be used to compute isometric muscle force as a function of muscle-tendon length. When this generic model is scaled by a muscle's peak isometric force (F_o^M), optimal muscle-fiber length (ℓ_o^M), pennation angle (α), and tendon slack length (ℓ_s^T), the force-length relation of a specific muscle-tendon actuator can be computed [62, 150].

Values for the muscle-tendon parameters were determined with a procedure similar to that used by Hoy *et al.* [62]. Values for muscle physiological cross-sectional area (PCSA), which determines F_o^M [122], were taken from the literature [43, 141]. Different factors were needed to scale the PCSA values reported by Friederich *et al.* [43] (25Ncm^{-2}) and Wickiewicz *et al.* [141] (61Ncm^{-2}) due to differences in their anatomical specimens. That is, we used the PCSA values from Friederich *et al.* [43] that were measured on a young cadaver, whereas the values from Wickiewicz *et al.* [141] were measured only on elderly cadavers. Thus, to scale the PCSA values that were measured on the elderly cadavers to match the moment curves measured on young subjects, we needed to use a factor (61Ncm^{-2}) that is larger than the "specific tension" reported by Spector *et al.* [122] (23Ncm^{-2}). Values for optimal fiber length (ℓ_o^M) and pennation angle (α) were taken from Wickiewicz *et al.* [141]. We scaled the fiber lengths reported by Wickiewicz *et al.* by a factor ($2.8/2.2$); this is the ratio of the optimal sarcomere length used in this study ($2.8\mu\text{m}$) to the optimal sarcomere length used by Wickiewicz *et al.* ($2.2\mu\text{m}$) [141]. We used $2.8\mu\text{m}$ as the optimal sarcomere length of human muscle because $2.8\mu\text{m}$ is the length at which a fiber develops peak force based on the sliding filament theory of muscle contraction [48], and human thick and thin filament lengths of $1.60\mu\text{m}$ and $2.55\mu\text{m}$, respectively [102]. For muscles not reported by Wickiewicz *et al.*, we used muscle-fiber lengths and pennation angles measured by Friederich *et al.* in the anatomical position [43].

Since no experimental data exist for tendon slack length (i.e., the length of tendon beyond which force develops when stretched), one application of our model was to estimate ℓ_s^T for each actuator. Tendon slack length includes both the length of free tendon and the length of tendon internal to the muscle belly (aponeurotic tendon). When muscle paths are specified, ℓ_s^T determines the joint angles where a muscle-tendon actuator develops force [62, 150]. We specified values for ℓ_s^T based on the following two criteria [62]. First, assuming that passive muscle contributes to the joint moment (called "passive moment") only when the muscle fibers are longer than ℓ_o^M , we selected ℓ_s^T so that each actuator was slightly longer than ℓ_o^M at joint angles corresponding to the onset of *in vivo* passive moment measured at the hip [148], knee [58, 85] and ankle [121]. We then compared total passive moment (i.e., the sum of the passive moments generated by all the muscles) that were calculated with the model to measured passive moments for a range of joint angles (e.g., Figure 4.6). Second, since ℓ_s^T determines the joint angles where an

Table 4.1 Muscle-tendon Parameters for 43 Lower-Limb Muscles*

muscle	peak muscle force (F_o^M) (N)	optimal fiber length (l_o^M) (cm)	pennation angle (α) (degrees)	tendon slack length** (l_s^T) (cm)	tendon length/fiber length** (l_s^T/l_o^M)
<i>hip muscles</i>					
gluteus medius1§	550	5.4	8	7.8	1.4
gluteus medius2§	380	8.4	0	5.3	0.6
gluteus medius3§	435	6.5	19	5.3	0.8
gluteus minimus1§	180	6.8	10	1.6	0.2
gluteus minimus2§	190	5.6	0	2.6	0.5
gluteus minimus3§	215	3.8	1	5.1	1.3
gluteus maximus1§	380	14.2	5	12.5	0.9
gluteus maximus2§	550	14.7	0	12.7	0.9
gluteus maximus3§	370	14.4	5	14.5	1.0
adductor magnus1§	345	8.7	5	6.0	0.7
adductor magnus2§	310	12.1	3	13.0	1.0
adductor magnus3§	445	13.1	5	26.0	2.0
adductor longus§	420	13.8	6	11.0	0.8
adductor brevis§	285	13.3	0	2.0	0.2
pectineus§	175	13.3	0	0.1	0.1
iliacus§	430	10.0	7	9.0	0.9
psoas§	370	10.4	8	13.0	1.3
quadratus femoris§	255	5.4	0	2.4	0.4
gemelli§	110	2.4	0	3.9	1.6
piriformis§	295	2.6	10	11.5	4.4
<i>hip and knee muscles</i>					
rectus femoris†	780	8.4	5	34.6	4.0
semimembranosus†	1030	8.0	15	35.9	4.5
semitendinosus†	330	20.1	5	26.2	1.3
biceps femoris(lh)†	720	10.9	0	34.1	3.1
gracilis†	110	35.2	3	14.0	0.4
sartorius†	105	57.9	0	4.0	0.1
tensor fasciae latae†	155	9.5	3	42.5	4.5
<i>knee muscles</i>					
vastus medialis†	1295	8.9	5	12.6	1.4
vastus intermedius†	1235	8.7	3	13.6	1.6
vastus lateralis†	1870	8.4	5	15.7	1.9
biceps femoris(sh)†	400	17.3	23	10.0	0.6
<i>knee and ankle muscles</i>					
medial gastrocnemius#	1115	4.5	17	40.8	9.0
lateral gastrocnemius#	490	6.4	8	38.5	6.0
<i>ankle muscles</i>					
soleus¶	2830	3.0	25	26.8	8.9
tibialis posterior†	1270	3.1	12	31.0	10.0
fl. digitorum longus†	310	3.4	7	40.0	11.8
fl. hallucis longus†	320	4.3	10	38.0	8.8
peroneus brevis†	350	5.0	5	16.1	3.2
peroneus longus†	755	4.9	10	34.5	7.0
tibialis anterior†	600	9.8	5	22.3	2.2
peroneus tertius§	90	7.9	13	10.0	1.3
ext. digitorum longus†	340	10.2	8	34.5	3.4
ext. hallucis longus†	110	11.1	6	30.5	2.6

* See Appendix A for muscle path coordinates

**Values generated in this study; see text for details.

§ Peak force derived from Brand et al. (1986); fiber length and pennation from Friederich and Brand (1990).

† Peak force, fiber length, and pennation angle derived from Wickiewicz et al. (1983).

Peak force derived from Brand et al. (1986); fiber length and pennation derived from Wickiewicz et al. (1983).

¶ Peak force derived from Wickiewicz et al. (1983) multiplied by 0.8; fiber length from Friederich and Brand (1990).

actuator develops peak joint moment, we adjusted ℓ_j^T so that the total moment about each joint peaked at a joint angle corresponding to *in vivo* joint moments measured during maximum voluntary contractions (e.g., Figure 4.7). Table 4.1 lists values for the muscle-tendon parameters.

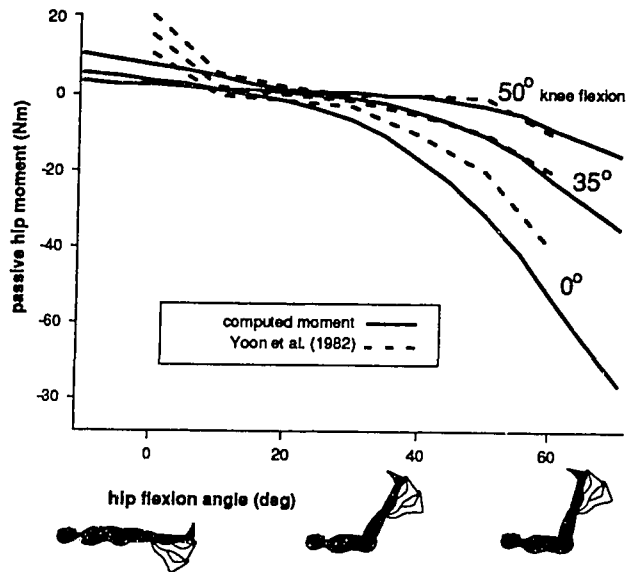


Figure 4.6. Passive hip moment vs. hip flexion angle with 50°, 35°, and 0° of knee flexion. Positive (negative) moments are flexion (extension) moments. Notice that both computed (solid lines) and experimental (dotted lines) hip extension moments increase as the knee is extended from 50° flexion to full extension (0°) because of hamstring stretch. Computed hip flexion moments are less than experimental moments because the model does not include ligament forces, which contribute to the experimental moment when the hip is in extension.

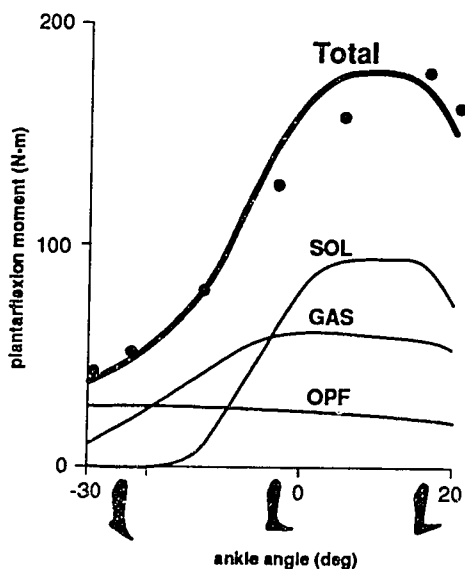


Figure 4.7. Comparison of computed and experimental plantarflexion moments. Computed moments of soleus (SOL), medial and lateral gastrocnemius (GAS), and the other plantarflexors (OPF) were summed to produce the total computed moment (thick-solid line). The total computed moment, with muscles fully activated, compared well with plantarflexion moments measured during maximum voluntary isometric contractions (large dots) [116]. From Delp et al. [30]

4.4 Model Output

By combining the musculoskeletal geometric data, joint models, and muscle-tendon models, we are able to compute the force and joint moment that each muscle can develop for any body position. For a given body position, we compute muscle-tendon length and moment arm with the

equations given in Section 3.2.4. Using the muscle-tendon models, we then compute the maximum (i.e., fully activated) isometric tendon force at the computed muscle-tendon length. The joint moment for each muscle is then computed as the product of the tendon force and the moment arm. This process is repeated for a range of joint motion to produce the joint moment vs. joint angle curve.

We summed the joint moments exerted by all muscles, and compared these total computed moments to joint moments measured during maximum voluntary isometric contractions (MVC). For example, Figure 4.7 compares the total plantarflexion moment computed with the model to the moment measured during maximum voluntary isometric contraction of the ankle plantarflexors [116]. Similar to Figure 4.7, we compared computed joint moments to moments measured at the hip [17, 66, 95, 96, 99, 137], knee [66, 75, 94, 119, 134], ankle [87, 116] and subtalar [130] joints. The next section shows these comparisons.

4.5 Computed Joint Moments Compared to Experimental Data

The figures in this section compare joint moments that have been measured during maximum voluntary contractions (MVC) of particular muscle groups (e.g., knee extensors) to calculated joint moments. Both the experiments and the model calculations assume isometric conditions. The calculated joint moments are the sum of the moments from all the muscles that contribute to the joint moment, assuming full muscular activation. At some joints, many muscles contribute to the total joint moment. For example, rectus femoris, iliacus, psoas, sartorius, and tensor fasciae latae all contribute to the total hip flexion moment. Since the contributions of each muscle to the total joint moment can be observed more easily on the computer-graphics system, we present here only the total joint moments. The problems associated with comparing calculated and measured joint moments are discussed in Section 2.6.

Passive muscle forces (i.e., the force developed in muscle when the fibers are stretched beyond optimal fiber length, see Figure 1.2) contribute significantly to the total joint moment for some ranges of joint motion, but not for others. In the figures below, two curves (“active + passive” and “active only”) are shown for the joint moments to which passive forces contribute significantly. For ranges of motion in which passive muscle forces do not contribute to the maximum isometric joint moment, only the active + passive curve is shown since it is the same as the active-only curve. It should be noted that the active-only curve is computed as the moment of active muscle force about the joint. It should also be noted that the contribution of passive muscle forces to joint moment during maximum voluntary contractions is less than during passive joint motion because of tendon stretch. Since muscle develops more force when it is activated, the stretch in tendon is greater. Thus, at a given body position (muscle-tendon length), the muscle fibers will be shorter (by the amount of tendon stretch) muscle is fully activated. Consequently, there is less force from fiber stretch.

4.5.1 Ankle Moments

Figures 4.8 and 4.9 compare computed plantarflexion moments to those measured by Sale *et al.* [116]. Computed and measured moments correspond very closely with the knee extended (Figure 4.8) and flexed (Figure 4.9). We found that the peak moment is greater with the knee extended because the gastrocnemius is longer and develops greater force when the knee is extended. In the model, when the knee is flexed 90° and the ankle is plantarflexed, the gastrocnemius fibers are too short to develop active force. We found that passive muscle force contributes nothing to the total moment when the muscles are fully activated over the range of ankle angles plotted in Figures 4.8 and 4.9. Thus, active and active+passive curves are the same for the ankle plantarflexors.

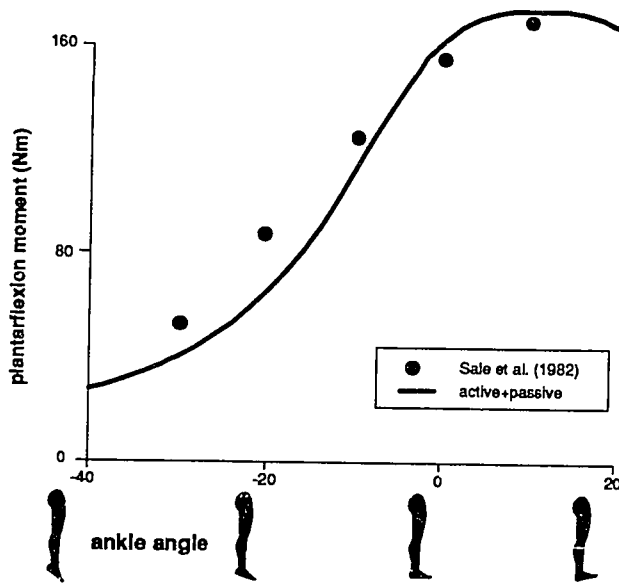


Figure 4.8. Plantarflexion moment vs. ankle angle with knee extended. Maximum isometric moments from soleus, gastrocnemius, tibialis posterior, flexor hallucis longus, and the peroneals were summed to produce the total (active+passive) computed moment.

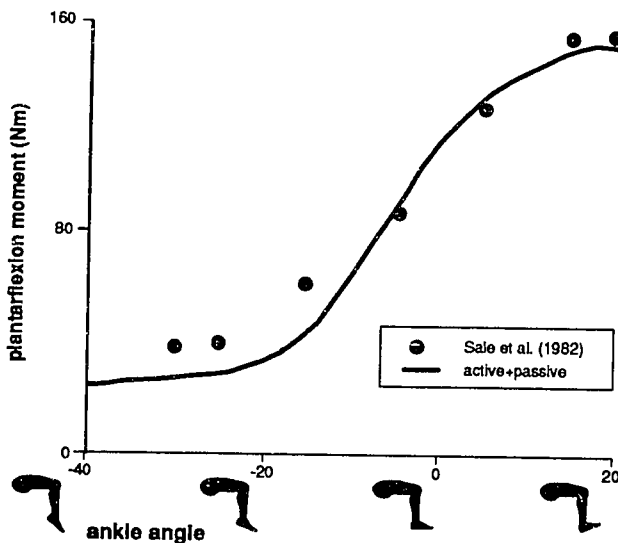


Figure 4.9. Plantarflexion moment vs. ankle angle with knee flexed 90°. Maximum isometric plantarflexion moments from soleus, gastrocnemius, tibialis posterior, and the peroneals were summed to produce the total (active+passive) computed moment.

Soleus and gastrocnemius, together, provide about 85% of the total plantarflexion moment at the ankle angle where the moment peaks. Also, these muscles account for most of the variation in the moment as the ankle is flexed. Since soleus and gastrocnemius have short fibers relative to their moment arms, the fibers change length (force) significantly as the ankle is moved. In contrast, tibialis posterior, flexor hallucis longus, and the peroneals have small moment arms, and therefore undergo a small change in length (force) as the ankle is flexed. These muscles play a significant role in contributing moment only near full plantarflexion because the fibers of gastrocnemius and soleus are almost fully shortened and develop very little force in that position.

We are fairly confident in our computed plantarflexion moments for three reasons. First, the experimental data of Sale *et al.* [116] is similar to moments measured by others [63]. Second, our computed moments match these data very closely. Third, since only the gastrocnemius crosses both the ankle and the knee, we can gain confidence in our estimates of gastrocnemius force by matching the ankle moment curves at various knee angles. Once we understand how gastrocnemius force changes with ankle and knee angles, we can adjust the tendon length of soleus until the total plantarflexion moment curves match. Since the other plantarflexors (tibialis posterior, flexor hallucis longus, and the peroneals) do not contribute much to the total moment because their moment arms are small, the effect of soleus on the total moment curve can be determined. Also, we found that the soleus force vs. ankle angle curve is extremely sensitive to changes in tendon length (see sensitivity study below). Thus, only small adjustments in soleus tendon length (1-2mm) were needed to match the experimental plantarflexion moments.

Figure 4.10 compares computed and experimental dorsiflexion moments. The peak moment calculated with the model (42 Nm) is similar to the peak moment measured by Marsh *et al.* (45 Nm) [87]. The joint angle where the moments peak are also similar. Tibialis anterior contributes over 50% of the total dorsiflexion moment over the entire range of ankle motion. Passive muscle forces contribute very little to the total moment.

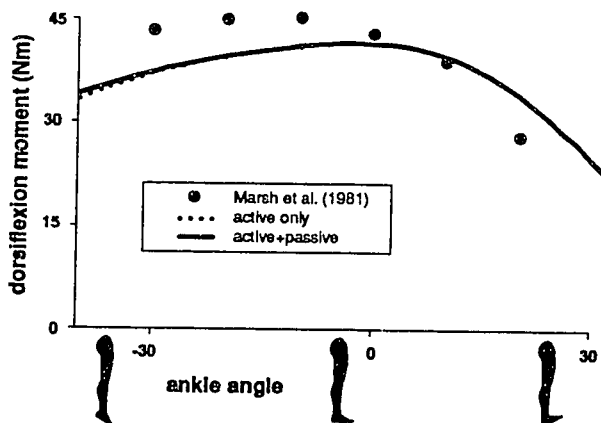


Figure 4.10. Dorsiflexion moment vs. ankle angle. Maximum isometric moments from tibialis anterior, peroneus tertius, extensor digitorum, and extensor hallucis longus were summed to produce the total computed moment (solid line).

4.5.2 Knee Moments

Knee Extension

Figure 4.11 compares computed knee extension moments to knee moments measured during maximum voluntary contraction of the quadriceps. The peak moment calculated with the model (215 Nm) is similar to the peak moment measured by Lindahl *et al.* [75] (230 Nm). However, the knee angles at which the computed and experimental moments peak are quite different.

The computed moment peaks near 30° of knee flexion, but the experimental moment peaks at about 60° of knee flexion. The computed moment peaks at 30° because the moment arm peaks near 30° and decreases with knee flexion (see Figure 4.4, above). The moment arm peak near 30° has been demonstrated in both theoretical and experimental investigations [134, 139, 146]. The MVC moment peak near 60° has also been observed by many different investigators [75, 134]. If moment arm indeed peaks at 30°, then the moment peak at 60° indicates that the quadriceps force is much higher at 60° than at 30°. However, since the fibers of the vastus muscles are fairly short (see Table 4.1), I found that it was impossible for the computed moment to peak at 60° while maintaining quadriceps force at full knee extension.

Our inability to reproduce the experimental moment curve may result from the simplicity of the muscle model. We simplify the muscle-tendon geometry in a number of ways. We represent each muscle with a series of line segments, not as a volume. This may be a reasonable approximation for muscles that have well-defined paths, such as tibialis posterior. However, muscles with large areas of origin, such as the vastus muscles, are only crudely approximated with lines. The approximation is improved by breaking the muscle into compartments (e.g., vastus medialis, intermedius, and lateralis), but lines are still a gross approximation of the actual three-dimensional anatomy. We also assume that the lengths and angles of all the muscle fibers are the same within a given muscle-tendon compartment. This assumption could be relaxed by allowing fiber length, at any given muscle length, to vary within a given muscle [60, 101]. Alternatively, a more complex model that represents both the geometric and the force-generating properties of the muscles in three dimensions might better represent architecturally complex muscles, such as the vastus group.

There is another possible explanation for the difference between computed and experimental knee moments that points out a limitation of our joint models. Our model of the knee accurately reproduces the kinematics and moment arms that have been measured experimentally. However, the knee model does not account for the effects of changing muscle forces on the motion of the knee. Thus, even though we can reproduce moment arms that were measured at fairly low muscle forces [139], this may not apply during MVC experiments when muscle forces are large. If the forces in the quadriceps alter the relative motion of the femur, tibia, and patella, the angle at which the moment arm peaks may change. This explanation seems reasonable in light of our finding that the knee moment arms are very sensitive to changes in knee kinematics.

That is, small changes in, say, the angle of the patella with respect to the femur significantly change the knee extension moment arm. Since the motions of our joint models do not depend on the muscle forces, we cannot account for this effect.

Figure 4.12 shows computed and measured knee extension moments with the hip flexed. The length of rectus femoris at each knee angle is the only change causing the difference between the computed moments in Figures 4.12 and 4.11. Flexing the hip shortens rectus femoris and thus shifts the angle at which it develops peak force toward greater knee flexion. It does not change the moment arms, however. So, the peak computed moment with the hip flexed is less than with the hip extended, and the peak occurs at greater knee flexion. Hence, the match with the experimental joint moments is slightly better. Also, flexing the hip decreases the contribution of passive moment to the total moment curve.

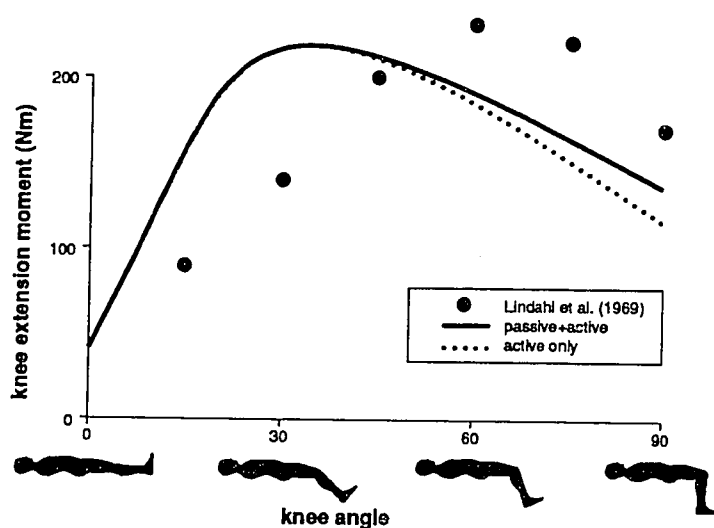


Figure 4.11. Knee extension moment vs. knee angle with the hip extended. Maximum isometric moments from rectus femoris and vastus medialis, lateralis, and intermedius were summed to produce the total computed moment (solid line).

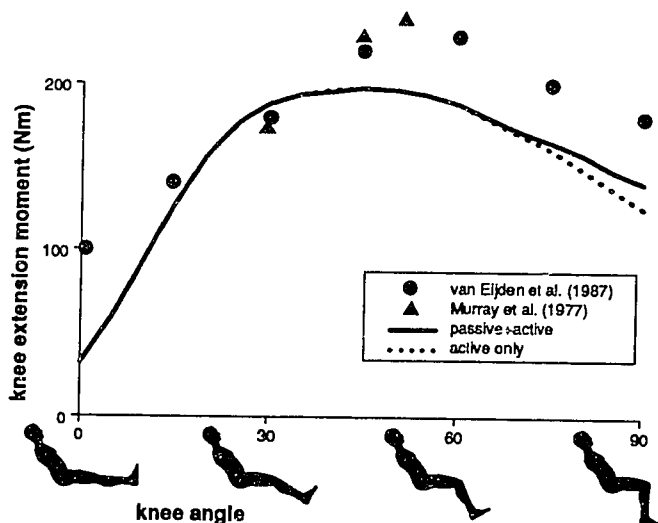


Figure 4.12. Knee extension moment vs. knee angle with the hip flexed. Maximum isometric moments from rectus femoris and vastus medialis, lateralis, and intermedius were summed to produce the total computed moment (solid line).

Knee Flexion

Inman *et al.* [66] measured isometric knee flexion moments on four subjects over a wide range of knee motion with the hip in extension. These experimental data are compared to the total computed moment in Figure 4.13. The computed and experimental moments both peak at about 15° of knee flexion. The calculated moment decreases as the knee is flexed from 15° to 90° because the hamstrings shorten with flexion and develop less force. Moment decreases as the knee is extended from 15° flexion because the moment arms of the hamstrings decrease near full extension. With the hip extended, passive muscle forces contribute nothing to the total joint moment.

Figure 4.14 compares computed and experimental moments with the hip flexed. Notice that the knee flexors are stronger (i.e., generate more moment) when the hip is flexed (*cf.* the peak moments in Figures 4.13 and 4.14). Passive muscle force contributes significantly to knee

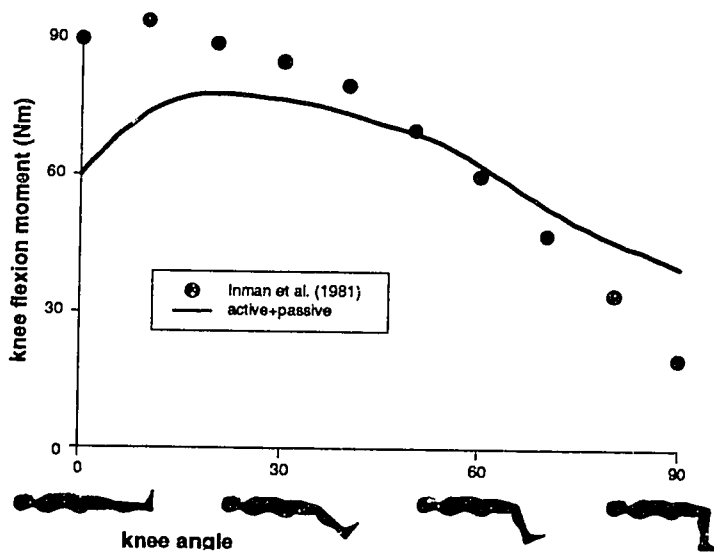


Figure 4.13. Knee flexion moment vs. knee angle with hip extended. Maximum isometric moments from semimembranosus, semitendinosus, biceps femoris (short and long heads), sartorius, gracilis, and gastrocnemius were summed to calculate the total computed moment (solid line).

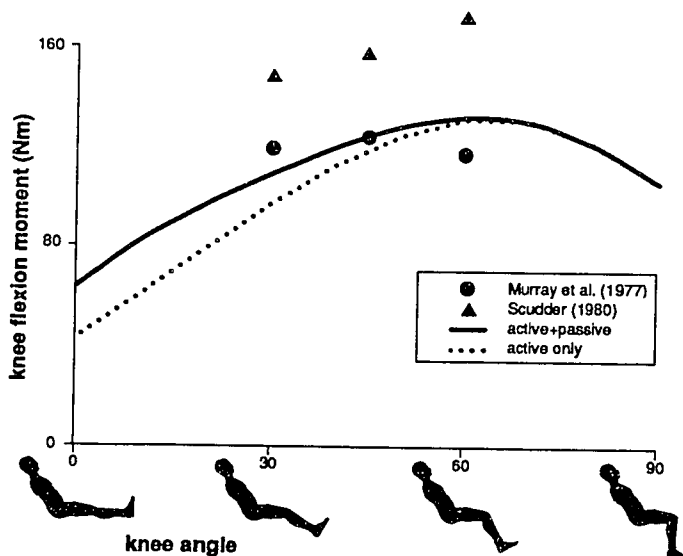


Figure 4.14. Knee flexion moment vs. knee angle with hip flexed 60°. Maximum isometric moments from all knee flexors (listed in Figure 4.13) were summed to calculate the total computed moment (solid line). The dotted line shows the contribution of active muscle only.

flexion moment near full knee extension when the hip is flexed. It is difficult to know how the knee flexion moments change with knee angle because experimental moments have only been measured over a small range of knee angles. Also, no investigations of knee flexion strength have controlled the ankle angle, and thus the contribution of the gastrocnemius to the knee flexion moment has not been determined.

4.5.3 Hip moments

Hip Extension/Flexion

Figure 4.15 compares computed and measured hip extension moments with the knee flexed 90°. The maximum computed and experimental moments are about 170 Nm. However, the computed

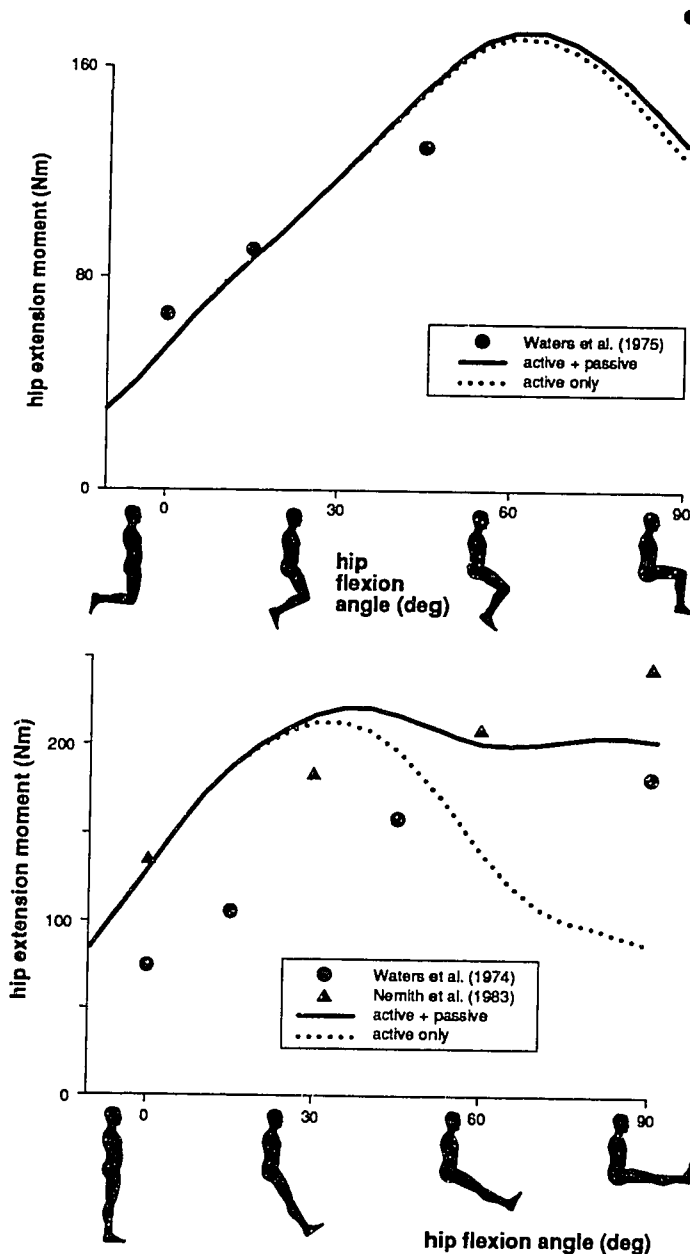


Figure 4.15. Hip extension moment vs. hip angle with knee flexed 90°. Maximum isometric moments from all the hip extensors (gluteus maximus, semimembranosus, semitendinosus, biceps femoris, adductor magnus, and gluteus medius) were summed to calculate the total computed moment (solid line). The dotted line shows the contribution of active muscle only.

Figure 4.16. Hip extension moment vs. hip angle with knee extended. Maximum isometric moments from all the hip extensors (listed in Figure 4.15) were summed to calculate the total computed moment (solid line). The dotted line shows the contribution of active muscle only. Note that passive muscle contributes significantly to the joint moment beyond about 45° of hip flexion.

moment decreases at hip flexion angles greater than 70° , whereas the experimental moment increases. In the model, the moment decreases beyond 70° because the moment arms of the hamstrings and the gluteus maximus decrease as the hip is flexed beyond about 40° . From observing the musculoskeletal geometry on the computer-graphics system, I have confidence that the model calculates accurate hip extension moment arms for the hamstrings because they are represented well by single lines from origin to insertion. Gluteus maximus, on the other hand, has widely distributed muscle fibers that wrap over the ischium and deeper muscles as the hip is flexed. Our model does not represent the lines of action of gluteus maximus well, especially when the hip is flexed. If gluteus maximus moment arms did not decrease with hip flexion, then computed and experimental moments would match more closely.

Figure 4.16 compares computed and measured hip extension moments with the knee extended. In an experimental investigation, Waters *et al.* [137] found little difference in hip extension strength with the knee flexed and extended. Through modeling, however, we uncovered two important differences. First, passive muscle forces contribute significantly to the hip extension moment when the knee is extended (*cf.* solid and dotted lines in Figure 4.16). Also, we found that the hamstrings contribute more to the total hip extension moment near full extension when the knee is extended. Thus, at the anatomical position, computed moment is greater with the knee extended (100 Nm) than flexed (50Nm).

Very little experimental data exist for hip flexion strength as a function of hip angle. Although Cahalan *et al.* [17] have measured hip flexion moments, they did not control the knee angle during their experiments. Thus, their data could not be compared to our model, which fixes the knee angle during hip flexion. Figure 4.17 compares computed moments with maximum iso-

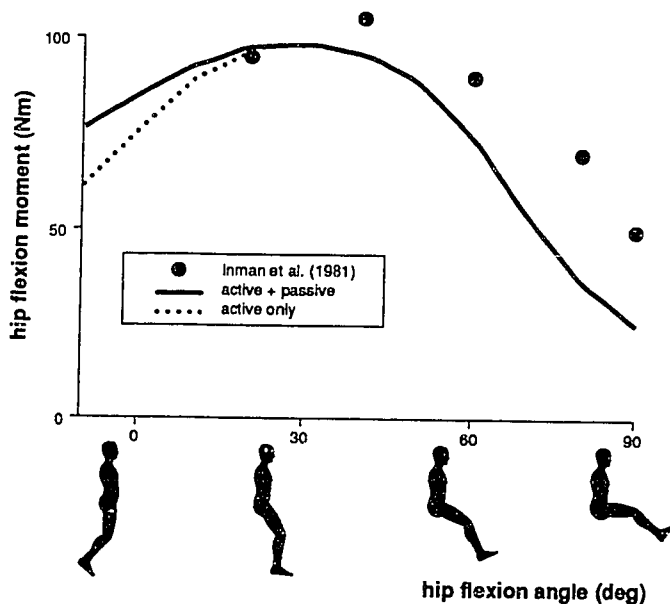


Figure 4.17. Hip flexion moment vs. hip angle with knee flexed 40° . Maximum isometric moments from all the hip flexors (rectus femoris, iliacus, psoas, sartorius, and tensor fasciae latae) were summed to calculate the total computed moment (solid line). The dotted line shows the contribution of active muscle only.

metric moments measured on three subjects [66]. The shape of the computed and measured moment curves correspond closely, but the magnitude of the computed moment is less than the measured flexion moment.

Hip Abduction/Adduction and Rotation

The hip abductors are an extremely important muscle group. Consequently, several research groups have quantified the strength of the hip abductors [17, 95, 99]. These groups have consistently reported that abduction moment increases with adduction. Figure 4.18 compares these experimental measurements with the abduction moments calculated with the model. A detailed comparison of the computed and experimental moments is presented in Section 6.4.

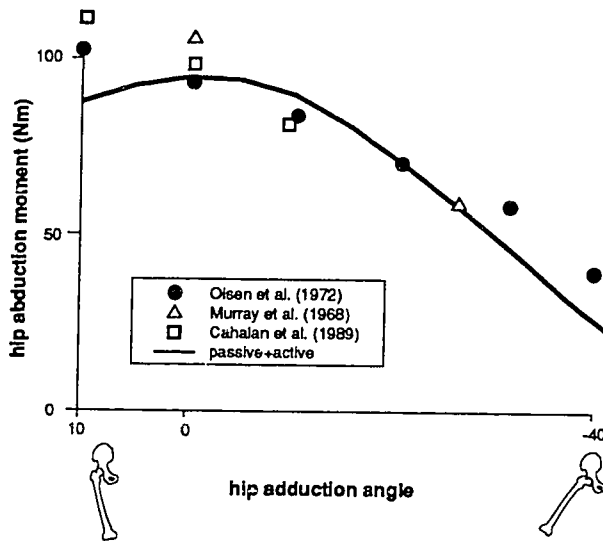


Figure 4.18. Hip abduction moment vs. hip adduction angle. Maximum isometric moments from all the hip abductors (gluteus medius, minimus, and maximus, tensor fasciae latae, and periformis) were summed to calculate the total computed moment (solid line).

The hip adductors can generate more moment when the hip is abducted. This has been shown experimentally [17, 95] and with our model (Figure 4.19). Although the shape of the computed hip adduction curve is similar to the experimental data, the magnitude of the computed moment is higher. The following observation may explain this difference. In addition to the muscles commonly considered to be adductors (i.e., adductor magnus, longus, and brevis, gracilis, and pectinius), I found that the hamstrings (semimembranosus, semitendinosus, and biceps femoris) also contribute significantly to adduction moment. Without the contribution from the hamstrings, the computed and experimental moments match almost exactly (Figure 4.19, dashed line). However, the additional moment of the hamstrings makes the computed moment greater.

Should the moment from the hamstrings be included? In computing the total adduction moment, we sum the moment generated by each muscle that has an adduction moment arm. We assume that each muscle is fully activated, and thus develops maximum force at the computed length. However, the hamstrings may not be fully activated in experimental measurements of

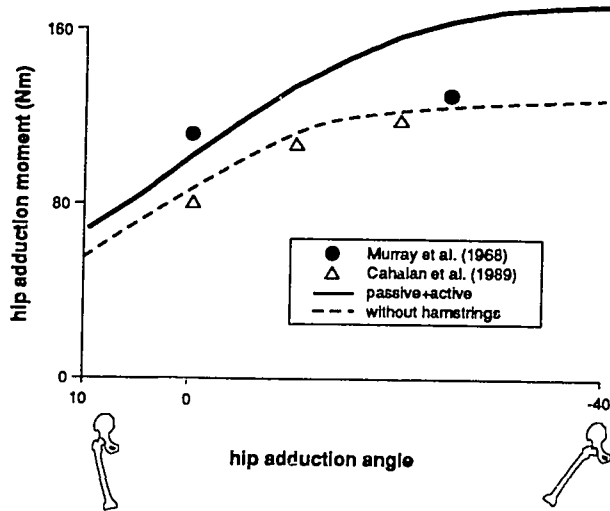


Figure 4.19. Hip adduction moment vs. hip adduction angle. Maximum isometric moments from all the hip adductors (adductor magnus, longus, and brevis, gracilis, pectinius, and the hamstrings) were summed to calculate the total computed moment (solid line). The dashed line shows adduction moment computed without the hamstrings.

adductor strength since they also generate hip extension moment and knee flexion moment. This raises several questions. During hip adduction experiments, are other muscles activated to counteract the hip extension and knee flexion moments generated by the hamstrings? Or, do subjects refrain from activating their hamstrings to avoid these “unwanted” moments? These issues need to be resolved, not only for the hip adductors, but for any muscle that generates moment about multiple joint axes.

Very few investigators have studied hip rotation strength. Figure 4.20 compares hip rotation moments measured by Cahalan *et al.* [17] to computed rotation moments. Computed internal rotation moments compare closely with measured moments, but computed external rotation moments are smaller than experimental moments. We found that the hip rotation moments depend strongly on the angle of hip flexion.

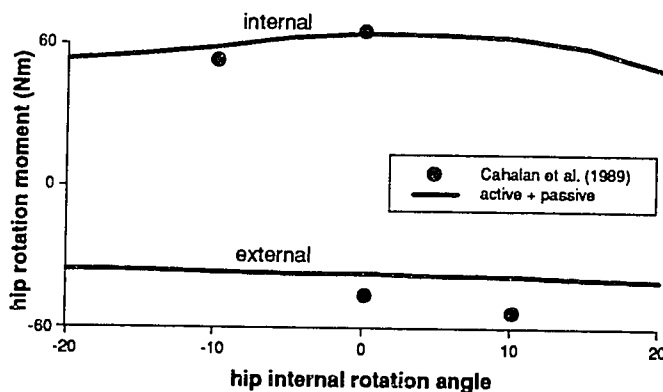


Figure 4.20. Hip rotation moment vs. hip rotation angle. Internal (positive) and external (negative) rotation moments were calculated with 60° hip flexion and 90° knee flexion are compared with experimental data [17] collected under the same conditions.

4.6 Sensitivity Study

We performed a sensitivity study to understand how the muscle-tendon parameters and musculoskeletal geometry affect muscle force. The joint angle at which a muscle develops peak force (θ_o) depends on tendon slack length (ℓ_s^T) (Figure 3.6, upper plot) and optimal muscle-fiber length (ℓ_o^M) (Figure 3.6, lower plot). To determine the sensitivity of muscle force to ℓ_s^T and ℓ_o^M we varied these parameters and determined the change in the *joint angle* at which each actuator develops peak force ($\Delta\theta_o$). This change in the joint angle also depends on the actuator's moment arm (ma), since $\partial\theta = \partial\ell / ma$ (see Section 3.2.5). The change in joint angle at which four actuators develop peak force resulting from a 5% change in ℓ_s^T and ℓ_o^M is shown in Figure 4.21.

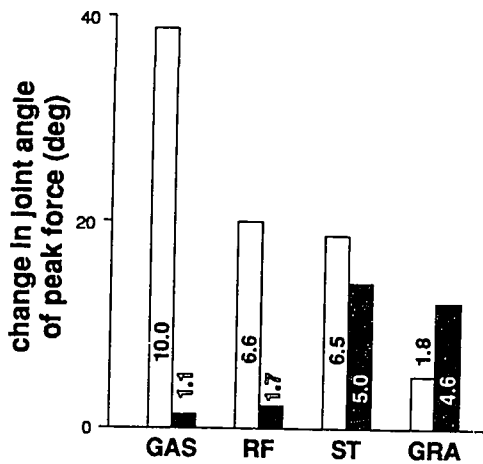


Figure 4.21. Change in joint angle at which four muscle-tendon actuators (gastrocnemius (GAS), rectus femoris (RF), semitendinosus (ST) and gracilis (GRA)) develop peak force resulting from a 5% change in tendon slack length (ℓ_s^T) (open bars) and optimal muscle-fiber length (ℓ_o^M) (filled bars). The number associated with each open (filled) bar is the ℓ_s^T / ma (ℓ_o^M / ma) ratio of that actuator. The moment arms (ma) were computed at the ankle (GAS), knee (RF and ST), and hip adduction (GRA) angles at which these actuators develop peak force. Note that actuators with high ℓ_s^T / ma ratios (ℓ_o^M / ma ratios) are most sensitive to a change in tendon length (fiber length).

We found that the angle of peak force (θ_o) is more sensitive to a change in tendon length for actuators with high ratios of tendon slack length to moment arm (ℓ_s^T / ma) than for actuators with low ℓ_s^T / ma ratios (Figure 4.21, open bars). For example, changing the ℓ_s^T of gastrocnemius by 5% shifted the joint angle of peak force by 38°, whereas a 5% change in the ℓ_s^T of gracilis shifted the angle by only 6°. Similarly, the angle of peak force is more sensitive to a change in optimal muscle-fiber length for actuators with long fibers relative to moment arm (i.e., high ℓ_o^M / ma ratios) than for actuators with low ℓ_o^M / ma ratios (Figure 4.21, filled bars). For instance, a 5% change in the ℓ_o^M of gracilis shifted the joint angle of peak force by 16° while the same percentage change shifted gastrocnemius force by only 2°. In general, θ_o is more sensitive to ℓ_s^T than ℓ_o^M since $\ell_s^T / \ell_o^M > 1$ for most actuators (*cf.* magnitude of open and filled bars).

The range of joint angles over which an actuator develops active force increases with the ratio of its optimal fiber length to its moment arm (i.e., range increases with ℓ_o^M / ma) [62]. Hence, muscles with small ℓ_o^M / ma ratios (e.g., gastrocnemius, soleus, rectus femoris) develop active force over a relatively limited range of motion (e.g., soleus develops active force over only

50° of ankle motion). Since ℓ_o^M has been measured for many muscles in the lower extremity [43, 141], and given that the muscle paths presented here yield reasonable moment arms, we expect that the calculated range of motion over which each actuator develops active force is fairly accurate.

Since no experimental measurements of ℓ_s^T have been reported, it is important to assess the adequacy of our ℓ_s^T estimates. We have shown that the angle of peak muscle force is most sensitive to ℓ_s^T for actuators with high ℓ_s^T / ℓ_o^M ratios (e.g., gastrocnemius, soleus, rectus femoris). We have also shown that actuators with low ℓ_o^M / ℓ_s^T ratios develop force over a limited range of motion. Consequently, ℓ_s^T must be specified accurately for actuators with both high ℓ_s^T / ℓ_o^M ratios and low ℓ_o^M / ℓ_s^T ratios (i.e., actuators with high ℓ_s^T / ℓ_o^M ratios), so that active force is developed in the physiologic range of motion. Since the modeled actuators indeed develop force in the physiologic range of motion, we are confident in the estimates of ℓ_s^T for muscles with high ℓ_s^T / ℓ_o^M ratios. We are less confident in our estimates of ℓ_s^T for muscles with low ℓ_s^T / ℓ_o^M ratios (e.g., sartorius, gracilis, iliacus); however, the force developed by these muscles is less sensitive to ℓ_s^T and thus accurate estimates of ℓ_s^T are less critical.

To study how increasing tendon length influences the *magnitude* of the forces generated by the muscles, we increased the ℓ_s^T of each actuator by 5% and measured the decrease in force at the angle of peak force (θ_o). Figure 4.22 shows that the magnitude of the force developed at θ_o by actuators with large ratios of tendon length to fiber length (ℓ_s^T / ℓ_o^M) is much more sensitive to a change in tendon length. For example, gastrocnemius force decreased by 40% at θ_o for a 5% (2.0cm) increase in ℓ_s^T , whereas gracilis force decreased only 1% at θ_o for a 5% (0.7cm) increase in ℓ_s^T . These results indicate that, in an actual surgery, a much larger decrease in force will be realized by lengthening the tendons of muscles with high ℓ_s^T / ℓ_o^M ratios (the ankle actuators) than by lengthening the tendons of muscles with low ℓ_s^T / ℓ_o^M ratios (the hip actuators).

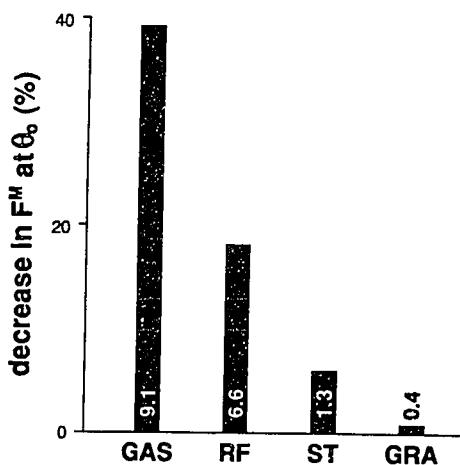


Figure 4.22. Decrease in muscle force (F^M) at the joint angle of peak force (θ_o) resulting from a 5% increase in tendon slack length (ℓ_s^T). The numbers associated with the bars for gastrocnemius (GAS), rectus femoris (RF), semitendinosus (ST) and gracilis (GRA) are the tendon slack length to muscle-fiber length ratios (ℓ_s^T / ℓ_o^M) for each actuator. Note that the magnitude of the muscle force is significantly more sensitive to a change in tendon length for actuators with high ℓ_s^T / ℓ_o^M ratios

4.7 Example Surgery Simulation

To determine how a planned surgical procedure affects muscle force and joint moment, we can adjust the model's parameters (e.g., origin-to-insertion paths and tendon lengths) according to a specific surgical technique. For example, to simulate the mechanical effects of an Achilles tendon lengthening with concomitant anterior transfer of the tibialis posterior (a procedure commonly performed to correct an equinovarus deformity [115]), we increase the model's Achilles tendon length and graphically detach the tendon of tibialis posterior from its insertion on the navicular bone, and reroute its path to insert on the dorsum of the foot. The results of this simulated surgery are then displayed as plots of presurgery and postsurgery plantarflexion and dorsiflexion moments versus ankle angle (Figure 4.23).

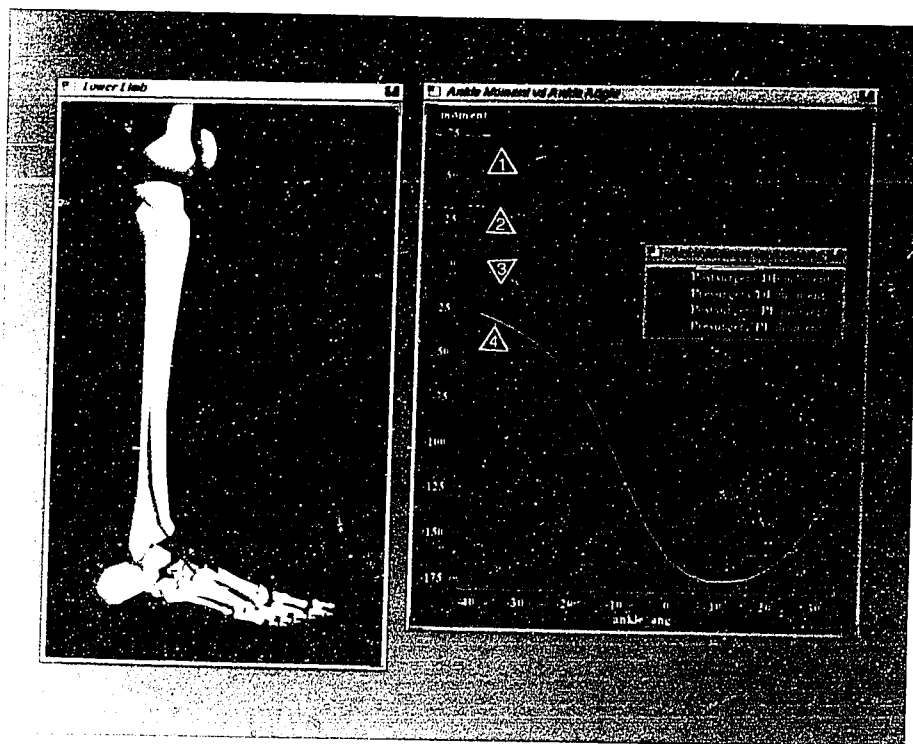


Figure 4.23. Display from a simulated surgery in which the Achilles tendon was lengthened (1 cm) and the tendon of tibialis posterior was transferred to the base of the third metatarsal. The left window shows the postsurgery musculoskeletal geometry with tibialis posterior passing anteriorly to the ankle. The plot on the right shows presurgery and postsurgery ankle dorsiflexion (DF) and plantarflexion (PF) moments (in Nm) vs. ankle angle. Positive (negative) ankle angles and moments indicate dorsiflexion (plantarflexion). Postsurgery dorsiflexion moment is increased significantly, but only in the range of ankle plantarflexion (cf. curves 1 and 2). Postsurgery plantarflexion moment is greatly decreased (cf. curves 3 and 4).

Notice that the magnitude and the shape of the plantarflexion moment versus ankle angle curve are changed by the surgery (*cf.* curves 3 and 4 in Figure 4.23). Two factors cause the significant decrease (65% at 0°) in the ankle plantarflexion moment. First, after surgery, the tibialis posterior does not contribute to the plantarflexion moment since it crosses the ankle anteriorly. Second, and more importantly, increasing the Achilles tendon length changes the ankle angle at which both the gastrocnemius and soleus produce maximum force. This combination of effects not only decreases the magnitude, but also shifts the angle of the peak moment toward greater dorsiflexion. We found that the plantarflexion moment is extremely sensitive to changes in Achilles tendon length. This may explain why it is clinically difficult to maintain plantarflexion strength after Achilles tendon lengthening procedures [9].

In this particular surgery simulation, the postsurgery dorsiflexion moment is greater than the presurgery moment, but only in the range of ankle plantarflexion (-30° to 0°) (*cf.* curves 1 and 2 in Figure 4.23). The significant increase in dorsiflexion moment in the range of ankle plantarflexion (100% at -30°) can be attributed to the large force developed by tibialis posterior in that range. Presurgery and postsurgery dorsiflexion moments are equal in the range of ankle dorsiflexion (0° to 20°) because the fibers of tibialis posterior are too short to develop force in dorsiflexion.

One reason for transferring the tibialis posterior is to correct the varus component of the equinovarus deformity. Indeed, the varus moment will be decreased by this transfer since, after surgery, the tendon passes lateral to the subtalar joint. However, in this particular simulation, tibialis posterior does not generate a corrective valgus moment when the ankle is dorsiflexed since its fibers are too short to develop force in dorsiflexion. If the attachment of the tendon were moved distally on the metatarsal, or if the tendon were shortened, the tibialis posterior would then generate force, and thus valgus moment, over the full range of ankle motion. Such variations in the surgical procedure are easily explored on the computer graphics system.

4.8 Assumptions and Limitations

This section discusses some of the assumptions and limitations of our model. First, we have simplified the knee model to represent motion in the sagittal plane only. While this does not account for rotation of the tibia about its longitudinal axis near full extension [55], or varus/valgus rotation, these non-planar rotations are small compared to motion in the sagittal plane [146]. Since our objective was to determine the effects of knee flexion and extension on muscle-tendon excursions, forces, and moments, the sagittal-plane model is adequate. We have also idealized the ankle and subtalar joints as fixed-axis revolutes. This is a reasonable assumption for the ankle, but the subtalar joint has more complex kinematic characteristics [121]. Thus, we are fairly confident in the ankle moment calculations, but less confident in the computed subtalar moments. Since our musculoskeletal modeling software allows for six degrees of freedom between any two bones, more complex joint models can easily be incorporated into the lower-extremity model.

Second, the musculoskeletal geometry and muscle-tendon parameters have been specified for only a single, nominal subject. However, there is a paucity of experimental data to indicate how the muscle-tendon parameters vary among subjects with different musculoskeletal geometry (i.e., different moment arms and body-segment lengths). If we assume that the range of joint angles over which each actuator develops active force is relatively constant across individuals, then ℓ_o^M would scale with the moment arm (ma) since the ℓ_o^M / ma ratio determines the range of joint angles over which active force is developed [62]. Further, if we assume that the joint angle at which each actuator develops peak force is also subject-independent, we would expect ℓ_s^T to vary to accommodate the change in muscle-tendon length in subjects with different body-segment lengths.

We make several assumptions when using this nominal model to study how the muscle function of an individual, or class of individuals, would be affected by surgery. We assume that the relative cross-sectional areas of muscles are about the same between individuals [12]. We also assume that the ratio of tendon length to muscle-fiber length (ℓ_s^T / ℓ_o^M) is relatively constant between individuals. That is to say, since my soleus muscle can be characterized by a large cross-sectional area, short muscle fibers, and a long tendon, but my sartorius muscle has a small cross-sectional area, long muscle fibers, and a short tendon, it is reasonable to assume that the relationship between the two muscles will be similar in other individuals. There is an extremely large variation in muscle-tendon parameters among the muscles in the lower extremity, yet a small variation of these parameters within specific muscles [43]. Thus, it seems justified to use the nominal model to compare the response of different muscles to surgical alterations, especially if the fundamental conclusions are insensitive to the perturbations of the parameter values that we expect among individuals.

In using our nominal model, we also make assumptions about the musculoskeletal geometry. For example, we assume that muscles attach in nearly the same locations in different individuals. Also we use “normal” joint models that yield moment arms similar to average experimental data. These nominal joint models may lead to unrealistic conclusions if they are blindly applied to study conditions in which joint pathology exists. On the other hand, one can gain insight into joint pathologies by graphically manipulating the nominal joint kinematics and determining the sensitivity of the joint function to joint geometry.

4.9 Advantages of Graphics

In the past, biomechanists have represented muscles as single lines from origin to insertion [13, 56, 57] and resorted to physical models, such as elastic threads attached to skeletons, to visualize the muscle paths [67, 108]. The ability to manipulate computer-generated images of musculoskeletal structures has allowed us to define more accurate muscle-tendon paths for all the major lower-extremity actuators, and to efficiently change these paths to study the biomechanical consequences of surgical reconstructions.

Display of the bone surfaces was also helpful in developing the joint kinematic models. Although the knee model has only one degree of freedom, there are five kinematic functions that specify the relative motion of the femur, tibia, and patella. The ability to graphically alter these kinematic functions and then view the motion of the knee allowed us to quickly refine the knee model (see Figure 3.5). Dynamic display was also helpful to position and orient the axes for the ankle, subtalar, and metatarsophalangeal joints.

The combined effects of musculoskeletal geometry and muscle-tendon parameters on the joint moment versus joint angle curve of a muscle are complex. We have found, however, that interacting with our model facilitates rapid discovery of how surgical manipulations of musculo-tendinoskeletal structures affect the moment generating capacity of the muscles. For example, in a few minutes, one can explore the effects of transferring the insertion of the rectus femoris to the tendon of sartorius (a procedure performed to correct stiff-legged gait [44]) on the knee flexion/extension moments. Further interaction with the model allows one to determine the sensitivity of the knee and hip moments to the exact location of rectus femoris attachment. Since the graphical mode of interaction eliminates the need for the user to focus on the model's mathematical basis, it can be used not only to analyze surgical procedures, but also to train surgeons.

The next two chapters represent applications of the lower-extremity model to study specific clinical problems.

5 Analysis of Tendon Lengthenings

5.1 Abstract

We applied the lower-limb model to study how surgical lengthening of tendon affects the force- and moment-generating capacity of the muscles. Tendon lengthenings were simulated by increasing tendon length and computing the change in maximum isometric muscle force and joint moment at a specific body position. We found that the forces and moments developed by the ankle plantarflexors are extremely sensitive to changes in tendon length. For example, the maximum isometric moment generated by soleus, at a body position corresponding to the midstance phase of gait, decreased 30% with a 1 cm increase in tendon length and 85% with a 2 cm increase in tendon length. In contrast, 1 and 2 cm increases in iliopsoas tendon length decreased its hip flexion moment by only 4% and 9%, respectively.

5.2 Introduction

Patients with muscular spasticity often undergo tendon transfers and tendon lengthenings aimed at normalizing joint moments and correcting gait abnormalities. For example, the Achilles tendon is commonly lengthened to correct an equinus deformity in stroke [91] and cerebral palsy patients [9]. Also, the hamstrings may be lengthened in patients who walk with excessive knee flexion, or a crouch gait [127]. While tendon lengthenings sometimes improve posture and walking, they often compromise the capacity of the muscles to generate force and moment about the joints. When a tendon is lengthened or transferred to a new location, the muscle fibers may be too long or too short to generate active force. Lack of sufficient muscle strength can leave the patient with weak or dysfunctional legs. For instance, over-lengthening of the Achilles tendon may weaken the plantarflexors and result in excessive dorsiflexion during stance [9, 136]. Lengthening the hamstrings may correct excessive knee flexion during stance by decreasing the forces in these muscles. However, weak hamstrings can lead to genu recurvatum [5, 9, 127], inadequate knee flexion during swing [127], and excessive hip flexion [37, 112]. An understanding of how changes in tendon length affect the force- and moment-generating characteristics of each muscle is needed to help design effective tendon surgeries.

The force-generating capacity of a muscle depends on several parameters. The peak force that a muscle can develop depends on its physiologic cross-sectional area (PCSA) [122]. The

range of joint angles over which a muscle can develop active force depends on its fiber length and moment arm. Muscles with long fibers can develop force over a greater range of lengths than muscles with short fibers. The change in muscle-tendon length (excursion) with joint angle depends on moment arm. For a given range of joint motion, muscle-tendon excursion increases with moment arm. Thus, the ratio of a muscle's fiber length to its moment arm determines the range of joint angles over which the muscle can develop active force [62]. The maximum isometric force developed by a muscle (i.e., the force developed when a muscle is maximally excited under isometric conditions) at each joint angle also depends on the fiber pennation angle and the length of tendon in series with the muscle fibers (see Sections 5.4.2 and 5.4.3). Since each muscle-tendon complex has different parameters (i.e., peak force, fiber length, tendon length, and pennation angle), each responds differently to surgical changes in tendon length. The combined effects of the muscle-tendon parameters and the musculoskeletal geometry (moment arms) in determining the sensitivity of muscle force and joint moment to changes in tendon length are complex.

We have applied our model of the human lower extremity to study how surgical lengthening of the tendons affects the force- and moment-generating capacity of the lower-extremity muscles. The specific objectives of this study were:

- (1) to quantify the sensitivity of the force developed by each lower-extremity muscle to changes in tendon length;
- (2) to determine the relative contributions of fiber length, tendon length, and pennation angle in determining the sensitivity of each muscle;
- (3) to quantify the changes in the maximum isometric joint moments that result from changes in tendon length for the most commonly lengthened tendons.

5.3 Methods

We used the lower-extremity model that was described in Chapter 4 to study the mechanical effects of tendon lengthenings. With this model, the maximum isometric force and joint moment that each muscle generates can be computed for any body position. It should be emphasized that the forces and moments computed with the model assume full muscle activation and isometric conditions. Thus, the calculated forces and moments represent each muscle's isometric strength, not the forces and moments that are developed during movement when muscles are, in general, neither fully activated, nor isometric.

With the model the parameters of each muscle-tendon complex can be changed and the effect on the muscle force curve observed. We define the "muscle force curve" as the maximum isometric force vs. joint angle curve (e.g., see Figures 5.3, 5.4, and 5.5). To study the effects of lengthening a particular tendon, we first plotted a muscle's nominal force curve. We then lengthened the tendon that is in series with the muscle fibers by a certain amount, and plotted the new force curve.

To quantify the sensitivity of muscle force to changes in tendon length, we increased the tendon length of each muscle and computed the change in the force at a specific body position from the muscle force curve. Since muscle force varies with joint angle, the change in force (for a given change in tendon length) depends on the body position at which it is computed. Consequently, we computed the changes in the muscle forces at many body positions. To limit the quantity of data, however, all the results presented in the following section were measured at one body position (Figure 5.1). We chose this position because it is used in many functional activities (e.g., the stance phase of walking). Also, we found that this position yields results that are representative of many other body positions.

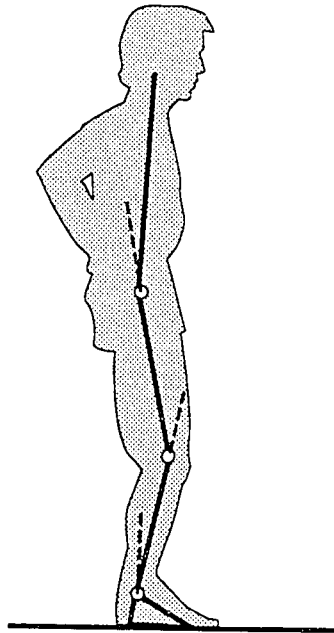


Figure 5.1. Body position for which changes in the forces and moments are presented. The joint angles are 10° dorsiflexion, 20° knee flexion, and 10° hip flexion. All other joint angles (hip adduction angle, hip rotation angle, subtalar angle, and metatarsophanangeal angle) are 0° (anatomical position).

5.4 Results

We found that the decrease in muscle force and joint moment for a given increase in tendon length is *different* for each muscle. Conversely, the increase in tendon length that reduced muscle force by a certain amount is different for each muscle. Figure 5.2 shows the change in tendon length that reduced muscle force 50% at the specified body position. Notice that there is a wide variation among the muscles in the sensitivity of force to a change in tendon length. For example, soleus force decreased 50% with only a 1.2 cm increase in tendon length. Biceps femoris (long head) and iliopsoas, on the other hand, required a 4 cm increase in tendon length to decrease force 50%.

In general, the forces developed by the muscles that cross the ankle are more sensitive to changes in tendon length than are the forces generated by the muscles that cross the hip. This

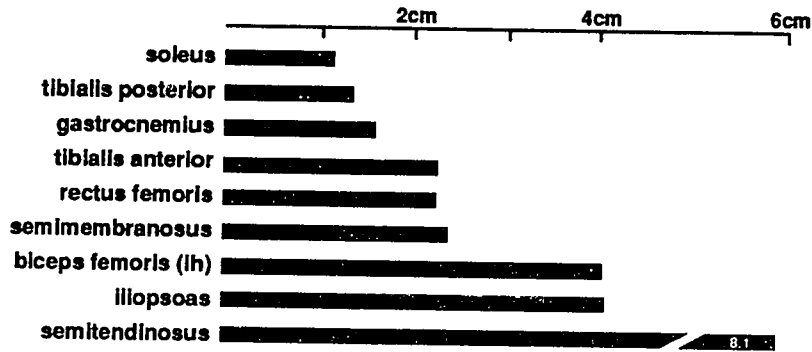


Figure 5.2. Change in tendon length resulting in a 50% decrease in muscle force. Forces in these commonly lengthened tendons were calculated at the body position shown in Figure 1. Tendon lengths are scaled for a 1.8 m adult skeleton.

variation in the sensitivity of the muscle forces to changes in tendon length is caused by differences in the parameters of each muscle-tendon complex. That is, each muscle has a different optimal fiber length, tendon length, and pennation angle, and thus responds differently to tendon lengthening. Table 5.1 shows the parameter values for the muscle-tendon complexes that are commonly lengthened.

Table 5.1. Muscle-tendon Parameters*

muscle	peak muscle force (N)	optimal fiber length (cm)	pennation angle (degrees)	tendon slack length (cm)	tendon length / fiber length
soleus	2830	3.0	30	26.8	8.9
tibialis posterior	1270	3.1	12	31.0	10.0
gastrocnemius §	1600	5.1	14	40.0	7.8
tibialis anterior	600	9.8	5	22.3	2.2
rectus femoris	780	8.4	5	34.6	4.0
semimembranosus	1030	8.0	15	35.9	4.5
semitendinosus	330	20.1	5	26.2	1.3
biceps femoris(lh)	720	10.9	0	34.1	3.1
biceps femoris(sh)	400	17.3	23	10.0	0.6
iliopsoas †	800	10.0	8	11.0	1.1

* See Section 4.3 for explanation of how the parameters were derived.

§ Peak force is the sum of the two heads; other parameters are the averages of the two heads.

† Peak force is the sum of iliacus and psoas; other parameters are the averages of the two muscles.

5.4.1 Effect of Optimal Fiber Length

The force developed by a muscle with short fibers is more sensitive to changes in tendon length than the force developed by a muscle with long fibers. A 1 cm increase in tendon length causes an excursion that is significant in terms of the force-length property for a muscle with 3 cm fibers.

In contrast, a 1 cm excursion is insignificant for a muscle with 40 cm fibers. Muscle fibers are of similar length within a muscle, but vary widely between muscles [43, 141]. For example, Friederich and Brand [43] report an optimal fiber length of about 3 cm for soleus and 44 cm for sartorius. Considering the effects of fiber length alone, changing muscle-tendon length by 1 cm represents a 33% change in fiber length for soleus, but only a 2% change for sartorius. Table 5.1 lists the fiber lengths of the most commonly lengthened muscle-tendon complexes.

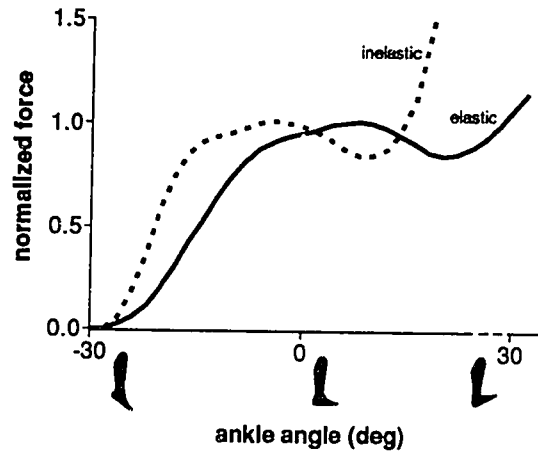
To study the effect of variations in optimal fiber length we constructed a muscle with a nominal fiber length of 5 cm. The muscle was given 0° pennation and no tendon (or inelastic tendon). At the joint angle where active force peaks (θ_o), force decreased 48% for a 2 cm change in tendon length for the nominal fiber length (5 cm). Fiber length was then altered and the decrease in force was measured at θ_o . Active force decreased 80% when the muscle fibers were 4 cm, and 23% when the fibers were 6 cm. Thus, even a 1 cm variation in the optimal fiber length has a large effect on the sensitivity of muscle force to changes in tendon length.

5.4.2 Effect of Tendon Length

Elastic tendon in series with the muscle fibers tends to increase the range of lengths over which the muscle-tendon complex develops force [150]. This occurs because tendon stretch accounts for part of the muscle-tendon excursion (i.e., muscle fiber excursion = muscle-tendon excursion - tendon stretch). Thus, the muscle fibers undergo less excursion than the muscle-tendon complex when tendon stretches. Long tendons stretch more than short tendons for a given force. The magnitude of the effect of tendon stretch on fiber excursion therefore depends on the ratio of tendon length to fiber length. Table 5.1 lists the tendon lengths and the ratios of tendon length to fiber length for the muscle-tendon complexes that are commonly lengthened. Tendon elasticity also decreases the slope of the (active + passive) muscle force curve [150]. For example, Figure 5.3 shows maximum isometric soleus force vs. ankle angle with nominal tendon stiffness (elastic) and with tendon stiffness equal to 100 times the nominal value (inelastic).

The normal variation of tendon lengths among muscles in the lower extremity is about 0-30 cm (see Table 4.1 and [62]). This leads to a variation in tendon elasticity. To quantify the effect of the variation in tendon elasticity on the sensitivity of muscle force, we constructed a muscle with 5 cm fibers, 0° pennation, and a 30 cm tendon. With nominal tendon elasticity (see Figure 3.2), active force decreased 29% for a 2 cm increase in tendon length. Without tendon elasticity active force decreased 48% for a 2 cm increase in tendon length. Thus, tendon elasticity decreases the sensitivity of muscle force to changes in tendon length.

Figure 5.3. Active + passive soleus force vs. ankle angle with elastic and inelastic tendon. The solid curve was calculated with nominal tendon elasticity (see Figure 3.2 for nominal tendon force-length curve). The dotted curve shows the effect of making the tendon inextensible; this also represents a muscle that has a very short or no tendon. The difference in the curves results from the tendon stretch. Notice that tendon elasticity tends to decrease the slope of the force vs. angle curve. This indicates that tendon compliance decreases the sensitivity of muscle force to changes in muscle-tendon length. Force is normalized by peak isometric force.



5.4.3 Effect of Pennation

Pennation increases the range of joint motion over which a muscle develops active force and decreases the peak force [150]. Because the muscle fibers are oriented at an angle with respect to the direction of force (see Figure 1.4), the excursion of the muscle fibers is less than the excursion of the muscle-tendon complex. Thus, pennation tends to decrease the slope of the muscle force vs. joint angle curve. For a given muscle cross section, pennation also decreases the peak force. Since muscle force (F^M) is directed along the fibers, the force in tendon (F^T) is decreased by a factor equal to the cosine of the pennation angle (α) (i.e., $F^T = F^M \cos(\alpha)$) [150].

Figure 5.4 shows the effect of pennation on the soleus force vs. ankle angle curve. With 30° of pennation (the nominal pennation angle for soleus at optimal fiber length), the range of

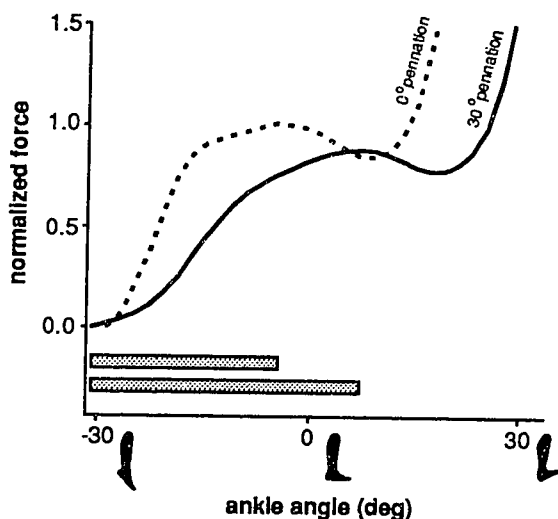


Figure 5.4. The effect of pennation on the soleus force vs. ankle angle curve. Active + passive soleus force is plotted for 0° (dotted curve) and 30° (solid curve) of pennation. The bars show the range of ankle angles over which active force increases with muscle length (the ascending region of the force-length curve). Notice that pennation increases the range of joint motion and decreases the peak force. Force in both curves is normalized by peak isometric force for 0° pennation.

joint angles over which soleus operates on the ascending region of its force-length curve is greater than with 0° pennation (*cf.* bars). The effect of pennation is enhanced when the fibers are shorter than optimal length because the pennation angle increases as the fibers shorten. On the other hand, the muscle fibers become more aligned with the tendon (i.e., pennation decreases) when they are stretched beyond optimal length. Consequently, pennation has a very small effect on the passive force characteristics (note the similarity of the slopes of the force curves near full dorsiflexion in Figure 5.4).

The normal variation in pennation angles among muscles in the lower extremity muscles is about 0-30° [43, 141]. To assess the effect of this variation in pennation angle on the sensitivity of muscle force to changes in tendon length, we constructed a muscle with 5 cm fibers and inelastic tendon. The decrease in force for a 2 cm increase in tendon length was 48% with 0° pennation, and 30% with 30° pennation. Thus, pennation decreases the sensitivity of force to changes in tendon length.

5.4.4 Relative Importance of Fiber Length, Tendon Length, and Pennation Angle

Optimal muscle-fiber length is the most important parameter in determining the sensitivity of isometric muscle force to changes in muscle-tendon length. There is a large variation in optimal fiber lengths among the muscles in the lower extremity [43, 141]. This variation in fiber length is the major factor contributing to the widely different sensitivities found among the muscles shown in Figure 5.2.

Tendon elasticity and fiber pennation both decrease the sensitivity of muscle force to changes in tendon length. Many muscles have tendons of sufficient length (elasticity) to significantly affect the sensitivity. Of the tendons that are commonly lengthened, soleus, gastrocnemius, tibialis posterior, peroneus longus, semimembranosus, rectus femoris, and biceps femoris (long head) all have tendon length to fiber length ratios greater than 3.0 (see Table 5.1). We found that tendon elasticity affected the slope of both active and passive muscle force curves for these muscles. On the other hand, few muscles have pennation angles large enough (>20°) to affect sensitivity significantly. The soleus and biceps femoris (short head) are exceptions, since they have pennation angles greater than 20° [43, 141].

5.4.5 Effect of Moment Arm

A muscle's moment arm affects its moment-generating capacity in two ways. First, since moment about a joint is the product of force and moment arm, increasing moment arm increases the joint moment, for a given muscle force. Moment arm also affects the change in length, or excursion, that a muscle-tendon undergoes as a joint is moved. Moment arm (*ma*) and muscle-tendon excursion ($\partial \ell^{MT}$) are related by the following equation: $ma = \partial \ell^{MT} / \partial \theta$, where θ is the joint angle [2]. Thus, muscles with larger moment arms exert more moment per unit muscle force, and

undergo larger excursions as the joints they span are flexed and extended.

At a given body position, the moment arm does not affect the change in muscle force or joint moment that results from tendon lengthening. However, since moment arm affects excursion, it affects the shape of the muscle force curve before and after tendon lengthening. Figure 5.5 shows the change in force caused by increasing tendon length for two muscles with the same parameters (fiber length, tendon length, and pennation angle), but different moment arms. (A physiologic example of this situation can be demonstrated by comparing soleus and tibialis posterior, since they have similar fiber lengths, tendon lengths, and pennation angles, but different moment arms.) Notice that the decrease in force (arrow) is the same for both muscles. However, the force developed by the muscle with the small moment arm (B) varies less with joint angle than the muscle with a large moment arm (A).

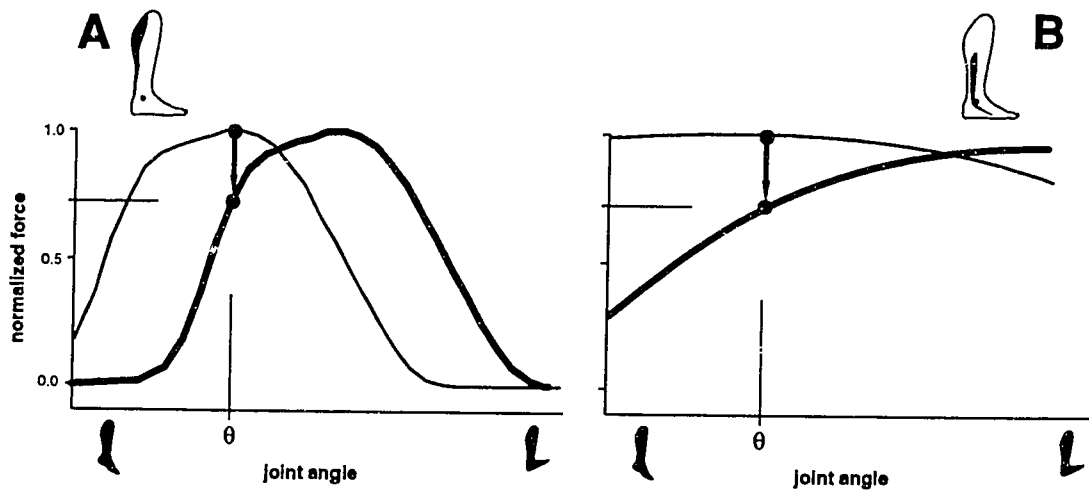


Figure 5.5. Force vs. joint angle for muscles with different moment arms. Active force is plotted for muscles with large (A) and small (B) moment arms. The thin (thick) lines are the muscle force curves before (after) tendon lengthening. Notice that the decrease in force caused by increasing tendon length (arrows) is the same for the two muscles at a specific joint angle (θ). This occurs because the two muscles were given the same fiber length, tendon length, and pennation angle. Thus, the decrease in force, at a particular joint angle, does not depend on moment arm. However, since the fibers of the muscle with the large moment arm (A) undergo a significant excursion as the joint is flexed, the slope of the muscle force curve is large. In contrast, the force in muscle B varies less with joint angle, both before and after tendon lengthening.

5.4.6 Sensitivity of joint moments

The percent change in muscle force for a given change in tendon length depends only on fiber length, tendon length, and pennation angle, as discussed above. Whether a change in muscle force has a significant effect on the total joint moment, however, depends on the muscle's physio-

logic cross-sectional area (PCSA) and moment arm, since PCSA determines peak force [122], and moment arm determines moment per unit force. Figures 5.6, 5.7, and 5.8 show the changes in the maximum isometric joint moments calculated for 1 and 2 cm increases in tendon length for the most commonly lengthened lower-extremity tendons.

Figure 5.6 shows that the plantarflexion moments developed by soleus, gastrocnemius, and tibialis posterior are extremely sensitive to changes in tendon length. For example, the maximum isometric moment that can be developed by soleus decreased 30% with a 1 cm increase in tendon length and 85% with a 2 cm increase in tendon length. Since soleus and gastrocnemius, together, provide a large percentage (about 90%) of the total plantarflexion moment in this body position, decreasing their moment has a significant effect on the total plantarflexion moment (strength). Tibialis posterior moment also decreases significantly with changes in tendon length. However, this has a small effect on total plantarflexion moment, since tibialis posterior contributes only a small percentage to the total plantarflexion moment due to its small moment arm.

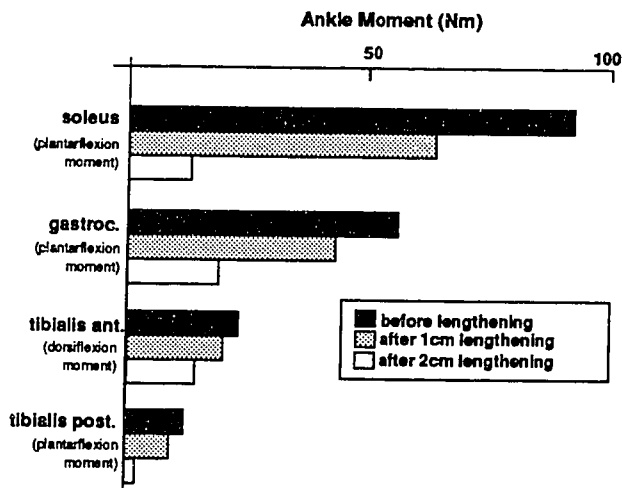


Figure 5.6. Maximum isometric ankle moments before and after simulated tendon lengthening. Moments were calculated with 10° dorsiflexion and 20° knee flexion (Figure 5.1).

Of the ankle muscles, the moment developed by tibialis anterior is the least sensitive to changes in tendon length. Tibialis anterior is less sensitive because it has relatively long fibers (9.8 cm) and a long tendon (22 cm), both of which decrease sensitivity.

Figure 5.7 shows the changes in the knee moments for 1 and 2 cm increases in tendon length. The knee extension moment developed by rectus femoris decreased 17% for 1 cm and 48% for 2 cm increases in tendon length. The knee flexion moments generated by semimembranosus and gastrocnemius are both fairly sensitive to changes in tendon length. However, the flexion moment generated by semitendinosus decreases very little with changes in tendon length. Since semimembranosus is more sensitive than semitendinosus, and provides a greater percentage of the total knee flexion moment, a much greater decrease in total knee flexion moment results from lengthening semimembranosus.

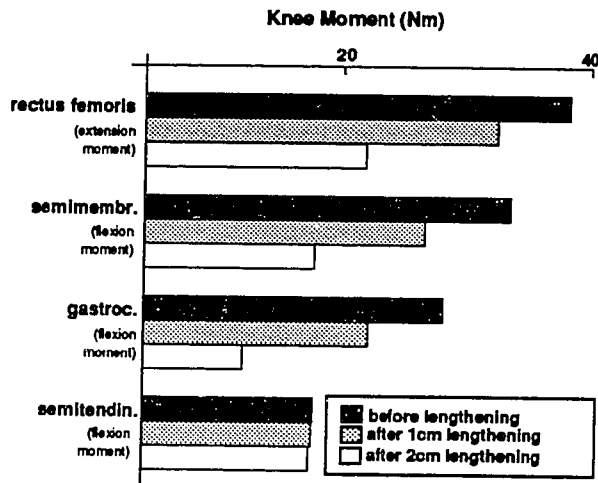


Figure 5.7. Maximum isometric knee moments before and after simulated tendon lengthening. Moments were calculated with 10° dorsiflexion, 20° knee flexion, and 10° hip flexion (Figure 5.1).

When the tendon of a biarticular muscle is lengthened, the effect on the moments about both spanned joints must be considered. For example, when the hamstrings are lengthened to correct excessive knee flexion during stance (i.e., "crouch gait"), the extension moment they exert about the hip is also changed. Figure 5.8 shows the changes in hip moments for 1 and 2 cm lengthening of the hamstrings and other tendons. For the hamstrings, note that semimembranosus is capable of generating more than twice as much extension moment than semitendinosus (cf. length of black bars), because it has a larger PCSA [43, 141]. Also, the moment developed by semimembranosus is much more sensitive to changes in tendon length because it has shorter fibers. Therefore, the hip extension moment (i.e., hip extension strength) is decreased significantly by lengthening semimembranosus, but is changed very little by lengthening

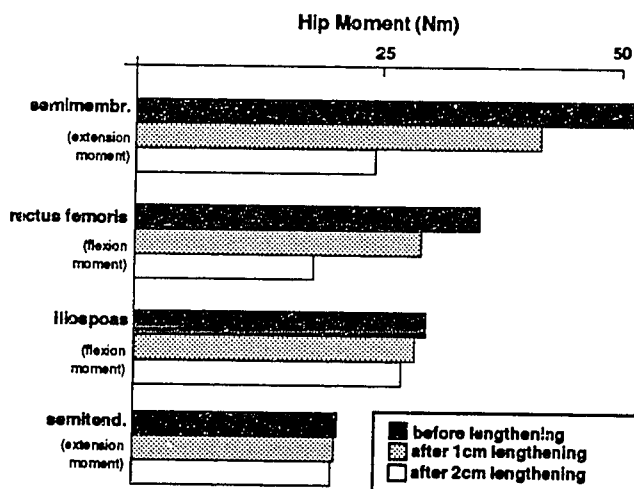


Figure 5.8. Maximum isometric hip moments before and after simulated tendon lengthening. Moments were calculated with 20° knee flexion and 10° hip flexion (Figure 5.1).

semitendinosus.

Figure 5.8 also shows that the maximum isometric moment developed by rectus femoris is more sensitive to changes in tendon length than the moment developed by iliopsoas. Also, rectus femoris can generate slightly more hip flexion moment than iliopsoas. Although iliopsoas has a larger PCSA [43, 141], it has less potential to generate flexion moment than rectus femoris because it has a smaller moment arm. Thus, rectus femoris is a slightly stronger hip flexor than iliopsoas, and is more sensitive to changes in tendon length.

5.5 Discussion

Each muscle has a unique set of muscle-tendon parameters (peak force, optimal fiber length, pennation angle, and tendon length) that determine its isometric force-generating characteristics. Furthermore, each muscle has a unique three-dimensional geometric relationship with respect to the joint(s) it spans. The combined effects of the muscle-tendon parameters and the musculoskeletal geometry determine each muscle's capacity to generate moment about the joints. We have applied a model that specifies the isometric force- and moment-generating capacity for all the major muscles in the lower extremity to simulate the biomechanical consequences of tendon lengthenings. Our simulations indicate that the forces developed by some muscles (particularly the ankle plantarflexors) are very sensitive to changes in tendon length. Thus, small changes in tendon length result in large changes in muscle force. In contrast, other muscles (e.g., iliopsoas, semitendinosus) are much less sensitive to changes in tendon length and must therefore be lengthened more aggressively to achieve a significant decrease in force. We have quantified this variation in the sensitivities of the muscle forces to changes in tendon length for the lower-extremity tendons that are most commonly lengthened.

5.5.1 Confidence in Muscle-tendon Parameters

The confidence in our simulation results are limited by the accuracy of the muscle-tendon parameters. Estimates of muscle-fiber length are particularly important. Three independent investigations of lower-extremity muscle architecture have reported remarkably consistent fiber lengths [43, 138, 141]. Thus, we are confident that reported fiber lengths are reasonably accurate.

However, the difference between fiber length and fascicular length, and complex muscle architectures must be considered. Wickiewicz *et al.* dissected bundles of 10-20 muscle fibers (called muscle fascicles) and measured fascicular length [141]. Friederich and Brand measured both fascicular and muscle-fiber lengths [43]. For many muscles, fascicular lengths and fiber lengths are very similar [43]. Based on these data, we assume that fascicular lengths and fiber lengths are equal. However, other data point out that fascicular length and muscle-fiber length are not equal in some parallel-fibered muscles [77]. For instance, Loeb *et al.* found that the fibers of the sartorius and semitendinosus in the cat hindlimb do not run from internal tendon to internal

tendon, as the fascicles do, and thus are shorter than the muscle fascicles [77]. If human parallel-fibered muscles (e.g. semitendinosus) have fibers shorter than the fascicular lengths used in this study, then the changes in force for a given change in tendon length for those muscles would be greater than the changes reported here.

Semitendinosus has another architectural specialization related to fiber length. There is a tendinous septum near the middle of the muscle belly that separates it into two distinct compartments. Since these compartments are in series, semitendinosus was treated as a single muscle with a fiber length equal to the sum of the fiber lengths of the two compartments [141].

Measured values for **physiologic cross-sectional area (PCSA)**, which scale peak force, [122] are less consistent than measured fiber lengths. PCSA is defined as the muscle volume divided by average fiber length. Friederich and Brand found that "normalized" PCSA (i.e., PCSA of a muscle / average PCSA of all muscles) measured in six cadavers by three different research groups were reasonably consistent (average standard deviation for all the muscles is 29%) [43]. Normalized PCSA measured by Brand *et al.* in fifteen cadaver arms had an average standard deviation of 26% (calculated from mass fraction in Table 1 of [12]). This inter-subject variability of each muscle's PCSA could be due to actual inter-subject variability or to measurement error. For example, some of the variability may be caused by inconsistent muscle shrinkage that occurs during muscle preparation [43]. The effects of shrinkage on muscle volume can be minimized by measuring volumes with CT (e.g., Clark *et al.* [25]). However, even if perfect measurements of PCSA were possible, we would expect some variability in normalized PCSA of muscles because of differences in body types, activity histories, *etc.* Since PCSA does not effect the percentage change in force for a given change in tendon length, the variability in this parameter does not affect the relative sensitivities (i.e., Figure 5.2 is not affected). However, it does affect the magnitude of the changes in force and moment. Thus, Figures 5.6, 5.7, and 5.8 are affected by PCSA.

Measurements of **pennation angle** are very consistent [43, 141]. We are therefore confident in the values used in this study, especially since small changes in pennation angle have very little effect on the sensitivity of muscle force to changes in tendon length.

Since no experimental measurements of **tendon slack length** have been reported, we have performed a sensitivity study to assess the accuracy of our estimates of tendon length (see Section 4.6). Briefly, we are confident in our estimates of tendon length for muscles with large ratios of tendon length to fiber length (e.g., soleus, tibialis posterior, gastrocnemius). We are less confident in our estimates of tendon length for muscles with small ratios of tendon length to fiber length (e.g., iliopsoas, semitendinosus). However, since force is less sensitive to changes in tendon length for these muscles, accurate estimates are less critical since an error in tendon length has a smaller effect on the muscle force curve.

5.5.2 Assumptions and Limitations

It is important to discuss the assumptions and limitations of using our model to study the mechanics of tendon lengthenings. First, our sensitivity results do not account for the effects of muscle-tendon adaptation. Patients are usually immobilized after tendon surgery. Immobilization can cause muscle atrophy, and thus a decrease peak muscle force [142]. Several investigators have shown that the number of sarcomeres in a muscle fiber changes as a result of immobilization, and that this change depends on the angle at which the joint is immobilized [125, 142]. Immobilization can also change the elasticity of tendon [144]. In our model, each muscle's peak force, fiber length, and tendon elasticity can be altered to simulate the mechanical effects of muscle-tendon adaptation. However, these parameters were kept constant in Figures 5.2, 5.6, 5.7, and 5.8. In these figures, our objective is to quantify the variation in the sensitivities of the muscle forces and joint moments that result from the normal differences in the muscle-tendon parameters.

The differences in the muscle-tendon parameters among muscles is much larger than the changes in these parameters that could result from adaptation. For example, optimal muscle-fiber lengths have been shown to increase 20% when held in an elongated position [125], whereas the differences in the fiber lengths between muscles in the lower extremity can be as large as 1000% [43, 141]. Thus, we do not expect that muscle-tendon adaptation would affect the relative sensitivities presented in Figure 5.2.

This is not to say that adaptation is unimportant in determining the biomechanical consequences of tendon lengthenings. It is in fact very important, especially for muscles that are sensitive to a parameter change. If a muscle's force curve is sensitive to a change in fiber length, then small changes in fiber length, caused by adaptation, could significantly affect the force-generating characteristics. For instance, muscle fibers may shorten as a result of being immobilized in a shortened position [142]. This not only decreases the range of joint angles over which the muscle develops force, but also changes the force developed at each angle. Muscles that are not sensitive to a parameter change must adapt much more to have a significant effect on the force-generating characteristics.

The effects of skeletal growth also confound biomechanical analysis of tendon lengthening. Truscilli *et al.* postulated that the lack of muscle growth during bone growth is often the cause of equinus in children with cerebral palsy [131]. We have not attempted to account for the effects of skeletal growth, or any temporal effects, on the muscle force curves. Thus, Figures 5.2, 5.6, 5.7, and 5.8 should be interpreted as the acute changes in the muscle forces and joint moments that result from increasing tendon lengths, not as the changes that would result after growth and adaptation.

A second limitation is that we have used a model of a nominal lower extremity. This model is assumed to have normal muscle-tendon properties and parameters. However, tendon lengthenings are frequently performed on stroke and cerebral palsy patients, whose condition may

be complicated by muscle-tendon contracture. How then can we use this nominal model to gain insight into the biomechanical aspects of surgeries performed on patients whose muscle-tendon parameters may not be normal?

If experimental data were available to indicate how the muscle-tendon parameters are affected by CNS lesions such as stroke or cerebral palsy, we could modify the parameters of the model to represent these pathologic changes. Unfortunately, no such experimental data exist. However, we can use the nominal model to study how pathologic changes would affect the sensitivity of the muscle forces. For example, if the muscle fibers in cerebral palsy patients are shorter than the average values used in this study, then the sensitivities of the muscle forces to changes in tendon length would be greater than the sensitivities presented here. Further, through analysis of the nominal model, we have found that very small changes in muscle-fiber lengths or tendon lengths of the ankle plantarflexors have significant effects on the muscle forces and ankle moments. The same changes in fiber length or tendon length have smaller effects at the hip and knee. This may explain why ankle equinus is the most common deformity requiring surgical attention in both stroke [107] and cerebral palsy [45], although this also may occur since spasticity generally increases distally in these patients.

Although a significant amount of experimental data is needed to understand how muscle-tendon parameters are affected by various pathologic conditions, our sensitivity studies can guide these experimental investigations to determine the most relevant parameters to be measured. We have found that muscle-fiber length is the most important parameter in determining the sensitivity of muscle force to changes in tendon length. Initial investigations should therefore focus on determining how fiber length is affected in pathologic states.

Finally, it is important to note that the results of tendon lengthenings are unpredictable, in part, because of the abnormal muscle activation patterns that occur in patients with CNS lesions. We have not attempted to account for abnormal muscle activity since it is highly variable [106] and difficult to quantify. Rather, we assumed that muscle activation is constant and quantified the effects of the muscle-tendon parameters and musculoskeletal geometry on the moment-generating capacity of the muscles. Since tendon surgery directly affects the moment-generating potential of the muscles, it is essential to understand these effects in order to design effective tendon surgeries.

5.5.3 Clinical Implications

The sensitivity results have practical implications with regard to tendon lengthenings. We found that the forces and moments developed by soleus and gastrocnemius change significantly with small changes in tendon length. This suggests that the Achilles tendon should be lengthened conservatively to avoid plantarflexion weakness. Clinical studies also suggest conservative lengthening of the Achilles tendon [9]. The observation that tendoachilles lengthening may weaken

soleus more than gastrocnemius supports those who recommend isolated gastrocnemius lengthening as a means to control plantarflexion weakness in cerebral palsy patients [98]. In contrast to soleus and gastrocnemius, the force and moment developed by iliopsoas is relatively insensitive to changes in tendon length. This suggests that it can be lengthened more aggressively without much decrease in force. The difference in the fiber lengths of the muscles of the hamstrings has similar implications for surgeons who lengthen more than one of the hamstrings.

Our results can also be applied to understand the mechanics of tendon transfers. If the force developed by a muscle is sensitive to changes in its tendon length, then it is also sensitive to changes in its origin-to-insertion length. That is, if a muscle's maximum isometric force decreases a certain amount from lengthening its tendon 2 cm, then the force would decrease by the same amount if a tendon transfer decreased the origin-to-insertion length 2 cm. Thus, the sensitivity results presented above apply to both tendon lengthenings and tendon transfers.

There are practical implications of this connection between tendon transfers and tendon lengthenings. If a muscle that is sensitive to length change (e.g., tibialis posterior) is to generate active force after a transfer, the transfer must be performed such that the muscle fibers are near optimal length. This may be difficult to accomplish for a muscle with high sensitivity to changes in length. On the other hand, muscles that are less sensitive to length change (e.g., rectus femoris) are more likely to generate active force after a transfer, even if the origin-to-insertion length is changed significantly.

6 *Analysis of the Chiari Pelvic Osteotomy*

6.1 Abstract

Although the Chiari osteotomy is usually effective in reducing pain, many patients are left with a long-term limp. The postoperative limp can at times be caused by hip abductors that have strength insufficient to counteract the moment from body weight during single-leg stance. To study how the surgical technique affects the hip abductor muscles, we developed a biomechanical model that computes the postsurgery pelvic geometry and the resulting hip abductor moment given three surgical parameters: angulation of the osteotomy, distance of medial displacement, and angle of internal rotation. The computer simulations of the Chiari osteotomy showed that some sets of surgical parameters conserve abductor moment while others greatly reduce it. Simulated surgeries with high angulation and large medial displacement reduce gluteus medius abductor moment by up to 65%. This combination of surgical parameters may, therefore, account for some instances of the postoperative limp. In the model, high angulation reduces the length of gluteus medius and is the primary cause of reduced abductor strength. Simulated horizontal osteotomies (0° to 10°) were found to best conserve both muscle length and abductor moment.

6.2 Introduction

Treating subluxation of the hip, whether from congenital disorders, neuromuscular problems, or acquired disease, remains a challenge. Subluxation of the hip with secondary acetabular dysplasia is particularly difficult to manage when it becomes irreducible. To solve this problem, Chiari devised a medial displacement osteotomy of the pelvis [22]. Initially, he recommended this procedure for all dysplastic hips; however, Chiari later stated that the medial displacement osteotomy is indicated only in children older than four years when Salter [117] and Pemberton [104] procedures are contraindicated [23]. Since its introduction, the Chiari osteotomy has become widely used to treat pain and instability of the hip in both children and adults [3, 8, 18, 24, 26, 31, 51, 52, 61, 79, 120].

In Chiari's procedure, the osteotomy starts from the lateral surface of the ilium at the level of the superior margin of the acetabulum, and is directed medially and superiorly. Once the osteotomy is complete, the distal fragment is displaced medially to create a bony ceiling above the femoral head. Increased femoral head coverage improves hip stability. Medial displacement of

the hip also reduces the body-weight moment arm (the perpendicular distance between the body-weight force vector and the hip joint center) thereby decreasing the abductor moment required to counteract gravity [90].

Even though the Chiari osteotomy putatively reduces the gravitational moment that must be counteracted by the hip abductors, many patients develop a Trendelenburg gait after surgery [3, 8, 18, 120]. The Trendelenburg gait occurs when the hip abductors are unable to support the moment from body-weight; consequently, the pelvis drops to the contralateral side during single-leg stance [64, 105]. Patients with weak abductors also frequently lurch over the involved hip to compensate for the weak muscles [65, 105]. The limp from abductor weakness must be differentiated from an antalgic gait which is similarly characterized by the patient leaning over the involved hip, in this case, however, to reduce the compressive joint load [66]. Although some have reported very few cases with the postoperative limp from abductor weakness [24, 79], others have reported many [3, 8, 18, 120]. For example, Schutze and Kramer [120] reported that the Chiari osteotomy gave unsatisfactory results in 39 of their 82 patients, primarily because of decreased abductor muscle strength. In a long-term follow-up study, Calvert *et al.* [18] reported a positive Trendelenburg sign in 76% and a severe limp in 56% of their 49 cases after surgery. Bailey and Hall [3] reported that 14 of 18 patients exhibited a Trendelenburg gait after a Chiari osteotomy was performed for acetabular dysplasia. It is puzzling that a procedure that presumably reduces the abductor moment required for pelvic stability, often leads to a Trendelenburg gait.

We hypothesize that surgical modification of the musculoskeletal geometry may substantially reduce hip abductor strength and thus cause the limp. Because the distal fragment, with the hip joint and muscle insertions, moves relative to the proximal fragment, muscle lengths and moment arms are changed by the surgery. These mechanical changes may hinder the capacity of the muscles to generate sufficient force and moment to support the pelvis during walking.

We developed a biomechanical model of the Chiari osteotomy to study how the surgical parameters affect hip abduction moment. Our objective was to determine if certain combinations of the surgical parameters significantly reduce abductor moment, and to find a surgical technique that conserves abductor moment. This chapter first describes mathematical models of both the surgical procedure and hip musculature. The results of two simulated surgeries are then shown to illustrate how the surgical parameters combine to affect abductor moment. Families of curves are also presented to show the change in hip abductor moment for each surgical parameter. Finally, we discuss the clinical significance of these findings.

6.3 Methods

To study how the Chiari osteotomy affects hip abductor moment, we developed a computer model to simulate the mechanical effects of the surgical procedure. The model is composed of

two parts: (1) a surgical model that computes the locations of the muscle insertions and the hip joint center given values for the surgical parameters, and (2) a musculoskeletal model that calculates the maximum isometric hip abductor moment given coordinates for the muscle attachments and the joint center, and values for the muscle-tendon parameters.

6.3.1 Surgical Model

We performed a preliminary anatomical study to ascertain how the changes in muscle attachment locations, resulting from a Chiari osteotomy, could be characterized. On each of three fresh cadavers, the most anterior and posterior points of the gluteus medius origin were first marked with metal pins. The line connecting these two points was bisected, and marked with a pin, to locate a third point representing the medial origin. The distance from origin to insertion (muscle-tendon length) was then measured as the distance from each of the three metal pins to the insertion on the greater trochanter. We performed a Chiari osteotomy on each cadaver with various angulation and displacement. The muscle-tendon lengths were again measured on each cadaver. Measured changes in muscle-tendon length showed that it was nearly impossible to perform the osteotomy with no relative rotation of the two bone fragments. We therefore included an internal rotation angle (representing the relative rotation) in the surgical model in addition to the angulation and the displacement.

As a result of the anatomical study and my colleagues' (Eugene Bleck and Gerard Bollini) clinical experience, we characterized the Chiari osteotomy with three geometric parameters: angulation of the osteotomy (*ang*), distance of medial displacement (*dis*), and angle of internal rotation (*rot*) (Figure 6.1). Angulation and displacement were defined by their projection in the frontal plane. Relative rotation of the two bone fragments was computed about a vertical axis

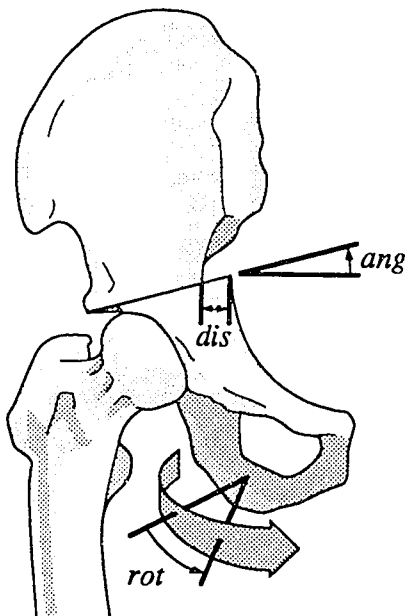


Figure 6.1. Surgical parameters. The Chiari osteotomy was characterized by the angulation of the osteotomy (*ang*), distance of medial displacement (*dis*), and the internal rotation angle (*rot*). From Delp et al. [29].

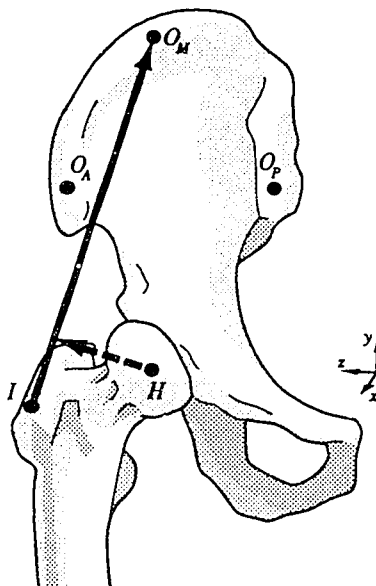
passing through the sacroiliac joint. Even though the proximal fragment of the innominate bone may rotate about the sacroiliac joint, it was assumed to remain fixed while the distal fragment translates and rotates as a rigid body. The abductor muscle origins are therefore unchanged in the surgical model, but the joint center and muscle insertions do change, and were computed with three-dimensional geometric transformations. The surgical model thus calculates the postsurgery hip joint center and muscle insertions given values for the surgical parameters.

6.3.2 Musculoskeletal Model †

The musculoskeletal model describes not only the geometric relationships of the muscles and bones (the musculoskeletal geometry), but also the muscle-tendon parameters, so that the maximum isometric hip abductor moment can be computed at any hip abduction angle. The musculoskeletal model thus consists of coordinates for muscle attachments and a model for each muscle-tendon compartment.

Presurgery coordinates for the three primary hip abductors were taken from data reported by Brand *et al.* [13]. Two of the hip abductors, gluteus minimus and tensor fasciae latae, were modeled as single lines from origin to insertion. The third, gluteus medius, was decomposed into anterior, medial, and posterior muscle-tendon compartments (Figure 6.2). From purely musculoskeletal geometric data, muscle moment arms and muscle-tendon lengths (origin to insertion lengths) can be computed. However, to find abductor moment (the product of force and moment arm), muscle force must also be calculated.

Figure 6.2. Musculoskeletal coordinates for the gluteus medius. O_A , O_M , and O_P , represent anterior, medial, and posterior muscle origins, respectively. I represents the muscle insertion. H is the hip joint center. Muscle-tendon length (solid line) and muscle moment arm (dashed line) can be computed from these coordinates. From Delp *et al.* [29].



† The musculoskeletal model of the human hip that was used to analyze the Chiari osteotomy was developed before the graphics-based model of the entire lower extremity. Thus, some of the muscle attachment coordinates and muscle-tendon parameters are slightly different than those presented in Appendices A and B. These slight differences do not affect the basic conclusions of this analysis.

To compute maximum isometric muscle force as a function of muscle-tendon length we formulated a model for each of the five muscle-tendon compartments (one for gluteus minimus, one for tensor fasciae latae, and three for gluteus medius). Each muscle-tendon model, which accounts for the static properties of both muscle [48] and tendon [144] of that compartment, was formed from a generic model [150]. When the generic model is scaled by a muscle's physiological cross-sectional area, optimal muscle-fiber length, and tendon slack length, the force-length relation of a specific muscle-tendon compartment can be computed [150]. Nominal values for physiological cross-sectional area were taken from Brand *et al.* [14]. Muscle-fiber lengths were taken from Friederich and Brand [43]. When muscle attachments are specified, as above, tendon slack length (tendon's length at which force begins to develop on elongation of a muscle-tendon complex) determines the joint angles where a muscle-tendon compartment develops moment [150]. Tendon slack length was specified so that the abductor moment computed with the musculoskeletal model matched moment measured during maximum voluntary contraction of the hip abductors under isometric conditions [99] (Figure 6.3, below). Passive muscle force was not included in this analysis; hence, the muscle-tendon model computes maximum, active muscle force at any muscle-tendon length.

Once muscle attachment sites and muscle-tendon parameters were specified, maximum isometric hip abductor moment was computed as follows. First, at each joint angle, the length of each muscle-tendon compartment was calculated as the magnitude of the vector from its origin to its insertion. The muscle-tendon model was then used to find the muscle force at the computed length. Abductor moment for each muscle compartment was computed as the moment of muscle force about the hip joint center. Individual muscle moments from gluteus medius (three components), gluteus minimus, and tensor fasciae latae were summed to find the total abduction moment.

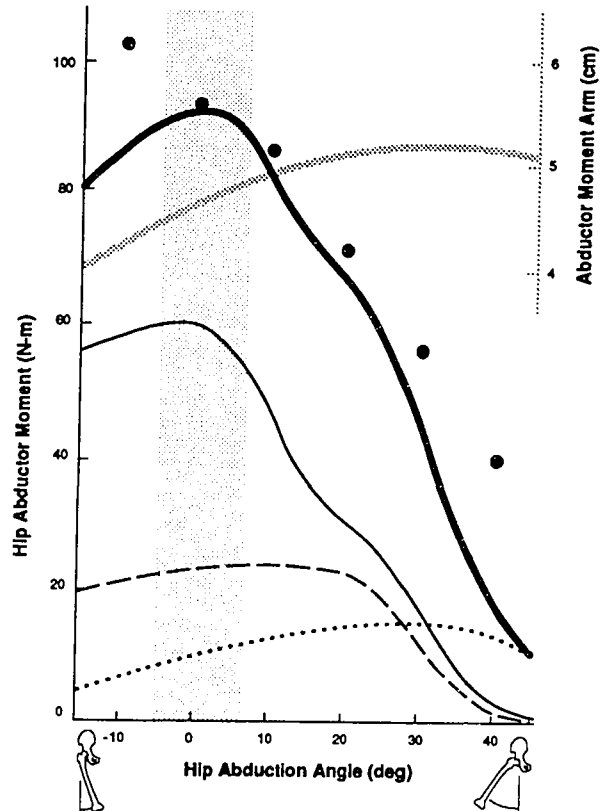
6.3.3 Simulations of Surgery

The surgical and musculoskeletal models were combined to simulate the effect of a Chiari osteotomy on abductor moment. To initiate a surgery simulation, a value for each surgical parameter was specified. The surgical model then computed the postsurgery muscle insertions and the joint center. These intermediate results were subsequently used in the musculoskeletal model to compute postsurgery gluteus medius abductor moment for joint angles ranging from 15° to 45° of abduction. Both presurgery and postsurgery moments were then plotted versus hip abduction angle.

6.4 Results

Figure 6.3 compares the computed presurgery hip abductor moment to the moment measured during maximum voluntary isometric contraction of the hip abductor muscles [99]. Notice the close correspondence between computed and measured hip abductor moment (compare the thick-

Figure 6.3. Comparison of computed and experimental hip abductor moments. Computed moments of tensor fasciae latae (dotted line), gluteus minimus (dashed line), and the three compartments of gluteus medius (thin-solid line) were summed to produce the total computed moment (thick-solid line) which compares well with abductor strength measurements [99] (large dots). The average gluteus medius moment arm is the gray line. The shaded area represents the range of hip abduction used in walking (-5° to $+7^{\circ}$). From Delp et al. [29].



solid line and the large dots). The peak moment and the shape of the curve (decreasing moment with abduction) generated by the model also correspond with other measurements of hip abductor strength [89, 95].

Moment decreases as the hip abducts because the muscles develop less force as their fibers shorten with abduction. The model shows that the gluteus medius moment arm does not decrease with abduction (gray line, Figure 6.3). Moment arms of similar magnitude have also been measured radiographically [99]. Since abductor moment is the product of muscle force and moment arm, and since moment arm does not decrease, the decrease in abductor moment with increasing abduction must result from decreased muscle force. It is also clear that abducting the hip brings the muscle origins and insertions closer together—shortening the muscle. As the muscle gets shorter with abduction, there is a decrease in muscle force. It can be concluded, therefore, that the hip abductors normally operate on the ascending region of their force-length curve.

Figure 6.3 also shows that the gluteus medius (thin-solid line) contributes about 70% and the gluteus minimus (dashed line) contributes about 20% to the total hip abductor moment (thick-solid line) near anatomical position (shaded region). Since these two muscles provide such a large proportion of the total moment, it is necessary that each muscle operates on the ascending

region of its force-length curve (i.e., force decreases as the muscle shortens) in order to match experimental data [89, 95, 99].

The gluteus medius and minimus have similar paths from the lateral surface of the ilium to the greater trochanter and were therefore affected similarly in the simulations of surgery. Because gluteus medius has more than twice the cross-sectional area of gluteus minimus [14, 25], and since the hip operates between -5° and 7° of abduction during gait [68], the results focus on moment produced by the gluteus medius in that region.

Simulation of the surgery showed that some sets of surgical parameters conserve gluteus medius abductor moment while others reduce it significantly. For example, with -5° of angulation, 10° of external rotation, and 15 mm of medial displacement (technique 1), postsurgery abductor moment is reduced by only 10% at anatomical position (Figure 6.4A). In contrast, 30° of angulation, 10° of internal rotation, and 30 mm of medial displacement (technique 2) reduces postsurgery abductor moment by 65% at anatomical position (Figure 6.4B).

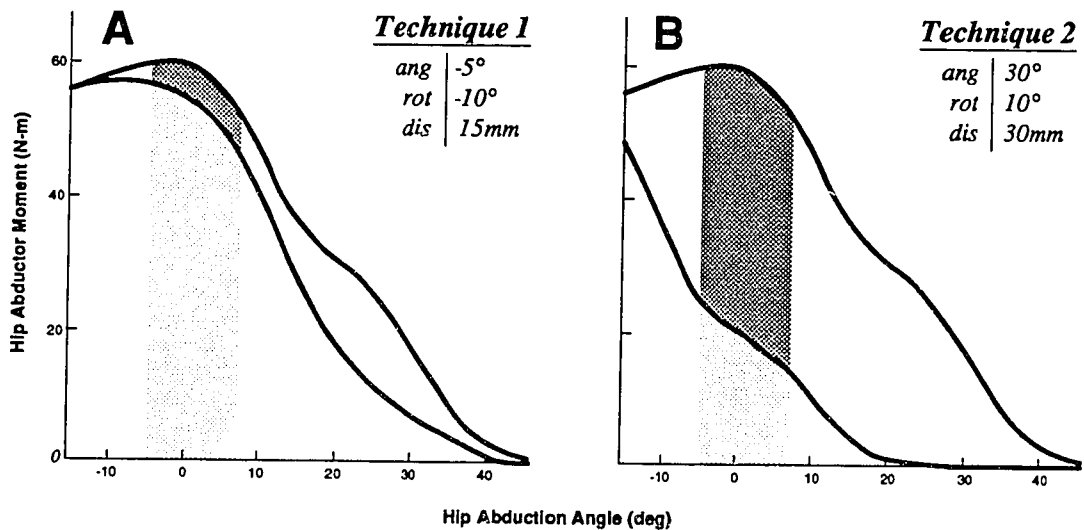


Figure 6.4. Results of two surgery simulations. Presurgery gluteus medius abductor moment (upper curve) is compared with postsurgery gluteus medius moment (lower curve). The darkly shaded area highlights the difference between presurgery and postsurgery curves in the range of hip abduction used in walking (entire shaded area). (A) Technique 1, a nearly horizontal osteotomy, conserves abductor moment. (B) Technique 2, with high angulation, reduces abductor moment significantly. From Delp et al. [29].

Table 6.1 shows moment arm, muscle force, muscle-tendon length, change in muscle-tendon length, and abductor moment computed in the two simulated surgeries. With technique 1, the average muscle moment arm is the same as before surgery; the muscle-tendon length is

decreased by only 1 cm, and consequently the muscle force, which depends on muscle length, is reduced by only 15%. Since both moment arm and muscle force are altered very slightly, technique 1 preserves abductor moment. Even though technique 2 increases the muscle moment arm, there is a decrease in abductor moment because of reduced muscle force. The muscle is able to develop much less force because the high angulation, combined with the large medial displacement, brings the gluteus medius insertion closer to the origin, reducing the muscle-tendon length by 2.6 cm. Because the muscle fibers of the gluteus medius are short (5-8 cm), the 2.6 cm change represents a large decrease in length (52-32%). This large decrease in muscle-fiber length causes a 68% reduction in muscle force in technique 2.

Table 6.1. Gluteus Medius Parameters at Anatomical Position

	Moment Arm (cm)*	Muscle Force (N)	Muscle- Tendon Length (cm)*	Change in Muscle- Tendon Length (cm)	Abduction Moment (Nm)†
Presurgery	4.5	1300	12.5	n/a	59
Technique 1 (Fig. 6.4A)	4.5	1100	11.5	-1.0	53
Technique 2 (Fig. 6.4B)	5.0	410	9.9	-2.6	21

* Average of the three gluteus medius components weighted by physiologic cross-sectional area.

† Abduction moment was computed as the sum of the individual moments from the three components of the gluteus medius, which does is not necessarily equal the average muscle moment arm times muscle force.

Figure 6.5 shows how each surgical parameter affects the postsurgery abductor moment. Postsurgery abductor moment decreases, as the angulation of the osteotomy increases (Figure 6.5A), suggesting that angulation should be kept near the horizontal to preserve gluteus medius strength. The internal rotation angle has little effect on the postsurgery abductor moment (Figure 6.5B). The effect of medial displacement depends on the angulation. Figure 6.5C shows that increasing displacement significantly reduces abductor moment, when angulation is above the horizontal. With a flat osteotomy (Figure 6.5D), increasing the length of medial displacement has a small effect on abductor moment. A nearly horizontal osteotomy therefore allows large displacement without a significant decrease in abductor moment.

Hip abductor moment may decrease from a reduction in either muscle force or muscle moment arm. Because muscle force is a function of its length, it is essential to consider the effect

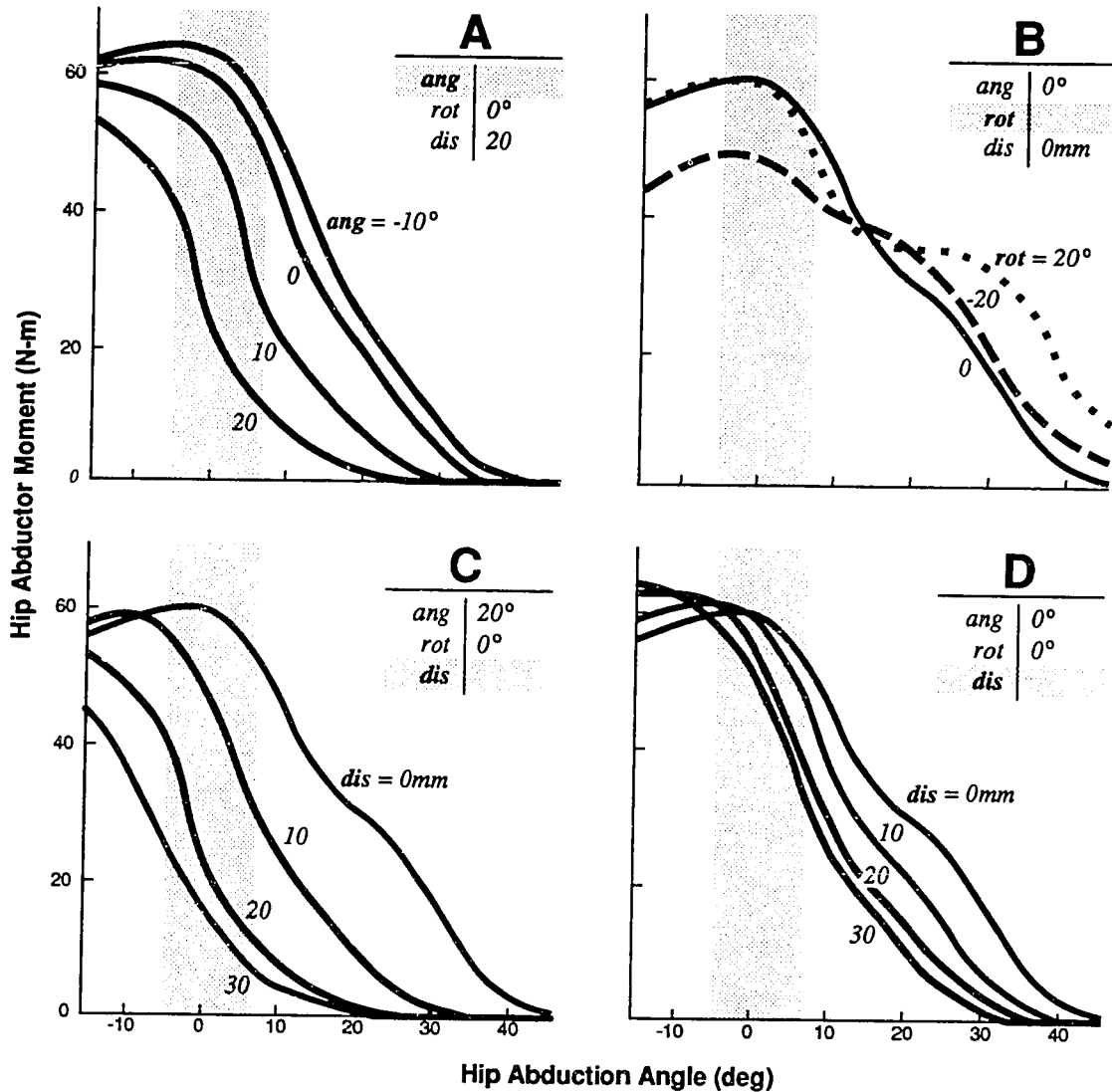


Figure 6.5. The effect of each surgical parameter on gluteus medius abductor moment. The shaded area represents the range of hip abduction used in walking. (A) Effect of angulation. Moment decreases as angulation increases, suggesting that the angulation should be kept as small as possible to preserve abductor moment. (B) Effect of internal rotation angle. Postsurgery gluteus medius abductor moment is higher with 20° of internal rotation (dots) than with 20° of external rotation (dashes) because the maximum moment arm occurs at 15° of internal rotation. The presurgery curve is the solid line. (C) Effect of medial displacement with large angulation. Abductor moment decreases as displacement increases when angulation is above the horizontal. (D) Effect of medial displacement with a flat osteotomy. Abductor moment is preserved, even with large displacement, when the osteotomy is horizontal. From Delp et al. [29].

of surgery on muscle-tendon length. As the angle of the osteotomy is increased cephalad, the gluteus medius length is decreased. Also, when the angulation is above the horizontal plane, increasing the length of medial displacement further reduces muscle-tendon length. Surgical simulations with both large angulation and displacement greatly reduce muscle length, leaving the muscle almost fully shortened at anatomical position. A reduction in muscle length reduces muscle force, causing a large decrease in abductor moment. Internal rotation lengthens the posterior aspect of the gluteus medius and shortens the anterior aspect. External rotation has the opposite effect. In the model, the maximum frontal plane moment arm occurs at about fifteen degrees of internal rotation. The reduction in abductor moment due to change in muscle moment arm was found to be much less significant than the reduction caused by decreased muscle length.

6.5 Discussion

Our computer simulations of Chiari osteotomy mechanics show that certain sets of surgical parameters (i.e., surgical techniques) cause a dramatic reduction (e.g., 65%) in gluteus medius abduction moment. Is this enough to cause a limp? It has been estimated the abductors must generate a force of approximately 1.5 times body weight for normal walking [90]. Under this assumption, a person weighing 78kg must generate about 1200N of abductor force to support the pelvis during gait. In a study of abductor muscle strength, thirty male subjects, with an average weight of 78kg, were able to produce an average abductor force of 2100N at anatomical position [99]. In this case, a 45% decrease in abductor strength would leave about 1200N—the amount required for normal walking. Therefore, a decrease in force (moment) greater than 45% would presumably cause a limp. These experimental results agree with the clinical finding that about half of the maximum moment of the hip abductors, unlike other muscle groups, is required for normal walking [105].

Because the changes in abductor moment due to moment arm effects are small compared to those caused by reduced muscle length, the limp from abductor weakness, after the Chiari osteotomy, is more likely caused by shortening the muscle than by reducing its moment arm. Bailey and Hall [3] have suggested that shortening the gluteus medius caused the Trendelenburg gait. However, they explained the limp in terms of reduced muscle moment arm instead of reduced muscle force, stating that the Chiari osteotomy “. . . brings the insertion of the gluteus medius closer to its origin and destroys the fulcrum around which it functions, thus the often persistent Trendelenburg gait [3].” The computer model, which isolated the effects of muscle length and muscle moment arm, clearly showed that changing muscle length is more important than muscle moment arm.

Gougeon *et al.* [51] have suggested that the Chiari osteotomy be performed as vertically as possible (i.e., with high angulation) to ease medial displacement and improve femoral head coverage. However, our simulations indicate that high angulation shortens the gluteus medius, causing

a reduction in abductor moment, thus increasing the risk of a persistent limp. These results suggest that the angulation be kept less than 10° above the horizontal to prevent excessive shortening of the gluteus medius and to preserve abductor strength. If a horizontal osteotomy is not possible, musculoskeletal geometry should still be adjusted to preserve the length of the gluteus medius.

Maintaining the length of the hip abductors is also important in other operative procedures. For example, trochanteric osteotomy has been proposed as a method for increasing the length of the hip abductor muscles to preserve abductor moment in patients undergoing total hip arthroplasty [21]. While some have seen good results with this technique [21, 34, 73], others have reported little or no evidence of improved abductor strength with increasing length [50, 92]. A recent study of 53 patients, however, showed that the best moment values were achieved by keeping the gluteus medius within 1 cm of its original length [10]. This clinical finding is in agreement with the model presented here, in which the gluteus medius operates near optimal length (producing maximum force) at anatomical position. In this case, both dramatic lengthening or shortening would result in decreased active muscle force at anatomical position. In Chiari's procedure, it is usually possible to maintain gluteus medius length without a trochanteric osteotomy.

It is important to discuss the assumptions and limitations of this study. First, with regard to the musculoskeletal model, we assumed that the muscle-tendon parameters (physiological cross-sectional area, optimal muscle-fiber length, and tendon slack length) were not affected by the surgery. Only the effect of musculoskeletal geometry on abductor moment was considered, even though muscle atrophy or nerve damage could certainly cause abductor weakness. In fact, a wide variety of biological and psychological factors that could lead to the Trendelenburg limp were neglected because they are very difficult to model. For example, a postoperative patient apprehensive of pain may instinctively lean over the involved hip to decrease the compressive joint load by reducing the tension in the hip abductors. If this pattern of walking should become habitual, it could lead to disuse atrophy of the hip abductors and a chronic Trendelenburg limp. The causes of a limp following surgery are multifarious, and it was not our intention to account for all of them. Rather, our objective was to determine if there could be a biomechanical basis for the decrease in abductor strength following the Chiari osteotomy. For this purpose, analysis of a computer model, which isolates the effects of each surgical parameter on abductor moment and leaves muscle physiological properties constant, as performed here, seems to be a reasonable approach.

Second, the contribution of gluteus maximus to abductor moment was not included. Although the anterior fibers of the gluteus maximus can contribute to abductor moment, modeling showed that they only become significant at high angles of abduction. Near the anatomical position (i.e., near 0° of abduction), gluteus maximus was found to contribute very little to abductor moment. Because the hip operates near 0° of abduction during walking [68], this study focused

on gluteus medius since it provides such a large proportion of the total abduction moment in that region. Considering gluteus medius alone is further justified by its similarity to gluteus minimus since they were affected similarly in the surgery simulations and, together, contribute over 80% of the total abductor moment near anatomical position.

Finally, the Chiari osteotomy was modeled with only three geometric parameters. Although the geometry of an actual osteotomy is certainly more complex, (e.g., there may be rotation about an anterior-posterior axis) many clinically reasonable configurations of pelvic geometry may be approximated with these three parameters. The geometric changes calculated with the surgical model make intuitive sense (e.g., high angulation combined with displacement shortens the gluteus medius) and are in accord with both our anatomical study and geometric models of proximal femoral osteotomies [15].

6.6 Conclusion

The conclusion that a nearly horizontal osteotomy preserves abductor moment is not sensitive to the details of the model, but is based only on the following general observations: (1) high angulation reduces the distance between origin and insertion of the gluteus medius. A more horizontal osteotomy preserves gluteus medius length; (2) decreasing the length of the gluteus medius reduces the force it can develop whereas maintaining its length preserves abductor muscle force and moment.

7 Conclusion

The goal of this dissertation was to explore the utility of simulating the effects of various surgical procedures on the moment-generating capacity of the lower-extremity muscles. To achieve this goal, we developed a computer graphics system to analyze and design musculoskeletal reconstructions of the lower limb. The summary result is that our existing surgery simulator can be used to gain insight into how the parameters of various surgical procedures affect muscle strength. A significant amount of future work is needed to simulate surgeries on individual patients.

Work on this surgery simulation project will continue beyond the scope of this dissertation. However, with the completion of the first graphics-based model of the human lower extremity, and its application to a variety of clinical problems, several punctuation marks are in order. This chapter summarizes the contributions of this dissertation, outlines some of the limitations of the existing system, and lays out plans to expand the limits and applications of surgery simulation.

7.1 Contributions

As described in Chapter 2, other surgery simulation and musculoskeletal modeling projects are underway. Within the context of these efforts, the main contributions of this dissertation are:

- creation of a software system that enables users to develop, alter, and analyze models of many different musculoskeletal structures on a computer graphics workstation,
- development of a graphics-based model that describes the isometric moment-generating characteristics of all the major muscles in the lower limb,
- analysis of the biomechanical consequences of tendon transfers, tendon lengthenings, and pelvic osteotomies.

The next three sections summarize each of these contributions and outline extensions of this work.

7.2 Applications and Extensions of the Musculoskeletal Modeling Software

As part of the surgery simulation project, we have developed a software system that allows one to create, modify, and analyze models of a wide variety of musculoskeletal structures. To date, we have used this software to develop a model of the human lower limb only. However, there are

several other applications of this software. For example, the software can be used to develop models of other musculoskeletal structures, such as the upper limb and hand. To develop these models, one must describe the surface geometry of the bones, define the paths and parameters of the muscles, and specify the kinematics of the joints. The software tools, such as the joint editor and the muscle editor, make the process of developing a model very efficient.

A model of the upper limb or hand could be used to simulate tendon transfers as we have done with the lower-limb model. Tendon transfers in the hand are commonly performed in stroke, trauma, cerebral palsy, and spinal cord injury patients [9, 11]. Since the objective of these procedures is to supplement the function of lost or dysfunctional muscles, correct selection of muscles for transfer and optimal routing of the tendon paths is essential so that the transferred muscles can generate the moments needed to regain the lost function. The graphical manipulation of muscle-tendon paths and joint kinematics that is possible with our software provides an excellent environment in which to explore various surgical options. This is similar to the approach used by Buford and Thompson [16] to simulate tendon transfers in the hand. However, since they do not calculate muscle-tendon forces, their analysis of simulated tendon transfers is limited to the effects on moment arms and muscle-tendon excursions. If their detailed models of the thumb and finger tendons [128] were implemented within our system, evaluation of simulated surgeries would include muscle forces and joint moments.

The applications of this software are not limited to simulating surgery. Musculoskeletal models are also needed to actuate dynamic models of human movement. For instance, in our lab alone, distinct musculoskeletal models have been developed to study walking [147], standing [70], jumping [103], and postural control [49]. Other research groups have developed musculoskeletal models to study the forces and moments generated in the frog [80] and the cat [76, 149]. Indeed, a large number of musculoskeletal models have been developed independently, each requiring a great deal of effort to create. Since our software assists in developing models of many different musculoskeletal structures, it can enhance the productivity of investigators working on diverse problems in biomechanics.

One of the limitations of using our existing software to develop models for studying the dynamics of movement is our model of muscle and tendon. The current muscle-tendon model computes maximum isometric force by assuming that the muscles are maximally activated and held isometric. These conditions are approximated when measuring isometric moments during maximum voluntary contractions, but rarely occur during movement. Thus, our muscle-tendon model must be modified to include muscle-tendon dynamics and variable activation to be used for dynamic analysis [150]. Since the muscle-tendon model is a distinct module within our software, including muscle-tendon dynamics and variable activation is straight-forward.

7.3 Applications and Extensions of the Lower-Extremity Model

Our model specifies the musculoskeletal geometry and musculotendon parameters of forty-three muscles in the lower limb. With this model the maximum isometric force and joint moments that each muscle develops can be computed at any body position. The model can be manipulated on the computer graphics system to study how each model parameter affects muscle strength.

We are enhancing the graphical interface to the model so that it can be used to analyze movement. Currently, the user interface allows only one joint angle to be varied at a time. We are now adding the capability to simultaneously vary multiple joint angles by reading an animation sequence that specifies the joint angles for an activity, such as walking or cycling. An animation sequence can be created from motion-analysis data or dynamic simulations of movement. Animating the lower limb model will provide a new tool for analyzing normal and pathologic movement. Imagine the following scenario. A child with cerebral palsy is examined in a gait-analysis laboratory. Rather than analyzing plots of the joint angles vs. percent of gait cycle, as is routinely done, we will be able to display the child's movement as an animated figure. The animated motion can be analyzed from any viewing perspective, at any speed, on the computer screen [28]. Further, the lengths and velocities of each muscle-tendon complex, as determined from the joint angles and velocities, will be plotted along with the animated figure. Thus, presurgery and postsurgery gait can be compared in terms of muscle-tendon lengths and velocities. Since lengths and velocities will be calculated using the nominal model, they must be normalized (e.g., muscle-tendon length can be normalized by length at anatomical position). This approach, which has been used to analyze the lengths of the hamstrings in cerebral palsy walking [111], will be extended to include all the muscles in the lower limb with our model.

We are also creating the capability to analyze the accelerations induced by the muscles [151] during any activity. To do this, additional input files that specify the body's inertial parameters and equations of motion are needed. For a given activity (e.g., walking), the software will calculate the muscle-induced accelerations at each point in the motion sequence. The motivation for this analysis is as follows. With surgery simulation, we now have a tool to study how surgery affects the capacity of muscles to generate force. But, we really have no idea of how the changes in the muscle forces affect the angular accelerations of the joints. To help design gait-correcting surgeries, both forces and induced accelerations should be analyzed.

7.4 Clinical Applications

This section summarizes the clinical findings from completed surgery simulations and suggests applications to other clinical problems.

Summary of clinical findings. We have applied our model of the lower limb to analyze tendon lengthenings and pelvic osteotomies. Our analysis of tendon lengthenings (Chapter 5) indicates that the forces generated by the ankle plantarflexors are extremely sensitive to surgical length-

ening of tendon. Other muscles are much less sensitive. Quantifying the sensitivity of the muscle forces and joint moments to changes in tendon length provides important new data needed to design effective tendon surgeries. Our simulations of the Chiari pelvic osteotomy (Chapter 6) revealed that the limp from abductor weakness, which often occurs after this procedure, may be caused by shortening of the abductors. Shortening the abductors can be avoided by keeping the angulation of the osteotomy less than 10° above the horizontal.

Application to muscle-tendon surgery. Surgery simulation can provide information relevant to three situations that arise in muscle-tendon surgery. In some situations, the forces and moments generated by a spastic or contracted (shortened) muscle are extremely disruptive to movement, so the surgeon chooses to eliminate the muscle completely (e.g., with tenotomy). Our model can estimate how total joint moment changes when a muscle is eliminated. A second situation arises when a surgeon wants to weaken a muscle via tendon lengthening, but not eliminate it completely, because this may cause too much weakness or an imbalance of joint moments. In this situation, we can estimate how force changes for a given increase in tendon length and how this change affects the total joint moments (strength). The third situation is transferring a tendon to change its function. We can answer three questions relevant to tendon transfers. They are: (i) Is it possible to achieve the desired postsurgery forces and moments given the parameters (i.e., peak force, fiber length, tendon length) of a candidate muscle? (ii) How can the geometry of the transfer be optimized to achieve maximum force and moment over the desired range of motion? (iii) How much strength is lost from the donor site?

Several common surgical procedures could be analyzed to answer the questions posed above. Results of these analyses should be presented to a clinical audience. Specifically, I suggest that a detailed analysis of Achilles tendon lengthening be performed to study the changes in the plantarflexion moment vs. ankle angle curve that are caused by this common surgical procedure. This analysis should consider the effects of muscle-tendon contracture. I also suggest an analysis of hamstring lengthenings to demonstrate the effects of these surgical procedures on the knee and hip moment curves. To support the analysis of hamstring lengthenings, it would be helpful to model lengthening of the internal tendon, since the aponeurosis of semimembranosus is commonly lengthened. Finally, I suggest a detailed analysis of an anterior transfer of the tibialis posterior to evaluate the tradeoffs among the various surgical techniques. This is an interesting procedure in that a muscle with short fibers (tibialis posterior) is used to supplement the function of a muscle with long fibers (tibialis anterior). Some controversy exists as to whether the tendon should be routed under the retinacula to reduce excursion or over the retinacula to increase moment arm. There is a wealth of clinical literature related to this problem, but very little biomechanical analysis.

Application to osteotomies. The primary conclusion of our analysis of the Chiari osteotomy is that the surgical procedure should be performed such that the length of the hip abductor muscles is maintained (Chapter 6). Our results suggest that osteotomies performed with high angulation shorten the length of the hip abductors and therefore may lead to a limp from abductor weakness. A logical extension of these surgery simulations is to perform a prospective or retrospective study to determine if patients who undergo a Chiari osteotomy with high angulation indeed have a higher incidence of the postoperative limp. Unfortunately, we (at Stanford) do not have a large series of patients on which we can perform such a clinical study. Our hope is that our recent journal article [29] will motivate a clinical investigation.

Simulating surgeries has both advantages and disadvantages with respect to clinical studies. The advantage of simulation is that the effect of a single change, such as the angle of an osteotomy, can be modeled without the confounding effects of poorly understood, unpredictable changes. This kind of advantage cannot be realized in a clinical study [15]. The disadvantage of simulations is that the actual surgery may, in fact, produce several changes (e.g. pain) that are not accounted for in the model. It may therefore be valuable to study a variety of patients before and after surgery, and to simulate their particular surgery. This approach may help gain confidence in the model, but it is not without problems. In comparing actual surgeries with simulations, effects that cannot be modeled (e.g., psychological factors) may, in some cases, determine the surgical outcome. Thus, it may not be clear whether the results of the actual and simulated surgeries agree (or disagree) because of these confounding effects, or because the surgery was modeled accurately. Clearly, both simulations and clinical studies are needed to design improved surgical procedures. To date, many more clinical studies have been performed. Thus, one important role of simulations is to analyze unexplained clinical results that are reported in the literature.

Application to joint replacements. In total hip replacement, surgeons often change the geometry of the hip joint and the surrounding musculature. For example, the center of the hip may be moved medially, or the greater trochanter may be transplanted to a new location [21]. These geometric changes affect the moment-generating capacity of the muscles that cross the hip. I have begun to study the effects of hip prosthesis design and surgical technique on hip muscular strength. This investigation will determine the positions of the hip center that maximize and minimize the isometric moments that can be generated by each muscle group (e.g., the hip abductors), and point out the trade-offs associated with various surgical alternatives.

A significant advance in the simulation of joint replacements could be made by interfacing our surgery simulation system with the bone remodeling algorithms developed by Carter *et al.* [19]. Prosthesis loosening and adverse bone remodeling are the main problems associated with total joint replacement. Since bone remodeling algorithms account for the effects of changing prosthesis geometry on bone structure, they provide ideal tools to investigate these problems. To

date, a major shortcoming of all studies of skeletal adaptation has been the oversimplification of the loads that are imposed on skeletal structures by the muscles. For example, in analyses of femoral loading, orthopaedic researchers typically include only a single abductor load. Recently, however, Orr has included the lines of action from our lower-limb model into bone remodeling simulations [100]. Integrating bone remodeling theories with our surgery simulation software would provide a powerful tool for analyzing the effects of prosthesis design and surgical technique on both muscular strength and skeletal adaptation.

Application to complex reconstructions. Some clinical problems, such as malignant tumors and severe traumatic injuries, require complex reconstructions of bone, muscle, and tendon. Historically, these problems were too complex or severe to allow reconstruction, and therefore required amputation. Surgeons are now able to salvage these limbs with microsurgical transfers and allografts. However, the ultimate function of the reconstructed limbs remains limited. There are many choices to be made when planning complex reconstructions; thus, analysis of these procedures is an ideal application of our surgery simulator. For example, surgeons must decide whether to use a “distant” muscle from some other part of the body or a “local” muscle that resides in the damaged limb to cover a defect [33, 82]. Our computer model may help improve the functional outcome of a reconstruction by guiding surgeons to the best approach to a specific, complex problem. These problems are particularly well suited for analysis with our simulator since trauma patients, unlike patients with chronic disease, have relatively normal muscle-tendon parameters. Joseph Rosen has initiated an investigation of soleus and gastrocnemius flaps that are used to cover type III tibial defects. Together, we will determine how the various surgical options affect plantarflexion strength. We plan to include a retrospective study of patients who have undergone these surgeries in this investigation.

7.5 Future Work

Some of the other possible future directions of this work include:

Improving joint models. Currently, our joint models are kinematic. That is, the motion of the joints does not depend on force. The main purpose of these kinematic models is to produce reasonable moment arms and excursions of the muscles that cross each joint. Developing kinetic joint models that move according to ligament, bone, and muscle forces may improve the accuracy of musculoskeletal models. These improved joint models would also provide additional information, such as bone-on-bone forces, that would be useful for simulating total joint replacements.

Obtaining patient-specific data. Data describing the bone surfaces for a specific patient can be derived from computed tomography (CT) or magnetic resonance (MR). However, no method has been implemented to automatically determine muscle geometry or muscle-tendon parameters from medical image data. Developing an automated means to determine both muscle and bone geometry of an individual patient would be a major step toward simulating patient-specific surgeries.

Representing muscles as volumes. We currently represent muscles as a series of line segments. Representing muscles as volumes has several advantages. The constraint that muscle fibers are of equal length within a given muscle could be relaxed by constructing 3D muscles from individual fibers that run between tendon plates. The force in the muscle would be calculated as the sum of the forces in the fibers, which could be at different lengths. The geometric relationships among the muscles and the bones could also be represented more realistically with 3D muscles, so more accurate moment arms could be computed. Thus, muscles that are geometrically and architecturally complex, such as the vastus muscles, could be represented more accurately. Volumetric muscles would also enhance visualization. The major problem associated with representing muscles as volumes is determining how they deform as the joints are moved and forces are developed.

Simulating postsurgery gait. We currently evaluate the results of simulated surgeries in terms of the maximum isometric joint moments that can be developed by the muscles. Simulating postsurgery gait would provide a more useful evaluation for analysis of gait-correcting surgeries. A major problem associated with dynamic simulation of gait is that the motions of the body segments are very sensitive to the muscle activation patterns [147]. Thus, it is difficult to determine the muscle activations such that a complex dynamic model walks normally. Simulation of pathologic gait is even more difficult. Dynamic optimization of walking may provide a means to simulate postsurgery gait. Dynamic optimization has been performed for jumping [103], kicking [57], the swing phase of gait [27], and recently for 96% of the gait cycle [147].

Improving the user interface. Our interface design has focused on engineering users. Thus, one interacts with our model much like one would interact with a computer-aided design (CAD) system. Virtual environments may provide a more natural interface for surgeons and other clinical users. In a 3-month project, Steve Pieper, of the MIT Media Lab, implemented our lower-limb model in NASA's virtual environment [41]. The ability to efficiently interact with the model was limited by the system performance. However, this pilot project showed that, with improved performance, the virtual environment holds promise as an improved user interface for simulating surgery.

Performing additional experiments. Additional experimental data are needed to gain confidence in the model. A consistent set of experimental data that indicate how maximum isometric joint moments vary with joint angles does not exist. Thus, we had to compare our simulated joint moments with experimental joint moments measured by a number of different investigators on a number of different populations. A complete set of strength curves that were obtained from a homogeneous population would bolster confidence in the model.

Other experimental and theoretical work could be directed at answering the following questions.

Some of the remaining questions are:

- How do the muscle-tendon parameters scale among subjects of different sizes, body types, and activity histories?
- How are the muscle-tendon parameters altered in stroke and cerebral palsy? How are these changes manifested in the active and passive moment curves?
- How do muscle and tendon adapt to an electromechanical milieu of imposed forces, lengths, velocities, and activation patterns? Can the adaptive response of muscle and tendon be formulated mathematically? How is adaptation altered in pathologic states?
- What are the actual muscle activations during maximum voluntary contraction (MVC) experiments?
- How do changes in the forces that can be developed by the muscles affect the dynamics of the resulting movement?
- Is it possible to model the *neuromusculoskeletal* system accurately enough so that simulated surgeries can be evaluated in terms of postsurgery gait rather than isometric joint moments?
- What user interface tools will make simulations accessible to a larger group of practicing surgeons? Will surgery simulators have a significant impact on surgical training as flight simulators have had on the training of pilots?

This dissertation has shown that computer graphics models are valuable tools for analyzing the biomechanical consequences of musculoskeletal reconstructions. Our lower-limb model has been used to determine which parameters of various surgical procedures have the greatest effect on muscle strength. However, a significant amount of future work is needed to make possible the simulation of surgeries specific to individual patients.

It is my hope that insight gained from surgery simulations will improve the quality of life for those suffering from musculoskeletal and neuromuscular diseases. There are two keys to maximizing the impact of surgery simulation on patient well-being. First, surgery simulations should focus on answering specific, clinically relevant questions. Second, we must understand the limitations of existing surgery simulations and direct future experimental and theoretical work toward eliminating those limitations.

Appendix A

Muscle File for Lower-Extremity Model

The muscle file shown on the following pages specifies the lines of action and parameters needed to compute isometric forces for 43 muscle-tendon complexes in the lower limb. The file is scanned by the musculoskeletal modeling software (Chapter 3) which creates a data structure that represents the muscles (Figure A1). The file is passed through the preprocessor “cpp” so that C-style comments (demarcated with `/* */`) and “#define” statements can be used in the muscle file.

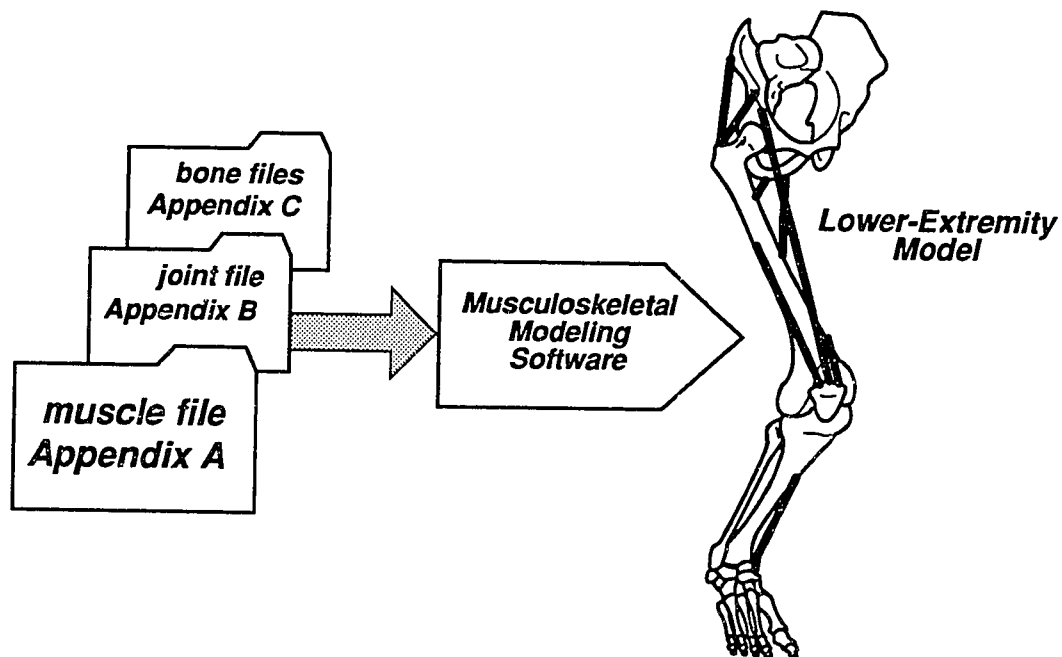


Figure A1. The muscle, bone, and joint files are scanned by the musculoskeletal modeling software to create a data structure that represents the lower limb. Appendix A gives a detailed description of the muscle input file.

 Muscle File
 August 20, 1990

Muscle Input file for use with 7 segment, 7 degree-of-freedom lower limb model

This muscle file specifies: (1) a dimensionless force-length curve for tendon, (2) dimensionless force-length curves for muscle, (3) a dimensionless force-velocity curve for muscle, and (4) definitions of each muscle. The definition of each muscle contains a list of coordinates that describe its line of action and the parameters (peak isometric force, optimal fiber length, tendon slack length, and pennation angle) needed to compute isometric muscle force. The model is assumed to be a right leg.

References are given for each muscle-tendon parameter. These references are:

Brand: Brand, Peterson, and Friederich, "The sensitivity of muscle force predictions to changes in physiologic cross-sectional area," *J. Biomech.*, Vol. 19, pp. 589-596, 1986.

Wick: Wickiewicz, et al., "Muscle architecture of the human lower limb," *Clin. Orthop. Rel. Res.*, Vol. 179, pp. 275-283, 1983.

Friederick: Friederick and Brand, "Muscle fiber architecture in the Human lower limb" *J. Biomech.* Vol. 23, pp. 91-95, 1990.

Delp: Delp, et al., "An interactive, graphics-based model of the lower extremity to study orthopaedic surgical procedures," *IEEE Trans. Biom.d. Eng.*, Vol. 37, pp. 557-567, 1990.

Location of Reference Frames: (see Figure 4.2)

Each muscle-tendon path is defined as series of three-dimensional coordinates. Each coordinate is fixed in a body-segmental reference segment. The location of these segments is as follows.

PELVIS: The pelvic reference segment is fixed at the midpoint of the line connecting the two anterior superior iliac spines.

FEMUR: The femoral segment is fixed at the center of the femoral head.

TIBIA: The tibial segment is located at the mid point of the line between the medial and lateral femoral epicondyles (see note below†).
 PATELLA: The patellar segment is located at the most distal point of the patella.

TALUS: The talar segment is located at the midpoint of the line between the apices of the medial and lateral malleoli.

CALCANUS: The calcaneal segment is located at the most distal, inferior point on the posterior surface of the calcanus.

TOES: The toe segment is located at the base of the second metatarsal.

†In the anatomical position, the X-axes point anteriorly, the Y-axes point superiorly, and the Z-axes point laterally. Also note that this muscle file must be used with a joint file that has the same reference segments.

†The coordinates of the tibial tuberosity in the tibia frame are $t = (0.039, -0.082, 0.000)$. The origin of the tibia reference frame could be moved to the tibial tuberosity using t . To do this, t would need to be subtracted from all the muscle points in the tibia segment and from the vertices in tibia and fibula bone files. Also, the translations in the femur-tibia joint, the tibia-patella joint, and the tibia-talus joint would need to be transformed.

```
#define PELVIS      1
#define FEMUR      2
#define TIBIA      3
#define PATELLA    4
#define TALUS      5
#define CALCN      6
#define TOES       7

#define HIPflex    q1
#define HIPadd     q2
#define HIProt     q3
#define KNEEang   q4
#define ANKLEang  q5
#define STang     q6
#define MTPang    q7
```

If parameters of a particular muscle are not specified within the muscle definition, then the values defined in the "default muscle" are used. The force-length curves of the default muscle are used in almost all of the muscles. However, each muscle-tendon complex must have a line of action defined by at least two 3D coordinates.

```
beginmuscle defaultmuscle
tendon_stress@max_force 32.0 /* MPa */
tendon_elastic_modulus 1200.0 /* MPa */
max_contraction_velocity 10.0 /* fiberlengths/sec, not used */

begin tendonforcelengthcurve
/* (tendon strain, normalized force) */
(-10.00,0.00) (-0.002,0.00)
(-0.001,0.00) (0.000,0.000)
(0.0013,0.011) (0.0028,0.026)
```

```

(0.0043,0.043) (0.0058,0.065)
(0.0073,0.091) (0.0088,0.123)
(0.0103,0.161) (0.0118,0.208)
(0.0123,0.227) (9.2000,345.0)
(9.2010,345.0) (9.2020,345.0)
(20.000,345.0)
endtendonforcelengthcurve

begininactiveforcevelocitycurve
/* (norm.length, norm.force) */
(-5.000,0.000) (0.000,0.000)
(0.401,0.000) (0.402,0.000)
(0.403,0.000) (0.522,0.226)
(0.628,0.636) (0.718,0.856)
(0.861,0.950) (1.045,0.993)
(1.217,0.770) (1.438,0.246)
(1.618,0.000) (1.620,0.000)
(1.621,0.000) (2.200,0.000)
(5.000,0.000)
endinactiveforcevelocitycurve

beginpassiveforcevelocitycurve
/* (norm.length, norm.force) */
(-5.00,0.00) (0.998,0.000)
(0.999,0.000) (1.000,0.000)
(1.100,0.035) (1.200,0.120)
(1.300,0.260) (1.400,0.550)
(1.500,1.170) (1.600,2.000)
(1.601,2.000) (1.602,2.000)
(5.000,2.000)
endpassiveforcevelocitycurve

beginforcevelocitycurve
/* (normalized velocity, normalized force) */
(-10.0,0.000) (0.055,0.000)
(0.403,0.000) (0.527,0.226)
(0.628,0.636) (0.718,0.856)
(0.861,0.950) (1.045,0.993)
(1.217,0.770) (1.438,0.246)
(1.618,0.000) (2.000,0.000)
(10.00,0.000)
endforcevelocitycurve
endmuscle

```

```

/******
The rest of the file gives definitions for each muscle by:
(1) giving the muscle a name
(2) defining the muscle path
(3) specifying the functional groups
(4) specifying for parameters that scale the generic muscle-tendon model.
These parameters are:
Peak isometric force, based on physiologic cross-sectional area (Newtons);
optimal muscle-fiber length (meters);
tendon slack length (meters);
penetration angle at optimal fiber length (degrees).
*****
beginmuscle GMED1 /*gluteus medius (anterior compartment) */
beginpoints
-0.0408 0.0304 0.1209 segment PELVIS
-0.0218 -0.0117 0.0555 segment FEMUR
endpoints
begingroups hip_abd hip_flex hip_inrot endgroups
force_max 546.0 /* units: Newtons, source: Brand */
optimal_fiber_length 0.0535 /* units: meters, source: Friederich */
tendon_slack_length 0.0780 /* units: meters, source: Delp */
penetration_angle 8.0 /* units: degrees, source: Friederich */
endmuscle

beginmuscle GMED2 /*gluteus medius (middle compartment) */
beginpoints
-0.0855 0.04450 0.0766 segment PELVIS
-0.0258 -0.0058 0.0527 segment FEMUR
endpoints
begingroups hip_abd endgroups
force_max 382.0 /* source: Brand */
optimal_fiber_length 0.0845 /* source: Friederich */
tendon_slack_length 0.0530 /* source: Delp */
penetration_angle 0.0 /* source: Friederich */
endmuscle

beginmuscle GMED3 /*gluteus medius (posterior compartment) */
beginpoints
-0.1223 0.0105 0.0648 segment PELVIS
-0.0309 -0.0047 0.0518 segment FEMUR
endpoints

```

```

beginngroups hip_abd hip_extrot hip_ext endgroups
force_max 435.0 /* source: Brand */
optimal_fiber_length 0.0646 /* source: Friederich */
tendon_slack_length 0.0530 /* source: Delp */
penetration_angle 19.0 /* source: Friederich */
endmuscle

beginmuscle GMIN1 /*gluteus minimus (anterior compartment) */
beginpoints
-0.0467 -0.0080 0.1056 segment PELVIS
-0.0072 -0.0104 0.0560 segment FEMUR
endpoints
beginngroups hip_abd hip_flex hip_inrot endgroups
force_max 180.0 /* source: Brand */
optimal_fiber_length 0.0680 /* source: Friederich */
tendon_slack_length 0.0160 /* source: Delp */
penetration_angle 10.0 /* source: Friederich */
endmuscle

beginmuscle GMIN2 /*gluteus minimus (middle compartment) */
beginpoints
-0.0633 -0.0065 0.0991 segment PELVIS
-0.0096 -0.0104 0.0560 segment FEMUR
endpoints
beginngroups hip_abd endgroups
force_max 190.0 /* source: Brand */
optimal_fiber_length 0.0560 /* source: Friederich */
tendon_slack_length 0.0260 /* source: Delp */
penetration_angle 0.0 /* source: Friederich */
endmuscle

beginmuscle GMIN3 /*gluteus minimus (posterior compartment) */
beginpoints
-0.0834 -0.0063 0.0836 segment PELVIS
-0.0135 -0.0083 0.0550 segment FEMUR
endpoints
beginngroups hip_abd hip_extrot hip_ext endgroups
force_max 215.0 /* source: Brand */
optimal_fiber_length 0.0380 /* source: Friederich */
tendon_slack_length 0.0510 /* source: Delp */
penetration_angle 1.0 /* source: Friederich */
endmuscle

```

```

beginmuscle SEMIMEM /* semimembranosus */
beginpoints
-0.1192 -0.1015 0.0695 segment PELVIS
-0.0243 -0.0536 -0.0194 segment TIBIA
endpoints
beginngroups hip_ext hip_add knee_bend endgroups
force_max 1030.0 /* source: Wickiewicz */
optimal_fiber_length 0.0800 /* source: Wickiewicz */
tendon_slack_length 0.3590 /* source: Delp */
penetration_angle 15.0 /* source: Wickiewicz */
endmuscle

beginmuscle SEMITEN /* semitendinosus */
beginpoints
-0.1237 -0.1043 0.0603 segment PELVIS
-0.0314 -0.0545 -0.0146 segment TIBIA
-0.0113 -0.0746 -0.0245 segment TIBIA
0.0027 -0.0956 -0.0193 segment TIBIA
endpoints
beginngroups hip_ext hip_add knee_bend endgroups
force_max 328.0 /* source: Wickiewicz */
optimal_fiber_length 0.2010 /* source: Wickiewicz */
tendon_slack_length 0.2620 /* source: Delp */
penetration_angle 5.0 /* source: Wickiewicz */
endmuscle

beginmuscle BIFEMLH /* biceps femoris (long head) */
beginpoints
-0.1244 -0.1001 0.0666 segment PELVIS
-0.0081 -0.0729 0.0423 segment TIBIA
endpoints
beginngroups hip_ext hip_add knee_bend endgroups
force_max 717.0 /* source: Brand (Wick lumps the two heads) */
optimal_fiber_length 0.1090 /* source: Wickiewicz */
tendon_slack_length 0.3410 /* source: Delp */
penetration_angle 0.0 /* source: Wickiewicz */
endmuscle

beginmuscle BIFEMSH /* biceps femoris (short head) */
beginpoints
0.0050 -0.2111 0.0234 segment FEMUR
-0.0101 -0.0725 0.0406 segment TIBIA

```

```

endpoints
beginngroups knee_bend endgroups
force_max 402.0 /* source: Brand (Wick lumps the two heads) */
optimal_fiber_length 0.1730 /* source: Wickiewicz */
tendon_slack_length 0.1000 /* source: Delp */
pennation_angle 23.0 /* source: Wickiewicz */
endmuscle

beginmuscle SAR /* sartorius */
beginpoints
-0.0153 -0.0013 0.1242 segment PELVIS
-0.0030 -0.3568 -0.0421 segment FEMUR
-0.0056 -0.0419 -0.0399 segment TIBIA
0.0060 -0.0589 -0.0383 segment TIBIA
0.0243 -0.0840 -0.0252 segment TIBIA
endpoints
beginngroups hip_flex hip_abd_knee_bend endgroups
force_max 104.0 /* source: Wickiewicz */
optimal_fiber_length 0.5790 /* source: Wickiewicz */
tendon_slack_length 0.0400 /* source: Delp */
pennation_angle 0.0 /* source: Wickiewicz */
endmuscle

beginmuscle ADDLONG /* adductor longus */
beginpoints
-0.0316 -0.0836 0.0169 segment PELVIS
0.0050 -0.2111 0.0234 segment FEMUR
endpoints
beginngroups hip_add hip_ext hip_flex endgroups
force_max 418.0 /* source: Wickiewicz */
optimal_fiber_length 0.1380 /* source: Wickiewicz */
tendon_slack_length 0.1100 /* source: Delp */
pennation_angle 6.0 /* source: Wickiewicz */
endmuscle

beginmuscle AADBREV /* adductor brevis */
beginpoints
-0.0587 -0.0915 0.0164 segment PELVIS
0.0009 -0.1196 0.0294 segment FEMUR
endpoints
beginngroups hip_add hip_flex endgroups

```

```

force_max 286.0 /* source: Wickiewicz */
optimal_fiber_length 0.1330 /* source: Wickiewicz */
tendon_slack_length 0.0200 /* source: Delp */
pennation_angle 0.0 /* source: Wickiewicz */
endmuscle

beginmuscle AMAG1 /* adductor magnus (superior component) */
beginpoints
-0.0732 -0.1174 0.0255 segment PELVIS
-0.0045 -0.1211 0.0339 segment FEMUR
endpoints
beginngroups hip_ext hip_add endgroups
force_max 346.0 /* source: Brand */
optimal_fiber_length 0.0870 /* source: Friederich */
tendon_slack_length 0.0600 /* source: Delp */
pennation_angle 5.0 /* source: Friederich */
endmuscle

beginmuscle AMAG2 /* adductor magnus (middle component) */
beginpoints
-0.0831 -0.1192 0.0308 segment PELVIS
0.0054 -0.2285 0.0227 segment FEMUR
endpoints
beginngroups hip_add endgroups
force_max 312.0 /* source: Brand */
optimal_fiber_length 0.1210 /* source: Friederich */
tendon_slack_length 0.1300 /* source: Delp */
pennation_angle 3.0 /* source: Friederich */
endmuscle

beginmuscle AMAG3 /* adductor magnus (inferior component) */
beginpoints
-0.0771 -0.1181 0.0276 segment PELVIS
0.0070 -0.3837 -0.0266 segment FEMUR
endpoints
beginngroups hip_ext hip_add endgroups
force_max 444.0 /* source: Brand */
optimal_fiber_length 0.1310 /* source: Friederich */
tendon_slack_length 0.2600 /* source: Delp */
pennation_angle 5.0 /* source: Friederich */
endmuscle

```

```

beginmuscle TFL /*tensor faciae latae */
beginpoints
-0.0311 0.0214 0.1241 segment PELVIS
0.0294 -0.0995 0.0597 segment FEMUR
0.0054 -0.4049 0.0357 segment FEMUR
0.0060 -0.0487 0.0297 segment TIBIA
endpoints
begingroups hip_abd hip_flex hip_inrot endgroups
force_max 155.0 /* source: Brand */
optimal_fiber_length 0.0950 /* source: Friederich */
tendon_slack_length 0.4250 /* source: Delp */
pennation_angle 3.0 /* source: Friederich */
endmuscle

beginmuscle PECT /* pectineus */
beginpoints
-0.0431 -0.0768 0.0451 segment PELVIS
-0.0122 -0.0822 0.0253 segment FEMUR
endpoints
begingroups hip_add hip_flex endgroups
force_max 177.0 /* source: Wickiewicz */
optimal_fiber_length 0.1330 /* source: Wickiewicz */
tendon_slack_length 0.0010 /* source: Delp */
pennation_angle 0.0 /* source: Wickiewicz */
endmuscle

beginmuscle GRA /* gracilis */
beginpoints
-0.0563 -0.1038 0.0079 segment PELVIS
-0.0154 -0.0475 -0.0358 segment TIBIA
0.0060 -0.0836 -0.0228 segment TIBIA
endpoints
begingroups hip_add knee_bend hip_flex endgroups
force_max 108.0 /* source: Wickiewicz */
optimal_fiber_length 0.3520 /* source: Wickiewicz */
tendon_slack_length 0.1400 /* source: Delp */
pennation_angle 3.0 /* source: Wickiewicz */
endmuscle

beginmuscle GMAX1 /* gluteus maximus (superior component) */
/* passes through deeper muscles beyond 70 degrees of hip flexion */
beginpoints

```

```

-0.1195 0.0612 0.0700 segment PELVIS
-0.1291 0.0012 0.0886 segment PELVIS
-0.0457 -0.0248 0.0392 segment FEMUR
-0.0277 -0.0566 0.0470 segment FEMUR
endpoints
begingroups hip_ext hip_abd endgroups
force_max 382.0 /* source: Brand */
optimal_fiber_length 0.1420 /* source: Friederich */
tendon_slack_length 0.1250 /* source: Delp */
pennation_angle 5.0 /* source: Friederich */
endmuscle

beginmuscle GMAX2 /* gluteus maximus (middle component) */
/* passes through deeper muscles beyond 70 degrees of hip flexion */
beginpoints
-0.1349 0.0176 0.0563 segment PELVIS
-0.1212 -0.0520 0.0914 segment PELVIS
-0.0426 -0.0530 0.0293 segment FEMUR
-0.0156 -0.1016 0.0419 segment FEMUR
endpoints
begingroups hip_ext endgroups
force_max 546.0 /* source: Brand */
optimal_fiber_length 0.1470 /* source: Friederich */
tendon_slack_length 0.1270 /* source: Delp */
pennation_angle 0.0 /* source: Friederich */
endmuscle

beginmuscle GMAX3 /* gluteus maximus (inferior component) */
/* Intersects ischial tuberosity beyond about 60 degrees of hip flexion. */
/* Moment arms are therefore too small in this range. */
beginpoints
-0.1556 -0.0314 0.0058 segment PELVIS
-0.1529 -0.1052 0.0403 segment PELVIS
-0.0299 -0.1041 0.0135 segment FEMUR
-0.0060 -0.1419 0.0411 segment FEMUR
endpoints
begingroups hip_ext endgroups
force_max 368.0 /* source: Brand */
optimal_fiber_length 0.1440 /* source: Friederich */
tendon_slack_length 0.1450 /* source: Delp */
pennation_angle 5.0 /* source: Friederich */
endmuscle

```

```

beginmuscle ILIACUS /* May want to define wrapping points */
/* Line of action passes through joint capsule when hip is extended */
beginpoints
-0.0674 0.0365 0.0854 segment PELVIS
-0.0218 -0.0550 0.0851 segment PELVIS
0.0017 -0.0543 0.0057 segment FEMUR
-0.0193 -0.0621 0.0129 segment FEMUR
endpoints
beginngroups hip_flex hip_inrot endgroups
force_max 429.0 /* source: Brand */
optimal_fiber_length 0.1000 /* source: Friederich */
tendon_slack_length 0.0900 /* source: Delp */
penetration_angle 7.0 /* source: Friederich */
endmuscle

beginmuscle PSOAS /* may want to define wrapping points */
/* Line of action passes through joint capsule when hip is extended */
beginpoints
-0.0647 0.0887 0.0289 segment PELVIS
-0.0238 -0.0570 0.0759 segment PELVIS
0.0016 -0.0507 0.0038 segment FEMUR
-0.0188 -0.0597 0.0104 segment FEMUR
endpoints
beginngroups hip_flex hip_inrot endgroups
force_max 371.0 /* source: Brand */
optimal_fiber_length 0.1040 /* source: Friederich */
tendon_slack_length 0.1300 /* source: Delp */
penetration_angle 8.0 /* source: Friederich */
endmuscle

beginmuscle QUADFEM /* quadratus femoris */
beginpoints
-0.1143 -0.1151 0.0520 segment PELVIS
-0.0381 -0.0359 0.0366 segment FEMUR
endpoints
beginngroups hip_extrot endgroups
force_max 254.0 /* source: Brand */
optimal_fiber_length 0.0540 /* source: Friederich */
tendon_slack_length 0.0240 /* source: Delp */
penetration_angle 0.0 /* source: Friederich */
endmuscle

```

```

beginmuscle GEM /* gemelli */
beginpoints
-0.1133 -0.0820 0.0714 segment PELVIS
-0.0142 -0.0033 0.0443 segment FEMUR
endpoints
beginngroups hip_extrot endgroups
force_max 109.0 /* source: Brand */
optimal_fiber_length 0.0240 /* source: Friederich */
tendon_slack_length 0.0390 /* source: Delp */
penetration_angle 0.0 /* source: Friederich */
endmuscle

beginmuscle PERI /* periformis */
beginpoints
-0.1396 0.0003 0.0235 segment PELVIS
-0.1193 -0.0276 0.0657 segment PELVIS
-0.0148 -0.0036 0.0437 segment FEMUR
endpoints
beginngroups hip_extrot hip_abd endgroups
force_max 296.0 /* source: Brand */
optimal_fiber_length 0.0260 /* source: Friederich */
tendon_slack_length 0.1150 /* source: Delp */
penetration_angle 10.0 /* source: Friederich */
endmuscle

/******
The quadriceps have points in their path definitions that are only part of the muscle path
over a specified range of knee angles. These so called "wrapping points" were defined by
finding the knee angles at which the muscle paths intersect the bone surface and then adding
muscle points to the path so that the muscle wraps over the bone. This is needed for the
quadriceps to wrap over the femur as the knee is flexed. Wrapping points can be specified
for ranges of any number of generalized coordinates. For example, a muscle definition that
included "ranges 2 HIPflex (0.0,0.5) HIPadd (0.25,0.30)" would have a muscle point that
only became part of the path when the hip flexion angle was (0.0 - 0.5) and the hip adduc-
tions angle was (0.25 - 0.30)
*****

beginmuscle RF /* rectus femoris */
beginpoints
-0.0295 -0.0311 0.0968 segment PELVIS
0.0334 -0.0430 0.0019 segment FEMUR ranges 1 KNEEang (-3.0, -1.46) /* radians */
/* The point above constrains the path of RF for knee angles between -3.0 and -1.46 */

```



```

0.0121 0.0437 -0.0010 segment PATELLA
endpoints
beginngroups hip_flex_knee_ext endgroups
force_max 779.0 /* source: Wickiewicz */
optimal_fiber_length 0.0840 /* source: Wickiewicz */
tendon_slack_length 0.3460 /* source: Delp */
pennation_angle 5.0 /* source: Wickiewicz */
endmuscle

beginmuscle VASMED /* vastus medialis */
beginpoints
0.0140 -0.2099 0.0188 segment FEMUR
0.0356 -0.2769 0.0009 segment FEMUR
0.0370 -0.4048 -0.0125 segment FEMUR ranges 1 KNEEang (-3.0, -1.21)
0.0274 -0.4255 -0.0131 segment FEMUR ranges 1 KNEEang (-3.0, -1.78)
0.0063 0.0445 -0.0170 segment PATELLA
endpoints
beginngroups knee_ext endgroups
force_max 1294.0 /* source: Wickiewicz */
optimal_fiber_length 0.0890 /* source: Wickiewicz */
tendon_slack_length 0.1260 /* source: Delp */
pennation_angle 5.0 /* source: Wickiewicz */
endmuscle

beginmuscle VASINT /* vastus intermedius */
beginpoints
0.0290 -0.1924 0.0310 segment FEMUR
0.0335 -0.2084 0.0285 segment FEMUR
0.0343 -0.4030 0.0055 segment FEMUR ranges 1 KNEEang (-3.0, -1.42)
0.0058 0.0480 -0.0006 segment PATELLA
endpoints
beginngroups knee_ext endgroups
force_max 1365.0 /* source: Wickiewicz */
optimal_fiber_length 0.0870 /* source: Wickiewicz */
tendon_slack_length 0.1360 /* source: Delp */
pennation_angle 3.0 /* source: Wickiewicz */
endmuscle

beginmuscle VASLAT /* vastus lateralis */
beginpoints
0.0048 -0.1854 0.0349 segment FEMUR
0.0269 -0.2591 0.0409 segment FEMUR

```

```

0.0361 -0.4030 0.0205 segment FEMUR ranges 1 KNEEang (-3.0, -1.21)
0.0253 -0.4243 0.0184 segment FEMUR ranges 1 KNEEang (-3.0, -1.92)
0.0103 0.0423 0.0141 segment PATELLA
endpoints
beginngroups knee_ext endgroups
force_max 1871.0 /* source: Wickiewicz */
optimal_fiber_length 0.0840 /* source: */
tendon_slack_length 0.1570 /* source: Delp */
pennation_angle 5.0 /* source: Wickiewicz */
endmuscle

beginmuscle MEDGAS /* gastrocnemius (medial head) */
beginpoints
-0.0127 -0.3929 -0.0235 segment FEMUR
-0.0239 -0.4022 -0.0258 segment FEMUR ranges 1 KNEEang (-0.77, 0.1)
-0.0217 -0.0487 -0.0295 segment TIBIA
0.0044 0.0310 -0.0053 segment CALCAN
endpoints
beginngroups knee_bend_ankle_pf endgroups
force_max 1113.0 /* source: Brand (Wick jumps the two heads) */
optimal_fiber_length 0.0450 /* source: Wickiewicz */
tendon_slack_length 0.4080 /* source: Delp */
pennation_angle 17.0 /* source: Wickiewicz */
endmuscle

beginmuscle LATGAS /* gastrocnemius (medial head) */
beginpoints
-0.0155 -0.3946 0.0272 segment FEMUR
-0.0254 -0.4018 0.0274 segment FEMUR ranges 1 KNEEang (-0.77, 0.1)
-0.0242 -0.0481 0.0235 segment TIBIA
0.0044 0.0310 -0.0053 segment CALCAN
endpoints
beginngroups knee_bend_ankle_pf endgroups
force_max 488.0 /* source: Brand (Wick jumps the two heads) */
optimal_fiber_length 0.0640 /* source: Wickiewicz */
tendon_slack_length 0.3850 /* source: Delp */
pennation_angle 8.0 /* source: Wickiewicz */
endmuscle

```

```

beginmuscle SOL /* solus */
beginpoints
-0.0024 -0.1533 0.0071 segment TIBIA
0.0044 0.0310 -0.0053 segment CALCN
endpoints
begingroups ankle_pf endgroups
force_max 2839.0 /* 4176.0 source: Wick 3340 = 0.8 * 4176 */
optimal_fiber_length 0.0300 /* Wick val=.025, Brand val=0.03 */
tendon_slack_length 0.2680 /* source: Delp */
pennation_angle 25.0 /* source: Wickiewicz */
endmuscle

/*****
A special muscle can be made by specifying its properties. For example, a muscle can be
given a unique force-length curve. Below a muscle was created (SOLSTIF) with tendon
stiffness 100 times greater than the nominal values specified in the "default muscle".
*****/
beginmuscle SOLSTIF /* soleus with stiff tendon */
begin tendonforlengthcurve
/* (strain, normalized force) */
(-10.0,0.00) (-0.002,0.00)
(-0.001,0.00) (0.000,0.00)
(0.0013,1.1) (0.0028,2.6)
(0.0043,4.3) (0.0058,6.5)
(0.0073,9.1) (0.0088,12.3)
(0.010,16.1) (0.012,20.8)
(0.013,22.7) (9.20,34500.0)
end tendonforlengthcurve
beginpoints
-0.0024 -0.1533 0.0071 segment TIBIA
0.0044 0.0310 -0.0053 segment CALCN
endpoints
begingroups endgroups
force_max 2839.0 /* 4176.0 source: Wick 3340 = 0.8 * 4176 */
optimal_fiber_length 0.0300 /* Wick val=.025, Brand val=0.03 */
tendon_slack_length 0.2680 /* source: Delp */
pennation_angle 25.0 /* source: Wickiewicz */
endmuscle

```

```

beginmuscle TIBPOST /* tibialis posterior */
beginpoints
-0.0094 -0.1348 0.0019 segment TIBIA
-0.0144 -0.4051 -0.0229 segment TIBIA
0.0417 0.0334 -0.0286 segment CALCN
0.0772 0.0159 -0.0281 segment CALCN
endpoints
begingroups ankle_pf inverter endgroups
force_max 1270.0 /* source: Wickiewicz */
optimal_fiber_length 0.0310 /* source: Wickiewicz */
tendon_slack_length 0.3100 /* source: Delp */
pennation_angle 12.0 /* source: Wickiewicz */
endmuscle

beginmuscle FLEXDIG /* flexor digitorum longus */
beginpoints
-0.0083 -0.2046 -0.0018 segment TIBIA
-0.0154 -0.4051 -0.0196 segment TIBIA
0.0436 0.0315 -0.0280 segment CALCN
0.0708 0.0176 -0.0263 segment CALCN
0.1658 -0.0081 0.0116 segment CALCN
-0.0019 -0.0078 0.0147 segment TOES
0.0285 -0.0071 0.0215 segment TOES
0.0441 -0.0060 0.0242 segment TOES
endpoints
begingroups ankle_pf inverter endgroups
force_max 310.0 /* source: Wickiewicz */
optimal_fiber_length 0.0340 /* source: Wickiewicz */
tendon_slack_length 0.4000 /* source: Delp */
pennation_angle 7.0 /* source: Wickiewicz */
endmuscle

beginmuscle FLEXHAL /* flexor hallucis longus */
beginpoints
-0.0079 -0.2334 0.0244 segment TIBIA
-0.0186 -0.4079 -0.0174 segment TIBIA
0.0374 0.0276 -0.0241 segment CALCN
0.1038 0.0068 -0.0256 segment CALCN
0.1726 -0.0053 -0.0269 segment CALCN
0.0155 -0.0064 -0.0265 segment TOES
0.0562 -0.0102 -0.0181 segment TOES
endpoints

```

```

beginngroups ankle_pf_inverter endgroups
force_max 322.0 /* source: Wickiewicz */
optimal_fiber_length 0.0430 /* source: Wickiewicz */
tendon_slack_length 0.3800 /* source: Delp */
penmatn_angle 10.0 /* source: Wickiewicz */
endmuscle

beginmuscle TIBANT /* tibialis anterior */
beginpoints
0.0179 -0.1624 0.0115 segment TIBIA
0.0329 -0.3951 -0.0177 segment TIBIA
0.1166 0.0178 -0.0305 segment CALCN
endpoints
beginngroups ankle_df_inverter endgroups
force_max 603.0 /* source: Wickiewicz */
optimal_fiber_length 0.0980 /* source: Wickiewicz */
tendon_slack_length 0.2230 /* source: Delp */
penmatn_angle 5.0 /* source: Wickiewicz */
endmuscle

beginmuscle PERBREV /* peroneus brevis */
beginpoints
-0.0070 -0.2646 0.0325 segment TIBIA
-0.0198 -0.4184 0.0283 segment TIBIA
-0.0144 -0.4295 0.0289 segment TIBIA
0.0471 0.0270 0.0233 segment CALCN
0.0677 0.0219 0.0343 segment CALCN
endpoints
beginngroups ankle_pf_everter endgroups
force_max 348.0 /* source: Wickiewicz */
optimal_fiber_length 0.0500 /* source: Wickiewicz */
tendon_slack_length 0.1610 /* source: Delp */
penmatn_angle 5.0 /* source: Wickiewicz */
endmuscle

beginmuscle PERLONG /* peroneus longus */
beginpoints
0.0005 -0.1568 0.0362 segment TIBIA
-0.0207 -0.4205 0.0286 segment TIBIA
-0.0162 -0.4319 0.0289 segment TIBIA
0.0438 0.0230 0.0221 segment CALCN
0.0681 0.0106 0.0284 segment CALCN

```

```

0.0852 0.0069 0.0118 segment CALCN
0.1203 0.0085 -0.0184 segment CALCN
endpoints
beginngroups ankle_pf_everter endgroups
force_max 754.0 /* source: Wickiewicz */
optimal_fiber_length 0.0490 /* source: Wickiewicz */
tendon_slack_length 0.3450 /* source: Delp */
penmatn_angle 10.0 /* source: Wickiewicz */
endmuscle

beginmuscle PERTERT /* peroneus tertius */
beginpoints
0.0010 -0.2804 0.0231 segment TIBIA
0.0229 -0.4069 0.0159 segment TIBIA
0.0857 0.0228 0.0299 segment CALCN
endpoints
beginngroups ankle_df_everter endgroups
force_max 90.0 /* source: Brand (not reported by wick) */
optimal_fiber_length 0.0790 /* source: Friederich */
tendon_slack_length 0.1000 /* source: Delp */
penmatn_angle 13.0 /* source: Friederich */
endmuscle

beginmuscle EXTDIG /* extensor digitorum longus */
beginpoints
0.0032 -0.1381 0.0276 segment TIBIA
0.0289 -0.4007 0.0072 segment TIBIA
0.0922 0.0388 -0.0001 segment CALCN
0.1616 0.0055 0.0130 segment CALCN
0.0003 0.0047 0.0153 segment TOES
0.0443 -0.0004 0.0250 segment TOES
endpoints
beginngroups ankle_df_everter endgroups
force_max 341.0 /* source: Wickiewicz */
optimal_fiber_length 0.1020 /* source: Wickiewicz */
tendon_slack_length 0.3450 /* source: Delp */
penmatn_angle 8.0 /* source: Wickiewicz */
endmuscle

```

beginmuscle EXTHAL /* extensor hallucis longus */

beginpoints

0.0012 -0.1767 0.0228 segment TIBIA
 0.0326 -0.3985 -0.0085 segment TIBIA
 0.0970 0.0389 -0.0211 segment CALCN
 0.1293 0.0309 -0.0257 segment CALCN
 0.1734 0.0139 -0.0280 segment CALCN
 0.0298 0.0041 -0.0245 segment TOES
 0.0563 0.0034 -0.0186 segment TOES

endpoints

begingroups ankle_df inverter endgroups

force_max 108.0 /* source: Wickiewicz */
 optimal_fiber_length 0.1110 /* source: Wickiewicz */
 tendon_slack_length 0.3050 /* source: Delp */
 pennation_angle 6.0 /* source: Wickiewicz */

endmuscle

Appendix B

Joint File for Lower-Extremity Model

The joint file defines the kinematics of a seven segment, seven degree-of-freedom model of the human lower limb. The file is scanned by the the musculoskeletal modeling software (Chapter 3) to create a data structure that defines the system kinematics (Figure B1). The file is passed through the preprocessor “cpp” so that C-style comments (demarcated with /* */) and “#define” statements can be used in the joint file. The actual joint file is shown on the following pages.

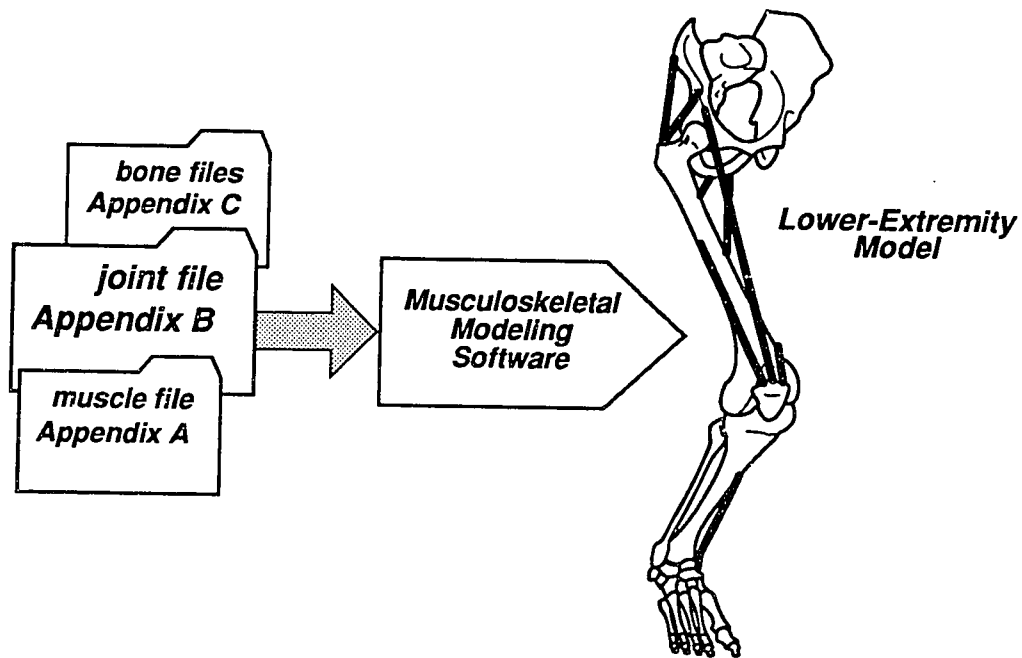


Figure B1. The muscle, bone, and joint files are scanned by the musculoskeletal modeling software to create a data structure that represents the lower limb. Appendix B gives a detailed description of the joint input file.

```

/*****
Joint File                               August 20, 1990
Input file for 7 segment, 7 degree-of-freedom kinematic model

This joint file specifies the four components (1) body segments, (2) generalized coordinates,
(3) joints, and (4) kinematic functions of the lower-limb model. These four components are
described below.

(1) body segments - The bones that make up each body segment are listed.

(2) generalized coordinates - Each generalized coordinate (gencoord) is defined. These de-
fine the ranges of motion for each degree-of-freedom (joint angle).

(3) joints - Each joint is defined. Each translation and rotation is defined by a sum of con-
stants and functions. For example, "tx 2 constant 1.0 function 1 2(gencoord)" means that tx
(x-translation) is a sum of two components. The first is the constant, 1.0, and the second is
function2 of gencoord. An example joint definition is shown here.

beginjoint (FRAME1,FRAME2) /* Begins definition of joint between 2 frames. */
name funnyjoint /* Names joint connecting frame1 and frame2. */
order t r3 r1 r2 /* Specifies order of translation and rotations. */
tx 1 constant .07 /* Translations between the frames are all */
ty 1 constant .06 /* constants in this example. However, they */
tz 1 constant .08 /* could be functions of the gencoords. (e.g., knee) */
axis1 1.0 0.0 0.0 /* Defines the directions of the rotation axes. */
axis2 0.0 1.0 0.0 /* In this example they are the same as the X, Y, */
axis3 0.0 0.0 1.0 /* and Z-axes, but they need not be (e.g., ankle). */
r3 1 function f1(gencoord1) /* Rotation about axis 3 is a f(gencoord1). */
r2 1 function f2(gencoord2) /* Rotation about axis 2 is a f(gencoord2). */
r1 1 constant 0.0 /* Rotation about axis 1 is a constant = 0.0. */
endjoint

(4) kinematic functions - The pairs of points that define each kinematic function are specified.
These points, when interpolated by a natural cubic spline, define each of the functions that
specify the kinematics of the joints. The first number in each pair is the independent variable
(gencoord value). The second number is the value of the dependent variable (translation or
rotation).

```

Location of reference frames: (see Figure 4.2)
The joint definitions specify the translations and rotations needed to transform between any two reference frames. The location of these frames is as follows.

PELVIS: The pelvic reference frame is fixed at the midpoint of the line connecting the two anterior superior iliac spines.
FEMUR: The femoral frame is fixed at the center of the femoral head.
TIBIA: The tibial frame is located at the mid point of the line between the medial and lateral femoral epicondyles (see note below†).
PATELLA: The patellar frame is located at the most distal point of the patella.
TALUS: The talar frame is located at the midpoint of the line between the apices of the medial and lateral malleoli.
CALCANUS: The calcaneal frame is located at the most inferior, lateral point on the posterior surface of the calcaneus.
TOES: The toe frame is located at the base of the second metatarsal.

In the anatomical position, the X-axes point anteriorly, the Y-axes points superiorly, and the Z-axes point laterally. Also note that the muscle file must use that same reference frames as this joint file.

†The coordinates of the tibial tuberosity in the tibia frame are $t = (0.039, -0.082, 0.000)$. The origin of the tibia reference frame could be moved to the tibial tuberosity using t . To do this, t would need to be subtracted from all the muscle points in the tibia frame and from the vertices in tibia and fibula bone files. Also, the translations in the femur-tibia joint, the tibia-patella joint, and the tibia-talus joint would need to be transformed.

```

*****
#define HIPflex      q1
#define HIPadd      q2
#define HIProt      q3
#define KNEEang     q4
#define ANKLEang    q5
#define STang       q6
#define MTPang      q7

#define PELVS      1
#define FEMUR     2
#define TIBIA     3
#define PATEL     4
#define TALUS    5
#define CALCN    6
#define TOES     7

```

```

/*****
(1) BONE FILES IN EACH BODY SEGMENT
*****
egInsegment PELVIS
name: pelvis
files: 2
filenames: bones/sacrum bones/r_pelvis
endsegment

beginsegment FEMUR
name: femur
files: 1
filenames: bones/r_femur
endsegment

beginsegment TIBIA
name: tibia
files: 2
filenames: bones/r_tibia bones/r_fibula
endsegment

beginsegment PATEL
name: patella
files: 1
filenames: bones/r_pat
endsegment

beginsegment TALUS
name: talus
files: 1
filenames: bones/r_talus
endsegment

beginsegment CALCN
name: foot
files: 1
filenames: bones/r_foot
endsegment

beginsegment TOES
name: toes
files: 1
filenames: bones/r_bofoot
endsegment

```

```

/*****
(2) GENERALIZED COORDINATES (degrees of freedom)
*****
begincoordinate HIPflex
range -10.0 120.0 hip_flex
endcoordinate
/* 10 degrees extension to 120 degrees flexion */

begincoordinate HIPadd
range -50.0 30.0 hip_add
endcoordinate
/* 50 degrees abduction to 30 degrees adduction */

begincoordinate HIProt
range -20.0 20.0 hip_inrot
endcoordinate
/* 20 degrees hip internal/external rotation */

begincoordinate KNEEang
range -90.0 0.0 knee_ang
endcoordinate
/* 90 degrees knee flexion */

begincoordinate ANKLEang
range -40 33.0 ankle_ang
endcoordinate
/* 40 degrees plantarflexion to 33 degrees dorsiflexion */

begincoordinate STang
range -20.0 20.0 subt_ang
endcoordinate
/* 20 degrees inversion/eversion (subtalar angle) */

begincoordinate MTPang
range -30.0 30.0 toe_ang
endcoordinate
/* 30 degrees flex/ext. (metatarsophalangeal angle) */

```

```

/*****
(3) JOINT DEFINITIONS
*****
beginJoint (PELVIS,FEMUR)
name hip
order t r3 r1 r2
tx 1 constant -0.707
ty 1 constant -0.661
tz 1 constant .0835
axis1 1.0 0.0 0.0
axis2 0.0 1.0 0.0
axis3 0.0 0.0 1.0
r3 1 function f1(HIPflex)
r1 1 function f2(HIPadd)
r2 1 function f3(HIProt)
endJoint

beginJoint (FEMUR,TIBIA)
name knee
order t r3 r1 r2
tx 1 function f5(KNEEang)
ty 1 function f6(KNEEang)
tz 1 constant 0.0
axis1 1.0 0.0 0.0
axis2 0.0 1.0 0.0
axis3 0.0 0.0 1.0
r3 1 function f4(KNEEang)
r1 1 constant 0.0
r2 1 constant 0.0
endJoint

beginJoint (TIBIA,PATEL)
name tp
order t r3 r1 r2
tx 1 function f7(KNEEang)
ty 1 function f8(KNEEang)
tz 1 constant 0.0024
axis1 1.0 0.0 0.0
axis2 0.0 1.0 0.0
axis3 0.0 0.0 1.0
r3 1 function f9(KNEEang)
r1 1 constant 0.0
r2 1 constant 0.0
endJoint

*****
/**** defines joint between pelvis and femur */
/**** translation, flexion, adduction, rotation */
/**** from midpoint between ASIS to hip center */
/**** meters */

/**** defines joint between femur and tibia */
/**** translation before rotation */
/**** from hip center to origin of tibial frame */

/**** defines joint between tibia and patella */
/**** translation before rotation */
/**** from origin of tibial frame to */
/**** distal point on patella */

/**** rotation of the patella about its z-axis */

```

```

endJoint
beginJoint (TIBIA,TALUS)
name ankle
order t r3 r1 r2
tx 1 constant 0.0
ty 1 constant -.43
tz 1 constant 0.0
axis1 1.0 0.0 0.0
axis2 0.0 1.0 0.0
axis3 -.0105 -0.174 0.979
r3 1 function f10(ANKLEang)
r1 1 constant 0.0
r2 1 constant 0.0
endJoint

beginJoint (TALUS,CALCN)
name subtalar
order t r1 r2 r3
tx 1 constant -.04877
ty 1 constant -.04195
tz 1 constant .00792
axis1 0.781 0.600 -0.120
axis2 0.0 1.0 0.0
axis3 0.0 0.0 1.0
r1 1 function f11(STang)
r2 1 constant 0.0
r3 1 constant 0.0
endJoint

beginJoint (CALCN,TOES)
name toe
order t r1 r2 r3
tx 1 constant 0.1788
ty 1 constant -.0020
tz 1 constant 0.00108
axis1 0.581 0.000 -0.814
axis2 0.0 1.0 0.0
axis3 0.0 0.0 1.0
r1 1 function f12(MTPang)
r2 1 constant 0.0
r3 1 constant 0.0
endJoint

/**** defines joint between tibia and talus */
/**** translation before rotation */
/**** from origin of tibial frame to ankle axis */

/**** ankle axis derived from Isman and Inman */

/**** defines joint between talus and calcaneus frames */
/**** translation before rotation */
/**** from ankle joint center to origin of */
/**** calcaneal frame (taken from the iris) */

/**** subtalar axis derived from Inman (1976) */

/**** defines joint between calcaneus and toe frames */
/**** translation before rotation */
/**** from calcaneal frame to base of second */
/**** metatarsal (taken from the iris) */

/**** Inman (1976) values are: 0.4695 0.0 -0.8829 */

```



```

/*****
(4) KINEMATIC FUNCTIONS
*****
beginfunction f1 /* hip flexion (+) and extension (-) */
/* (hip flexion angle (radians), rotation about axis 3 (radians) *)
(-5.0,-5.0)
(5.0,5.0)
endfunction
beginfunction f2 /* hip adduction (+) and abduction (-) */
/* (hip adduction angle, rotation about axis 1) *)
(-5.0,-5.0)
(5.0,5.0)
endfunction
beginfunction f3 /* hip internal (+) and external rotation (-) */
/* (hip rotation angle, rotation about axis 2) *)
(-5.0,-5.0)
(5.0,5.0)
endfunction
beginfunction f4 /* 0 degrees is full extension, neg. angles are flexion */
/* (knee flexion angle, rotation about axis 3) *)
(-5.0,-5.0)
(5.0,5.0)
endfunction

/*****
FEMUR-TIBIA KINEMATICS
TX and TY for femoral-tibial kinematics were determined by the following process. I first
printed a medial view of the femur and tibia from the iris. I next fit an ellipse to the femoral
condyles (semimajor axis = 3.54 cm, semiminor axis = 2.42cm). The tibial plateau was char-
acterized by a line of length 5.5 cm. Using Eric Topp's modification of Gary Yamaguchi's
cmknee program (Yamaguchi and Zajac, 1989) I determined the translations that make the el-
lipse (femur) and the line (tibia) contact according to Nissel's data (1985) for tibial-femoral
contact.
*****
/

```

```

/* tx for femoral-tibial joint */
beginfunction f5 /* range of motion: 120 degrees flexion to 0 degrees extension */
/* knee angle (radians), x-translation from femoral to tibial frame (meters) */
(-2.09,-0.0032)
(-1.74,0.00179)
(-1.39,0.00411)
(-1.04,0.00410)
(-0.69,0.00212)
(-0.35,-0.0010)
(-0.17,-0.0031)
(0.00,-0.00525)
endfunction

/* ty for femoral-tibial joint */
beginfunction f6 /* range of motion: 120 degrees flexion to 0 degrees extension */
/* knee angle (radians), y-translation from femoral to tibial frame (meters) */
(-2.09,-0.4226)
(-1.22,-0.4082)
(-0.52,-0.3990)
(-0.35,-0.3976)
(-0.17,-0.3966)
(0.00,-0.3960)
endfunction

/*****
TIBIA-PATELLA KINEMATICS
TX and TY for tibial-patellar motion were determined by assuming that the patellar liga-
ment is inextensible and has length 5.5cm. The patellar ligament angle was taken from Ya-
maguchi and Zajac (1989) because it fits experimental data (Nissel, 1985 and VanEijden,
1985) well. From patellar length and angle, tx and ty were computed. I subtracted 8mm
from all of the tx values because the patella was tracking too far from the femur. This is be-
cause the tibial tuberosity of my bone model is too large. Effectively, subtracting the 8mm
reduces the size of the tuberosity. RZ was taken directly from VanEijden, 1985. I subtract-
ed 5 degrees from all rz values because my patella model was oriented about 5 degrees dif-
ferently. I visually compared the iris display of the knee kinematics to xerograms of knee in
four different positions. I also compared knee moment arms to experimental data.
*****
/

```

```

/* tx for tibial-patellar motion */
beginfunction f7 /* range of motion: 120 degrees flexion to 0 degrees extension */
/* knee angle (radians), x-translation from tibial to patellar frame (meters) */
(-2.09,0.0173)
(-1.39,0.0324)
(-1.04,0.0381)
(-0.69,0.0430)
(-0.35,0.0469)
(-0.17,0.0484)
(0.000,0.0496)
endfunction

/* ty for tibial-patellar motion */
beginfunction f8 /* range of motion: 120 degrees flexion to 0 degrees extension */
/* knee angle (radians), y-translation from tibial to patellar frame (meters)*/
(-2.09,-0.0219)
(-1.57,-0.0202)
(-1.39,-0.0200)
(-1.04,-0.0204)
(-0.69,-0.0211)
(-0.35,-0.0219)
(-0.17,-0.0223)
(0.005,-0.0227)
endfunction

/* tz for tibial-patellar motion */
beginfunction f9 /* range of motion: 120 degrees flexion to 0 degrees extension */
/* knee angle (radians), z-rotation from tibial to patellar frame (radians) */
(-2.09,0.308)
(-2.00,0.308)
(-1.45,0.306)
(-0.52,0.270)
(0.027,-0.0936)
(0.170,-0.280)
endfunction

/* ankle motion */
beginfunction f10:
/* ankle angle (radians), rotation about axis 3 (radians) */
(-5.0,-5.0)
(5.0,5.0)
endfunction

```

```

/* subtalar motion */
beginfunction f11
/* inversion angle, rotation about axis 1 */
(-5.0,-5.0)
(5.0,5.0)
endfunction

/* metatarsophalangeal motion */
beginfunction f12
/* toe angle, rotation about axis 1 */
(-5.0,-5.0)
(5.0,5.0)
endfunction

```

Appendix C

Format of Bone Files

In the musculoskeletal modeling software, a body segment consists of one or more bones. The bones that make up each body segment are specified as shown in the following example.

```
beginsegment FEMUR
name right_femur
files: 1
filenames: r_femur.dat
endsegment
```

The files listed in the definitions of the body segments (e.g. `r_femur.dat`) define the polygon meshes that describe the bone surfaces. These files list the 3D coordinates of the polygon vertices (in a vertex list) and define how the vertices are connected to form polygons (in a polygon list). The reference frame that is associated with each body segment serves as the coordinate system for the polygon vertices. The first number on each line of the polygon list specifies the number of vertices in the polygon; the rest of the numbers on the line are the vertices in that polygon. For example, the first polygon in the polygon list has three vertices, which are the first three vertices in the vertex list. The format of the bone files is shown below.

```
260      290      (number of vertices, number of polygons)

( X      Y      Z )
0.0101  0.0443  -0.0139 (vertex list)
0.0120  0.0339  -0.0165
0.0110  0.0238  -0.0151
0.0085  0.0164  -0.0117
0.0069  0.0087  -0.0095
.
.

3      1 2 3      (polygon list)
3      2 3 4
4      3 4 7 8
4      4 5 13 12
4      5 6 14 13
.
.
```

The bone files are not passed through the C-preprocessor, so comments must not be used in these files. Also, the bone files are not needed to define a musculoskeletal model. If the definitions of the body segments specify `files: 0`, the model will be displayed without bones.

References

- [1] Aho, A. V., Hopcroft, J. E., and Ullman, J. D., *Data Structures and Algorithms*. Reading: Addison-Wesley, 1985.
- [2] An, K. N., Takakashi, K., Harrigan, T. P., and Chao, E. Y., "Determination of muscle orientation and moment arms," *J. Biomech. Eng.*, vol. 106, pp. 280-282, 1984.
- [3] Bailey, T. E. and Hall, J. E., "Chiari medial displacement osteotomy," *J. Pediatr. Orthop.*, vol. 5, pp. 635-641, 1985.
- [4] Barillot, C., Gibaud, B., Lis, O., Min, L. L., Bouliou, A., Certen, G. L., Collorec, R., and Coatrieux, J. L., "Computer graphics in medicine: a survey," *CRC Crit. Rev. in Biomed. Eng.*, vol. 15, pp. 269-307, 1988.
- [5] Bassett, F. H., Poehling, G. G., Morrefield, W. G., and Riley, K., "Hamstring procedures in cerebral palsy: a sequelae after long follow up. Recommendations for current practice," *J. Bone and Joint Surg.*, vol. 58-A, pp. 725, 1976.
- [6] Belanger, A. Y. and McComas, A. J., "Extent of motor unit activation during effort," *J. Appl. Physiol.*, vol. 51, pp. 1131-1135, 1981.
- [7] Bellemare, F. J., W. J., Johansson, R., and Bigland-Ritchie, B., "Motor unit discharge rates in maximal voluntary contractions of three human muscles," *J. Neurophysiol.*, vol. 50, pp. 1380-1392, 1983.
- [8] Betz, R. R., Kumar, S. J., Palmer, C. T., and MacEwen, G. D., "Chiari pelvic osteotomy in children and young adults," *J. Bone Joint Surg.*, vol. 70-A, pp. 182-191, 1988.
- [9] Bleck, E. E., *Orthopaedic Management in Cerebral Palsy*. Philadelphia: Mac Keith Press, 1987.
- [10] Borja, F., Latta, L., Stinchfield, F., and Obreron, L., "Abductor muscle performance in total hip arthroplasty with and without trochanteric osteotomy," *Clin. Orthop.*, vol. 197, pp. 181-190, 1985.
- [11] Brand, P. W., *Clinical Mechanics of the Hand*. St. Louis: C.V. Mosby, 1985.

- [12] Brand, P. W., Beach, R. B., and Thompson, D. E., "Relative tension and potential excursion of muscles in the forearm and hand," *J. Hand Surg.*, vol. 6, pp. 209-219, 1981.
- [13] Brand, R. A., Crowninshield, R. D., Wittstock, C. E., Pederson, D. R., Clark, C. R., and van Krieken, F. M., "A model of lower extremity muscular anatomy," *J. Biomech. Eng.*, vol. 104, pp. 304-310, 1982.
- [14] Brand, R. A., Pedersen, D. R., and Friederich, J. A., "The sensitivity of muscle force predictions to changes in physiologic cross-sectional area," *J. Biomech.*, vol. 19, pp. 589-596, 1986.
- [15] Brand, R. A. and Pederson, D. R., "Computer modeling of surgery and a consideration of the mechanical effects of proximal femoral osteotomies," *The Hip. Proceeding of the Twelfth Open Scientific Meeting of the Hip Society*, pp. 193-210, St. Louis: C. V. Mosby, 1984.
- [16] Buford, W. L. and Thompson, D. E., "A system for three-dimensional interactive simulation of hand biomechanics," *IEEE Trans. Biomed. Eng.*, vol. BME-34, pp. 444-453, 1987.
- [17] Cahalan, T. D., Johnson, M. E., Liu, S., and Chao, E. Y. S., "Quantitative measurements of hip strength in different age groups," *Clin. Orthop. Rel. Res.*, vol. 246, pp. 136-145, 1989.
- [18] Calvert, P. T., August, A. C., Albert, J. S., Kemp, H. B., and Catterall, A., "The Chiari pelvic osteotomy: a review of the long-term results," *J. Bone Joint Surg.*, vol. 69-B, pp. 551-555, 1987.
- [19] Carter, D. R., Orr, T. E., and Fyhrie, D. P., "Relationships between loading history and femoral cancellous bone architecture," *J. Biomech.*, vol. 22, pp. 231-244, 1989.
- [20] Chang, G., "Computer-aided surgery: an interactive simulation system for intertrochanteric osteotomy," M.S. Thesis, Massachusetts Institute of Technology, 1987.
- [21] Charnley, J. C. and Ferreira, S. D., "Transplantation of the greater trochanter in arthroplasty of the hip," *J. Bone Joint Surg.*, vol. 46-A, pp. 191-197, 1964.
- [22] Chiari, K., "Ergebnisse mit der Beckenosteotomie als Pfannendachplastik," *Z. Orthop.*, vol. 87, pp. 14-26, 1955.
- [23] Chiari, K., "Medial Displacement Osteotomy of the Pelvis," *Clin. Orthop.*, vol. 98, pp. 55-71, 1974.
- [24] Chiari, K. and Schwager, X., "L'osteotomie pelvienne: Indications et resultats," *Rev. Chir. Orthop.*, vol. 62, pp. 560-568, 1976.
- [25] Clark, J. M. and Haynor, D. R., "Anatomy of the abductor muscles of the hip as studied by computed tomography," *J. Bone Joint Surg.*, vol. 69-A, pp. 1021-1031, 1987.

- [26] Colton, C. L., "Chiari osteotomy for acetabular dysplasia in young subjects," *J. Bone Joint Surg.*, vol. 54-B, pp. 578-589, 1972.
- [27] Davy, D. T. and Audu, M. L., "A dynamic optimization technique for predicting muscle forces in the swing phase of gait," *J. Biomech.*, vol. 20, pp. 187-201, 1987.
- [28] Delp, D. B. and Delp, S. L., "Understanding human movement with computer graphics," *Soma.*, vol. 3, pp. 17-25, 1989.
- [29] Delp, S. L., Bleck, E. E., Zajac, F. E., and Bollini, G., "Biomechanical analysis of the Chiari pelvic osteotomy: preserving hip abductor strength," *Clin. Orthop. Rel. Res.*, vol. 254, pp. 189-198, 1990.
- [30] Delp, S. L., Loan, J. P., Hoy, M. G., Zajac, F. E., Topp, E. L., and Rosen, J. M., "An interactive, graphics-based model of the lower extremity to study orthopaedic surgical procedures," *IEEE Trans. Biomed. Eng.*, vol. 37, pp. 757-767, 1990.
- [31] DeWaal Malefut, M. C., Hoogland, T., and Neilsen, H. K. L., "Chiari osteotomy in the treatment of congenital dislocation and subluxation of the hip," *J. Bone Joint Surg.*, vol. 64-A, pp. 996-1004, 1982.
- [32] Dul, J., Shiavi, R., and Green, N. E., "Simulation of tendon transfer surgery," *Eng. Med.*, vol. 14, pp. 31-38, 1985.
- [33] Edwards, C. C., Simmons, S. C., Browner, B. D., and Weigel, M. C., "Severe open tibial fractures," *Clin. Orthop. Rel. Res.*, vol. 230, pp. 98-115, 1988.
- [34] Eftekhari, N. S., "Surgical approaches to the hip," in *Principles of Total Hip Arthroplasty*. pp. 35-37, St. Louis: C.V. Mosby, 1978.
- [35] Enoka, R. M., "Muscle strength and its development: new perspectives," *Sports Med.*, vol. 6, pp. 146-168, 1988.
- [36] Enoka, R. M. and Fuglevand, A. J., "Neuromuscular basis of the maximum voluntary force capacity of muscle," in *Current Issues in Biomechanics. a Prospectus*. (edited by Grabiner, M. D.) Champaign, IL: Human Kinetics, 1990.
- [37] Evans, E. B. and Julian, J. D., "Modifications of the hamstring transfer," *Develop. Med. and Child. Neurol.*, vol. 8, pp. 539-551, 1966.
- [38] Eycleshymer, A. C. and Shoemaker, D. M., *A cross section anatomy*. New York: Appleton-Crofts, 1970.
- [39] Farrell, E. J. and Zappulla, R. A., "Three-Dimensional data visualization and biomedical applications," *CRC Crit. Rev. in Biomed. Eng.*, vol. 16, pp. 323-363, 1989.

- [40] Fellingham, L. L., Vogel, J., Lau, C., and Dev, P., "Interactive graphics and 3-D modelling for surgical planning and prosthesis and implant design," *Proc. 7th Annual Conference, National Computer Graphics Association*, pp. 132, 1986.
- [41] Fisher, S. S., McGreevy, M., Humphries, J., and Robinett, W., "Virtual Environment display system," *Proc. ACM Workshop on Interactive 3D Graphics*, pp. 1-11, 1986.
- [42] Forsythe, G. E. and Malcolm, M. A., *Computer Methods for Mathematical Computations*. Englewood Cliffs: Prentice-Hall, 1977.
- [43] Friederich, J. A. and Brand, R. A., "Muscle fiber architecture in the human lower limb," *J. Biomech.*, vol. 23, pp. 91-95, 1990.
- [44] Gage, J. R., J. Perry, R. R. Hicks., Koop, S., and Wernitz, J. R., "Rectus femoris transfer as a means of improving knee function in cerebral palsy," *Develop. Med. Child Neurolgy.*, vol. 29, pp. 159-166, 1987.
- [45] Gaines, R. W. and Ford, T. B., "A systematic approach to the amount of Achilles tendon lengthening in cerebral palsy," *J. Pediatr. Orthop.*, vol. 4, pp. 448-451, 1984.
- [46] Garg, A. and Walker, P. S., "Prediction of total knee motion using a three-dimensional computer-graphics model," *J. Biomech.*, vol. 23, pp. 45-58, 1990.
- [47] Goldwasser, S. M., Reynolds, R. A., Talton, D. A., and Walsh, E. S., "Techniques for the rapid display and manipulation of 3D biomedical data," *Comp. Med. Imag. and Graphics.*, vol. 12, pp. 1-24, 1988.
- [48] Gordon, A. M., Huxley, A. F., and Julian, F. J., "The variation in isometric tension with sarcomere length in vertebrate muscle fibres," *J. Physiol.*, vol. 184, pp. 170-192, 1966.
- [49] Gordon, M. G., "An analysis of the biomechanics and muscular synergies of human standing," Ph. D. Thesis, Stanford University, 1990.
- [50] Gore, D. R., Murray, M. P., Gardner, G. M., and Sepic, S. B., "Roentgenographic measurements after Muller total hip replacement," *J. Bone Joint Surg.*, vol. 59-A, pp. 948, 1977.
- [51] Gougeon, F., D., A., and Fontaine, C., "L'osteotomie de Chiari: Difficultes de realisation du contrat biomecanique," *Revue de Chirurgie Orthopedique.*, vol. 70, pp. 599-611, 1984.
- [52] Graham, S., Wentin, G. W., Dawson, E., and Oppenheim, W. L., "The Chiari osteotomy. a review of 58 cases," *Clin. Orthop.*, vol. 208, pp. 249-258, 1986.
- [53] Granholm, J. W., Robertson, D. D., Walker, P. S., and Nelson, P. C., "Computer design of custom femoral stem prostheses," *IEEE Comput. Graphics Appl.*, vol. pp. 26-35, 1987.
- [54] Gromie, W. J., "Computer-aided surgery," *MIT Report.*, vol. XVI, pp. 4-5, 1988.

- [55] Hallen, L. G. and Lindahl, O., "The screw home movement in the knee-joint," *Acta Orthop. Scand.*, vol. 37, pp. 97-106, 1966.
- [56] Hardt, D. E., "Determining muscle forces in the leg during normal human walking — an application and evaluation of optimization methods," *J. Biomech. Eng.*, vol. 100, pp. 72-78, 1978.
- [57] Hatze, H., "The complete optimization of a human motion," *Math. Biosci.*, vol. 28, pp. 99-135, 1976.
- [58] Heerkens, Y. F., Woittiez, R. D., Huijing, P. A., Huson, A., Schenau, G. J. I., and Rozendal, R. H., "Passive resistance of the human knee: the effect of remobilization," *J. Biomed. Eng.*, vol. 9, pp. 69-76, 1987.
- [59] Herman, G. T., "Applications of three-dimensional computer graphics to surgical planning and evaluation," *Proc. 5th Ann. Conf. Natl. Comput. Graphics Assoc.*, pp. 1984.
- [60] Herzog, W. and ter Keurs, H. E. D. J., "Force-length relation of in-vivo human rectus femoris muscles," *J. Physiol. (Europ.)*, vol. 411, pp. 642-647, 1988.
- [61] Hogh, J. and MacNicol, M. F., "The Chiari pelvic osteotomy: a long-term review of clinical and radiographic results," *J. Bone Joint Surg.*, vol. 69-B, pp. 365-373, 1987.
- [62] Hoy, M. G., Zajac, F. E., and Gordon, M. E., "A musculoskeletal model of the human lower extremity: the effect of muscle, tendon, and moment arm on the moment-angle relationship of musculotendon actuators at the hip, knee, and ankle," *J. Biomech.*, vol. 23, pp. 157-169, 1990.
- [63] Huijing, P. A., Greuell, A. E., Wajon, M. H., and Wottiez, R. D., "An analysis of human maximal isometric voluntary plantar flexion as a function of ankle and knee joint angle," *Biomechanics: Basic and Applied Research. Selected Proceedings from the Fifth Meeting of the European Society of Biomechanics*. pp. 667-672, Berlin, F. R. G., 1986.
- [64] Inman, V. T., "Functional aspects of the abductor muscles of the hip," *J. Bone Joint Surg.*, vol. 29-A, pp. 607-619, 1947.
- [65] Inman, V. T., *The joints of the ankle*. Baltimore: Williams & Wilkins, 1976.
- [66] Inman, V. T., Ralston, H. J., and Todd, F., *Human Walking*. Baltimore, MD: Williams & Wilkins, 1981.
- [67] Jensen, R. H. and Davy, D. T., "An investigation of muscle lines of action about the hip: a centroid line approach vs the straight line approach," *J. Biomech.*, vol. 8, pp. 103-110, 1975.
- [68] Johnston, R. C., "Mechanical considerations of the hip joint," *Arch. Surg.*, vol. 107, pp. 411-417, 1973.

- [69] Johnston, R. C., Brand, R. A., and Croninshield, R. D., "Reconstruction of the hip: a mathematical approach to determine optimum geometric relationships," *J. Bone Joint Surg.*, vol. 61-A, pp. 639-652, 1979.
- [70] Khang, G. and Zajac, F. E., "Paraplegic standing controlled by functional neuromuscular stimulation: part I— computer model and control-system design," *IEEE Trans. Biomed. Eng.*, vol. 36, pp. 873-884, 1989.
- [71] Kinnucan, P. and Stiefel, R. A., "3D reconstruction systems bring a fresh perspective to patient care," *S. Klein Comp. Graphics Rev.*, vol. pp. 65-69, 1988.
- [72] Kulig, K., Andrews, J. G., and Hay, J. G., "Human Strength Curves," *Exercise and Sport Sciences Reviews.*, vol. 12, pp. 417-466, 1984.
- [73] Lazansky, M. G., "Osteotomy of the greater trochanter. Part II. Trochanteric osteotomy in total hip replacement," *The Hip. Proceedings of the Second Open Scientific Meeting of the Hip Society.* pp. 231-237, St. Louis: C. V. Mosby, 1974.
- [74] Lieber, R. L., "Skeletal muscle adaptability. I: Review of basic properties," *Develop. Med. Child Neurol.*, vol. 28, pp. 390-397, 1986.
- [75] Lindahl, O., Movin, A., and Ringqvist, I., "Knee extension: Measurement of the isometric force in different positions of the knee joint," *Acta Orthop. Scand.*, vol. 40, pp. 79-85, 1969.
- [76] Loeb, G. E., He, J., and Levine, W. S., "Spinal cord circuits: are they mirrors of musculoskeletal mechanics?," *J. Motor Behavior.*, vol. 21, pp. 473-491, 1989.
- [77] Loeb, G. E., Pratt, C. A., Chanaud, C. M., and Richmond, F. R. J., "Distribution and innervation of short, interdigitated muscle fibers in parallel-fibered muscles of the cat hindlimb," *J. Morph.*, vol. 191, pp. 1-15, 1987.
- [78] Lord, P. J., "3-D gait: a three dimensional computer graphic display for human motion analysis from track gait data," B.S. Thesis, Massachusetts Institute of Technology, 1987.
- [79] MacNicol, M. F., Uprichard, H., and Mitchell, G. P., "Exercise testing after the Chiari pelvic osteotomy," *J. Bone Joint Surg.*, vol. 63-B, pp. 326-331, 1981.
- [80] Mai, M. T. and Lieber, R. L., "A model of semitendinosus muscle sarcomere length, knee and hip joint interaction in the frog hindlimb," *J. Biomech.*, vol. 23, pp. 271-279, 1990.
- [81] van Mameran, H. and Drukker, J., "Attachment and composition of skeletal muscles in relation to their function," *J. Biomech.*, vol. pp. 859-867, 1979.
- [82] Manktelow, R. T., Zucker, R. M., and McKee, N. H., "Functioning free muscle transplantation," *J. Hand Surg.*, vol. 9A, pp. 32-39, 1984.

- [83] Mann, R. W., "Computer-aided surgery," *Proc. 8th Ann. Conf. Rehab. Eng. Soc. North Am. (RESNA)*, pp. 160-162, 1985.
- [84] Mann, R. W. and Antonsson E. K., "Gait analysis - precise, rapid, automatic, 3-D position and orientation kinematics and dynamics," *Bull. Hosp. Jt. Diseases Orthop. Inst.*, vol. XLIII, pp. 137-146, 1983.
- [85] Mansour, J. M. and Audu, M. L., "The passive elastic moment at the knee and its influence on human gait," *J. Biomech.*, vol. 19, pp. 369-373, 1986.
- [86] Mansour, J. M. and Pereira, J. M., "Quantitative functional anatomy of the lower limb with application to human gait," *J. Biomech.*, vol. 20, pp. 51-58, 1987.
- [87] Marsh, E., Sale, D., McComas, A. J., and Quinlan, J., "Influence of joint position on ankle dorsiflexion in humans," *J. Appl. Physiol.: Respirat. Environ. Exer. Physiol.*, vol. 51, pp. 160-167, 1981.
- [88] Marsh, J. L., Vannier, M. W., Stevens, W. G., Warren, J. O., Gayou, D., and Dye, D. M., "Computerized imaging for soft tissue and osseous reconstruction in the head and neck," *Clin. Plastic Surg.*, vol. 12, pp. 279-291, 1985.
- [89] May, W. W., "Relative isometric force of the hip abductor and adductor muscles," *Phys. Ther.*, vol. 48, pp. 845-851, 1968.
- [90] McLeish, R. D. and Charnley, J. C., "Abduction forces in the one-legged stance," *J. Biomech.*, vol. 3, pp. 191-209, 1970.
- [91] Mooney, V. and Goodman, F., "Surgical approaches to lower-extremity disability secondary to strokes," *Clin. Orthop.*, vol. 63, pp. 142-152, 1969.
- [92] Muller, M. E., "Osteotomy of the greater trochanter. Part I. Total hip replacement without trochanteric osteotomy," *The Hip. Proceedings of the Second Open Scientific Meeting of the Hip Society*. pp. 231-237, St. Louis: C. V. Mosby, 1974.
- [93] Murphy, S. B., Kijewski, P. K., Millis, M. B., Hall, J. E., Simon, S. R., and Chandler, H. P., "The planning of orthopaedic reconstructive surgery using computer-aided simulation and design," *Comp. Med. Imag, and Graphics.*, vol. 12, pp. 33-45, 1988.
- [94] Murray, M. P., Baldwin, J. M., Gardner, G. M., Sepic, S. B., and Downs, W. J., "Maximum isometric knee flexor and extensor muscle contractions," *Phys. Ther.*, vol. 57, pp. 637-643, 1977.
- [95] Murray, M. P. and Sepic, S. B., "Maximum isometric torque of hip abductor and adductor muscles," *Phys. Ther.*, vol. 48, pp. 1327-1335, 1968.
- [96] Nemeth, G., Ekholm, J., Arborelius, U., Harms-Ringdahl, K., and Schuldt, K., "Influence of knee flexion on isometric hip extensor strength," *Scand. J. Rehabil. Med.*, vol. 15, pp. 97-101, 1983.

- [97] Nisell, R., Nemeth, G., and Ohlsen, H., "Joint forces in extension of the knee," *Acta Orthop. Scand.*, vol. 57, pp. 41-46, 1986.
- [98] Olney, B. W., Williams, P. F., and Menelaus, M. B., "Treatment of spastic equinus by aponeurosis lengthening," *J. Pediatric Orthop.*, vol. 8, pp. 422-425, 1988.
- [99] Olson, V. L., Smidt, G. L., and Johnston, R. C., "The maximum torque generated by the eccentric, isometric, and concentric contractions of the hip abductor muscles," *Phys. Ther.*, vol. 52, pp. 149-158, 1972.
- [100] Orr, T. E., "The role of mechanical stresses in bone remodeling," Ph.D. Thesis, Stanford University, 1990.
- [101] Otten, E., "Concepts and models of functional architecture in skeletal muscle," *Exercise and Sport Science Reviews.*, vol. 16, pp. 89-138, 1988.
- [102] Page, S. G. and Huxley, H. E., "Filament lengths in striated muscle," *J. Cell Biol.*, vol. 19, pp. 369-390, 1963.
- [103] Pandy, M. G., Zajac, F. E., Sim, E., and Levine, W. S., "An optimal control model for maximum-height human jumping," *J. Biomech.*, (in press), 1990.
- [104] Pemberton, P. A., "Pericapsular osteotomy of the ilium for treatment of congenital subluxation and dislocation of the hips," *J. Bone Joint Surg.*, vol. 47-A, pp. 65-86, 1965.
- [105] Perry, J., "Normal and pathologic gait," *American Academy of Orthopaedic Surgeons Atlas of Orthodics*. pp. 76-111, St. Louis: C.V. Mosby, 1985.
- [106] Perry, J. and Hoffer, M., "Preoperative and postoperative dynamic electromyography as an aid in planning tendon transfers in children with cerebral palsy," *J. Bone Joint Surg.*, vol. 59-A, pp. 531-537, 1977.
- [107] Perry, J., Waters, R. L., and Perrin, T., "Electromyographic analysis of equinovarus following stroke," *Clin. Orthop. Rel. Res.*, vol. 131, pp. 47-53, 1978.
- [108] Pierrynowski, M. R. and Morrison, J. B., "A physiological model for the evaluation of muscular forces in human locomotion: theoretical aspects," *Math Biosci.*, vol. 75, pp. 69-101, 1985.
- [109] Pizer, S. M. and Fuchs, H., "Three dimensional image presentation techniques in medical imaging," *Proc. Int. Symp. Comput. Assist. Radiol.*, pp. 589, 1987.
- [110] Proske, U. and Morgan, D. L., "Tendon stiffness: methods of measurement and significance for the control of movement. a review," *J. Biomech.*, vol. 20, pp. 75-82, 1987.
- [111] Rab, G. T., "Hamstring length in crouch gait," *Proc. XII International Congress of Biomechanics*, pp. 277, 1989.

- [112] Ray, R. L. and Ehrlich, M. G., "Lateral hamstring transfer and gait improvement in the cerebral palsy patient," *J. Bone and Joint Surg.*, vol. 61-A, pp. 719-723, 1979.
- [113] Rhodes, M. L., Luo, Y.-M., and Rothman, S. L. G., "An application of computer graphics and networks to anatomic modeling and prosthesis manufacturing," *IEEE Comput. Graphics Appl.*, vol. pp. 12-25, 1987.
- [114] Robb, R. A. and Barillot, C., "Interactive Display and Analysis of 3-D Medical Images," *IEEE Trans. Med. Imag.*, (in press), 1990.
- [115] Root, L., Miller, S. R., and Kirz, P., "Posterior tibial-tendon transfer in patients with cerebral palsy," *J. Bone and Joint Surg.*, vol. 69-A, pp. 1133-1139, 1987.
- [116] Sale, D., Quinlan, J., E. Marsh, A. J. M., and Belanger, A. Y., "Influence of joint position on ankle plantarflexion in humans," *J. Appl. Physiol.: Respirat. Environ. Exer. Physiol.*, vol. 52, pp. 1636-1642, 1982.
- [117] Salter, R. B., "Role of the innominate osteotomy in the treatment of congenital dislocation and subluxation of the hips in the older child," *J. Bone Joint Surg.*, vol. 48-A, pp. 1413-1439, 1966.
- [118] Schwartz, J. R., Carr, W., Bassett, F. H., and Coonrad, R. W., "Lessons learned in the treatment of equinus deformity in ambulatory spastic children," *Orthop. Trans.*, vol. 1, pp. 84, 1977.
- [119] Scudder, G. N., "Torque curves produced at the knee during isometric and isokinetic exercises," *Arch. Phys. Med. Rehabil.*, vol. 61, pp. 68-72, 1980.
- [120] Shultze, H. and Kramer, J., "Ergebnisse der bekenosteotomie nach Chiari," *Z. Orthop.*, vol. 113, pp. 891, 1975.
- [121] Siegler, S., Chen, J., and Schneck, C. D., "The three-dimensional kinematics and flexibility characteristics of the human ankle and subtalar joints—part I: kinematics," *J. Biomech. Eng.*, vol. 110, pp. 364-373, 1988.
- [122] Spector, S. A., Gardiner, P. F., Zernicke, R. F., Roy, R. R., and Edgerton, V. R., "Muscle architecture and force-velocity characteristics of cat soleus and medial gastrocnemius: implications for neural control," *J. Neurophysiol.*, vol. 44, pp. 951-960, 1980.
- [123] Spoor, C. W., van Leeuwen, J. L., de Windt, F. H. J., and Huson, A., "A model study of muscle forces and joint-force direction in normal and dysplastic neonatal hips," *J. Biomech.*, vol. 22, pp. 873-884, 1989.
- [124] Stredney, D. L., "The representation of anatomical structures through computer animation for scientific, educational, and artistic applications," Masters Thesis, The Ohio State University, 1982.

- [125] Tabary, J. C., Tabary, C., Tardieu, C., Tardieu, G., and Goldspink, G., "Physiological and structural changes in the cat's soleus muscle due to immobilization at different lengths by plaster casts," *J. Physiol. (Lond.)*, vol. 224, pp. 231-244, 1972.
- [126] Tello, R., Chang, G., Mann, R. W., and Rowell, D., "Generation of surface anatomy from CT and MRI images," *Proc. 10th Ann. Conf. Rehabilitation Eng. Soc. North America*, pp. 817-819, 1987.
- [127] Thometz, J., Simon, S., and Rosenthal, R., "The effect on gait of lengthening of the medial hamstrings in cerebral palsy," *J. Bone and Joint Surg.*, vol. 71-A, pp. 345-353, 1989.
- [128] Thompson, D. E. and Giurintano, D. J., "A kinematic model of the flexor tendons of the hand," *J. Biomech.*, vol. 22, pp. 327-334, 1989.
- [129] Trivedi, S. S., Herman, G. T., Udupa, J. K., Margasahayam, P., and Chen, L.-S., "Measurements on 3-D displays in the clinical environment," *Proc. 7th Annual Conference, National Computer Graphics Association*, pp. 93-99, 1986.
- [130] Tropp, H., "Pronator muscle weakness in functional instability of the ankle joint," *Int. J. Sports Med.*, vol. 7, pp. 291-294, 1986.
- [131] Truschelli, D., Lespargot, A., and Tardieu, G., "Variation in the long-term results of elongation of the tendo achillis in children with cerebral palsy," *J. Bone Joint Surg.*, vol. 61-B, pp. 466-469, 1979.
- [132] Udupa, J. K., "Simulation of surgical procedures using computer graphics," *Proc. 7th Annual Conference, National Computer Graphics Association*, pp. 80-92, 1986.
- [133] van Eijden, T. M. G. J., de Boer, W., and Weijs, W. A., "The orientation of the distal part of the quadriceps femoris muscle as a function of the knee flexion-extension angle," *J. Biomech.*, vol. 18, pp. 803-809, 1985.
- [134] van Eijden, T. M. G. J., Weijs, W. A., Kouwenhoven, E., and Verberg, J., "Forces acting on the patella during maximal voluntary contraction of the quadriceps femoris muscle at different knee flexion/extension angles," *Acta Anat.*, vol. 129, pp. 310-314, 1987.
- [135] Vannier, M. W., Marsh, J. L., and Warren, J. O., "Three dimensional CT reconstruction images for craniofacial surgical planning and evaluation," *Radiology*, vol. 150, pp. 179-184, 1984.
- [136] Waters, R. L., Perry, J., and Garland, D., "Surgical correction of gait abnormalities following stroke," *Clin. Orthop.*, vol. 131, pp. 54-63, 1978.
- [137] Waters, R. L., Perry, J., McDaniels, J. M., and House, K., "The relative strength of the hamstrings during hip extension," *J. Bone Joint Surg.*, vol. 56-A, pp. 1592-1597, 1974.
- [138] Weber, E., *Wagner's Handwörterbuch der Physiologie*. Braunscheig, Vieweg: 1846.

- [139] Werdt, P. P. and Johnson, R. P., "A study of quadriceps excursion, torque, and the effect of patellectomy on cadaver knees," *J. Bone and Joint Surg.*, vol. 67-A, pp. 726-731, 1985.
- [140] White, S. C., Yack, H. J., and Winter, D. A., "A three-dimensional musculoskeletal model for gait analysis. Anatomical variability estimates," *J. Biomech.*, vol. 22, pp. 885-893, 1989.
- [141] Wickiewicz, T. L., Roy, R. R., Powell, P. L., and Edgerton, V. R., "Muscle architecture of the human lower limb," *Clin. Orthop. Rel. Res.*, vol. 179, pp. 275-283, 1983.
- [142] Williams, P. E. and Goldspink, G., "Changes in sarcomere length and physiological properties in immobilized muscle," *J. Anat.*, vol. 127, pp. 459-468, 1978.
- [143] Williams, R. and Seireg, A. A., "Interactive computer modeling of the musculoskeletal system," *IEEE Trans. Biomed. Eng.*, vol. BME-24, pp. 213-219, 1977.
- [144] Woo, S. S.-Y., Gomez, M. A., Woo, Y.-K., and Akeson, W. H., "Mechanical properties of tendons and ligaments. II. The relationships of immobilization and exercise on tissue remodeling," *Biorheology*, vol. 19, pp. 397-408, 1982.
- [145] Wood, J. E., Meek, S. G., and Jacobsen, S. C., "Quantification of human shoulder anatomy for prosthetic arm control —I. surface modelling," *J. Biomech.*, vol. 22, pp. 273-292, 1989.
- [146] Yamaguchi, G. T. and Zajac, F. E., "A planar model of the knee joint to characterize the knee extensor mechanism," *J. Biomech.*, vol. 22, pp. 1-10, 1989.
- [147] Yamaguchi, G. T. and Zajac, F. E., "Restoring unassisted natural gait to paraplegics via functional neuromuscular stimulation: a computer simulation study," *IEEE Trans. Biomed. Eng.*, vol. 37, (in press), 1990.
- [148] Yoon, Y. S. and Monsour, J. M., "The passive elastic moment at the hip," *J. Biomech.*, vol. 15, pp. 905-910, 1982.
- [149] Zajac, F. E., "Thigh muscle activity during maximum-height jumps by cats," *J. Neurophysiol.*, vol. 53, pp. 979-994, 1985.
- [150] Zajac, F. E., "Muscle and tendon: properties, models, scaling, and application to biomechanics and motor control," *CRC Critical Reviews in Biomedical Engineering*, vol. 17, pp. 359-411, 1989.
- [151] Zajac, F. E. and Gordon, M. E., "Determining muscle's force and action in multi-articular movement," *Exercise and Sport Sciences Reviews*, vol. 17, pp. 187-230, 1989.